i

The Dissertation Committee for Sue-jie Koo Certifies that this is the

approved version of the following dissertation:

UNDERSTANDING AND MODULATING MACROPHAGE METABOLISM FOR IMPROVING INFLAMMATORY FUNCTIONS AGAINST TRYPANOSOMA CRUZI INFECTION
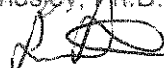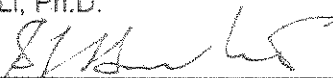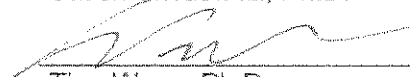
Committee:

Nisha J. Garg, Ph.D, Mentor

Janice Endsley, Ph.D.

Liwu Li, Ph.D.

Satish Srivastava, Ph.D.

Tian Wang, Ph.D.

Dean, Graduate School

UNDERSTANDING AND MODULATING MACROPHAGE METABOLISM FOR IMPROVING INFLAMMATORY FUNCTIONS AGAINST TRYPANOSOMA CRUZI INFECTION

by

Sue-jie Koo, B.S.

Dissertation

Presented to the Faculty of the Graduate School of

The University of Texas Medical Branch

in Partial Fulfillment

of the Requirements

for the Degree of

Doctor of Philosophy

The University of Texas Medical Branch
October, 2017

Acknowledgements

I would like to express my gratitude to everyone who were a part of my journey in the completion of this work; the unlimited support from my family, husband, and friends without whom I would have not persisted in even trying to achieve my goals.

I also thank my preliminary exam committee and the Pathology department faculty who taught me how to structure a grant and were the evaluators of my first research proposal. Their patience and kindness sent me well on my way toward the start of this dissertation work. I thank the GSBS deans, past and present, who were always available and even went out of their way to help me address any concerns that I had.

I extend my heartfelt gratitude to my committee members who not only advised in my research, but also gave counsel in my times of personal difficulty, helped me unconditionally to get back on my feet, provided reassurance, and advised on my next steps after graduate school. No matter how short our one-on-one meetings were in the office or at a conference, every one of them helped me to see and energized me to continue and run to the finish line.

Lastly, but certainly not least, I am deeply indebted to my supervisor, Nisha Garg, who served as my biggest critic yet my greatest advocate in my graduate school journey. Her patience, optimism, and dedication in her mentorship helped me grow to who I am today and taught me to fully embrace uncertainties in research and work with them. I am grateful for the opportunity to have worked on this project.

UNDERSTANDING AND MODULATING MACROPHAGE METABOLISM FOR IMPROVING INFLAMMATORY FUNCTIONS AGAINST TRYPANOSOMA CRUZI INFECTION

Sue-jie Koo

The University of Texas Medical Branch, 2017

Supervisor: Nisha J. Garg

This dissertation aims to illuminate how metabolism regulates the pro-inflammatory functions in macrophages for improving the clearance of *Trypanosoma cruzi* infection. *T. cruzi* is the etiologic agent of Chagas disease, which affects over 8 million people and current therapy has limited efficacy. Macrophages are one of the first sentinels to *T. cruzi* infection yet are susceptible to infection. Prior research indicated that glycolysis and broken Krebs cycle support pro-inflammatory functions of macrophages. This study advances our understanding of how *T. cruzi* infection shifts the metabolism of macrophages and suppress accumulation of oxidative mediators. The first is to evaluate the pro-inflammatory macrophage response to *T. cruzi* with respect to production of pro-inflammatory mediators and metabolic state. The second is to modulate the macrophage metabolism during infection and evaluate the functional outcome, with the focus on a lipid metabolism transcription factor, peroxisome proliferator-activated receptor-α (PPAR-α), and oxidative species generation. This study tested two hypotheses: that macrophages infected with *T. cruzi* fail to metabolically and phenotypically shift to the pro-inflammatory phenotype, and that modulating PPAR-α is a strategy to improve

macrophage function against *T. cruzi*. The findings of this research demonstrate that macrophages infected with *T. cruzi* poorly accumulate reactive oxygen species and nitric oxide, in which the shunt to the pentose phosphate pathway is important for oxidative species generation and suppressing *T. cruzi* survival and replication.

Contrary to our expectations, inhibition of PPAR-α and mitochondrial pyruvate transport moderately suppressed oxidative species levels. Supplying macrophages with IFN-γ during infection succeeded in shifting metabolism to glycolysis and enhancing oxidative species levels. We conclude that the pentose phosphate pathway is vital in the *T. cruzi* clearing response of macrophages and could serve as a novel basis for a strategy to improve the innate immune response to *T. cruzi* infection and prevent Chagas disease progression.

TABLE OF CONTENTS

LIST OF TABLES

LIST OF FIGURES

Chapter 1: Review of Literature

Part A. Chagas Disease

A1. Public Health Concern of Chagas Disease

Chagas disease, also known as American Trypanosomiasis, is one of the five neglected parasitic infections prioritized by the United States Centers for Disease Control for public health solutions. Over 8 million people worldwide are affected by Chagas disease primarily in Latin America, and approximately 300,000 persons are infected in the United States. Chagas disease is caused by the vector-borne protozoan, *Trypanosoma cruzi*, which can be transmitted by blood transfusions and congenitally but primarily are transmitted by triatomine insects. Triatomines become infected when they blood-feed on mammals positive for *T. cruzi* trypomastigotes, and carry the transformed replicative epimastigote parasite stage in their small intestine (Garcia et al., 2010). In the rectum of infected triatomines, epimastigotes mature to the infective trypomastigote stage which are defecated near feeding sites. The mammalian host becomes infected with *T. cruzi* when the triatomine feces contaminate the feeding site wound, typically due to scratching of the wound site by the host.

There are three phases to Chagas disease: first, the acute phase where it presents with general symptoms of fever, rash, body aches, and swelling at the infection site; then the asymptomatic phase where patients are seropositive yet do not show complications. Lastly, the chronic phase occurs in approximately 30% of those infected, where cardiomyopathy and digestive symptoms are the most common and occur decades after infection. Benznidazole and nifurtimox are the current therapeutics for Chagas disease, but have limited efficacy, require long-term treatment and cause adverse side effects (Pinazo et al., 2010) (Coura et al., 1997) (Jackson et al., 2010). *T. cruzi* strains are currently classified phylogenetically within 6 discrete typing units

from I to VI, and are variable in their geography, epidemiology, and pathogenic characteristics. The Sylvio X10 isolate is a prototype of type I and has been shown to cause pathology in mice (Zago et al., 2016b). *T. cruzi* culture strain (TCC) is also type I but experimentally infected animals do not show disease and has been studied in the past for its potential as a vaccine candidate but the risk of its reversion to cause pathology is unknown (Basombrio and Besuschio, 1982) (Perez Brandan and Basombrio, 2012).

A2. *Trypanosoma cruzi* Alters Metabolism of Host Cells

Chagas disease patients and animal models have suggested that *T. cruzi* infection dysregulates host metabolism. Murine models of Chagas disease have shown hypoglycemia, defect in liver gluconeogenesis (Nagajyothi et al., 2013), increase in parasitism and mortality in diabetic animals (Nagajyothi et al., 2010), and increase in insulin resistance and pro-atherogenic particles in obese chagasic mice (Cabalen et al., 2016). In human patients seropositive for *T. cruzi*, clinical surveys in Brazil observed over 70% of participants with dyslipidemia, an atherosclerotic risk factor, and 85% to be overweight or obese (Geraix et al., 2007) (Elaine Cristina Navarro, 2013).

Macrophages are one of the first and vital responders to *T. cruzi* infection, yet their incomplete control of the parasite leads to dissemination to peripheral tissues (Celentano and Gonzalez Cappa, 1993) (Silva et al., 2004). Infected HeLa cells and chagasic myocardium show decreased expression of pyruvate dehydrogenase, indicative of reduced use of glycolysis and instead utilize fatty acid metabolism (Caradonna et al., 2013) (Garg et al., 2004). Additionally, the immune deficiency of *T. cruzi*-infected macrophages is indicated by its down-regulation of antigen presentation via MHC-II (La Flamme et al., 1997). Peritoneal mφ from *T. cruzi*-infected mice elicit poor T cell proliferation via presentation of programmed death ligands (PDL) 1 and 2.

Blocking PDL-2 in infected mφ presents with increased arginase 1 expression and activity, and decreased the production of nitric oxide and nitric oxide synthase gene expression (Dulgerian et al., 2011).

Conversely, accumulation of lipid droplets which store inflammatory mediators have been shown in infected macrophages; however, their role in parasite clearance has not been delineated (Johndrow et al., 2014). These studies indicate that altering the host metabolism is essential in the persistence of *T. cruzi*, and understanding the mechanics of metabolism could aid in devising a strategy to control parasite dissemination and persistence.

Part B. Macrophages

B1. Introduction to Role of Macrophages in Host Defense

Macrophages (Mφ) are innate immune cells named after their characteristics as large cells that eat or phagocytose. They reside in almost all of the tissues in the body as patrollers and responders. Two lineages are currently known: those differentiated from blood-circulating monocytes derived from myeloid progenitor cells in the bone marrow and migrate to sites of host insult, or in the tissues as resident mφ which are derived from the yolk sac. Both lineages of mφ serve as one of the first line of host defense at multiple levels; for their properties to engulf and digest microbes, synthesize compounds for microbial damage and for recruitment of immune cells, and present antigens to T cells for the initiation of adaptive immunity. These types of macrophages are named M1, respective to their ability to activate T helper 1 (Th1) cells.

Mφs also regulate the resolution of inflammation by further phagocytosing apoptotic bodies and debris, and secreting wound healing factors for tissue repair. These immunosuppressive macrophages are alluded to as M2 for their phenotype being

associated to T helper 2 (Th2) or regulatory T cells. Proteomics studies have revealed that there are differences in surface receptors of M1 vs M2, (Becker et al., 2012) which can be used as phenotypic markers in addition to functional studies. Because of these range of characteristics, mφ are essential players in inflammation and the immune control of many infectious diseases. The criticality of macrophages in the appropriate response to infectious pathogens and shaping disease progress is particularly evident shown by depletion and phenotyping studies.

B2 Overview of activation of Mφ Functions

B2.1. Recognition by Mφ for pro-inflammatory activation of effector functions

Mφs directly recognize pathogens through pattern recognition receptors (PRRs) which include toll-like receptors, C-type lectin receptors, NOD-like receptors, and RIG-I-like receptors. These receptors recognize conserved pathogen associated molecular patterns (PAMPs) (Zhang and Mosser, 2008). A common example of PAMP is a component of the outer membrane of gram negative bacteria, lipopolysaccharide, which activates TLR4 of mφ and elicit a signaling cascade resulting in a pro-inflammatory response. Activation of TLRs commonly signal through a series of phosphorylation for recruitment and degradation of proteins and kinases, including tumor necrosis factor receptor-associated factor (TRAF) 6, MyD88, and TAK, that result in the induction of the nuclear factor κB (NFκB) transcription factor for the expression of pro-inflammatory cytokine genes (reviewed in (Akira and Takeda, 2004)). Mφ also recognize damage-associated molecular patterns (DAMPs), which are endogenous molecules that serve as immune activators when they are exposed out of a cell which occur under conditions of stress or injury. Some DAMPs are recognized by PRRs. Activation of PRRs initiate a signaling cascade which result in the activation of the immune cell such as cytokine secretion and phagocytosis.

Cytokines and chemokines produced by macrophages or other nearby cells are modes of communication, recognized by their respective receptors and enhance the activation of macrophages. Macrophages sense chemoattractants produced by other cells and migrate to the site by rapid rearrangements of the actin cytoskeleton (reviewed by (Jones, 2000)). Pro-inflammatory cytokines, namely interferon-γ (IFN-γ) and tumor necrosis factor (TNF)-α, enhance the pro-inflammatory activation of the mφ program by transcriptional mechanisms including by NFκB or hypoxia inducible factor-1α, or translational control (Su et al., 2015). IFN-γ and TNF-α are recognized by the IFN-γ receptor and TNF-α receptor, respectively. The IFN-γ receptor is composed to two chains with dimerize upon binding of IFN-γ, and Janus kinases phosphorylate and activate signal transducers and activators of transcription (STAT) 1 or STAT 3 to translocate to the nucleus and bind to DNA elements for gene transcription (reviewed in (Green et al., 2017)). TNF-α activates macrophages through Fas-associated protein with death domain or TRAF2-dependent manner which result in caspase-mediated apoptosis or activation of NFκB (reviewed in (Sedger and McDermott, 2014). Hence, the classical *in vitro* model of pro-inflammatory macrophage M1 activation is by LPS and IFN-γ and which result in the production of an extensive profile of inflammatory cytokines.

Pro-inflammatory macrophages also generate high levels of reactive oxygen and nitrogen species as oxidative molecules which contribute to the killing of many pathogens. Reactive oxygen species (ROS) are free radicals resulting from the reduction of molecular oxygen, to superoxide anion, peroxide, and hydroxyl radical. The unpaired electrons are highly reactive with lipids, proteins, and nucleic acids thus disrupting their functions. ROS can be produced by mitochondrial respiration or enzymatically by NADPH oxidase. Nitric oxide (NO) is also a free radical and is formed by the reaction of oxygen and L-arginine, catalyzed by nitric oxide synthases.

B2.2. Phagocytosis

Phagocytosis in mφ are activated by recognition through its complement, Fc, or

mannose receptors (reviewed in (Aderem and Underhill, 1999). Upon recognition of the

material for phagocytosis, the mφ membrane protrudes around the attached material

and forms a phagosome. The lysosome, filled with hydrolytic enzymes, fuses with the

phagosome forming a phagolysosome where the engulfed material is digested. The

digested material is then disposed from the cell by exocytosis or the resulting peptides

can be processed to be presented as antigens. It is here as a professional antigen

presenting cell to T cells, that macrophages serve as the bridge linking the innate

immune system to the initiation of adaptive immunity. Macrophages also uptake

apoptotic bodies by recognizing "eat-me" signals including nucleotides, chemokines, and

lipid phosphatidylserine. This results in the release of anti-inflammatory cytokines to

dampen the inflammatory response (Arandjelovic and Ravichandran, 2015). When

macrophages encounter necrotic debris, macropinocytosis, where multiple pockets

uptake necrotic debris (Krysko et al., 2006), and result in the induction of antigen

presentation (Barker et al., 1999).

B2.3. Activation of the resolution of inflammation phase of mφ.

Inflammatory events require resolution to maintain host tissue integrity, and

macrophages play significant roles also in the immunosuppressive phase (reviewed in

(Ortega-Gomez et al., 2013)). The uptake of apoptotic immune cells activate the

immunomodulatory program of macrophages and the reduction of chemokine production

by immunomodulatory mφ halts the recruitment of neutrophils to the original site of insult.

Immunoregulatory cytokines activate the anti-inflammatory and wound-fixing programs in

macrophages. IL-4 and IL-13 are commonly used for the polarization of

immunomodulatory macrophages, as they elicit phenotypes associated with supporting a

type 2 immune response and tissue homeostasis. IL-4 are produced by Th2 cells and macrophages, and IL-13 is produced by various T cell subsets; primarily by Th2 but also Th1 and Th17 cells (Gallo et al., 2012) and by natural killer cells (Hoshino et al., 1999). IL-4 and IL-13 initiate the STAT6 transcription activator and also increase the expression of the mannose receptor, dectin-1, and resistin-like molecule α which are important for recognition of fungal infections and are involved in type 2 immunity. These responses are due to kinases and phosphatases that interact with the tyrosine motif in the IL-4 receptor (reviewed by (Van Dyken and Locksley, 2013)). IL-10 is another immunosuppressive cytokine which can polarize macrophages to M2, activating STAT 1 and 3 and inhibiting LPS-stimulated TNF-α and IL-1β production (O'Farrell et al., 1998). IL-10 is produced by macrophages and by a variety of immune cells including dendritic cells, T cells, and B cells (reviewed in (Couper et al., 2008)). Therefore, appropriate signals are required for macrophages for the coordinated control of inflammation.

B2.3. Antigen Presentation

Mφ as antigen presenting cells (APCs) express major histocompatibility complexes (MHC) for the presentation of peptides to T cells to initiate immune memory. The peptides, either products from phagolysosomal or endosomal degradation in mφ, are loaded onto MHC II molecules then are presented on the mφ surface and recognized by CD4+ T cells. Peptides derived from proteasomal degradation are loaded on MHC I molecules which are recognized by CD8+ T cells. APCs stimulate naïve T cell subsets to differentiate to effector T cells which result in cytokine release, effector T cell expansion, and further activation of macrophages for pathogen killing by enhanced cytotoxic means. The activation of T cells from APCs requires the antigen peptide presented on MHC to the T cell receptor, and 2 signals: activation of the CD3 and ζ chain, and co-stimulation through the CD28/CD4/CD8 receptors. Upon activation of the T cells, they proliferate

and differentiate to effector T cells which aid in direct killing (cytotoxic T cells) or stimulate other immune cells (helper T cells). MHC II can be inhibited by IL-10, an immunomodulatory cytokine produced by several immune cells including macrophages , as has been previously reviewed (Couper et al., 2008). Therefore, the appropriate mφ response and its coordination with the adaptive arm of immunity allows the larger and efficient immune response for host protection and defense.

B3 Metabolic Signatures of Activated Mφs.

B3.1: Introduction to Pro-inflammatory vs Immunomodulatory Metabolic Profiles

Metabolism generates ATP to meet energy demands for enzyme function, substrates for the synthesis of cell components, and electron carriers for molecular chemical reactions. In macrophages, the metabolic processes have been described to differ among its diverse activation types; naïve (M_0) and immunomodulatory (M2) macrophages use oxidative phosphorylation while pro-inflammatory macrophages (M1) rely on the glycolysis that although oxygen is available, result in the reduction of pyruvate to lactate, known as the Warburg effect. Transcriptome profiling of M1 and M2 macrophages revealed that there were significant differences in cytokine and chemokine gene expression, but very few genes related to metabolism differed in expression (Martinez et al., 2006). This suggest that the metabolic pathway used by macrophages may not first be regulated at the transcriptional level, but rather at the enzymatic levels. Indeed, combinatory metabolomics and transcription analyses on polarized mouse bone marrow-derived macrophages indicated that the differential metabolic status between the two subsets can be determined at the metabolite level (Jha et al., 2015). The U-^{13}C-labeling study revealed that glycolysis, fatty acid synthesis, and pentose phosphate pathways were predominant in M1. Similar patterns of observations in the accumulation of

metabolites resulting from differential activation stimulus have been reported by several others.

With regard to infectious diseases, macrophages are one of the first responders for infection control yet serve as susceptible hosts for several intracellular pathogens. Here, metabolism plays an additional crucial role in the host-pathogen relationship as the host-generated substrates are required for the function of both the host cell and the invading pathogen, therefore influence the final outcome of infection. In-depth investigation of these mechanisms is important because it can provide new avenues for infectious disease control and give insight into evaluating disease susceptibility from the host side, which may reduce the probability of drug-resistance of pathogens when host innate immune system is boosted. Herein, we review the metabolic processes in activated macrophages and the interplay in pathogen control.

B3.2 Metabolism of Pro-inflammatory Mφ.

Upon activation of macrophages via pattern recognition receptors (PRRs) or cytokine receptors, which initiate signaling cascades that result in the activation of a vast variety of transcription factors. Gene transcription is increased for inflammatory mediators and glycolysis (Hu et al., 2003) (Kim et al., 2006), production of reactive oxygen and nitrogen species, and the metabolic shift to aerobic glycolysis from oxidative phosphorylation occur. In addition, the pentose phosphate pathway and fatty acid synthesis have also been described to be active in pro-inflammatory macrophages (Moon et al., 2015) (Haschemi et al., 2012). These changes in metabolism has been shown to be important for supporting the various pro-inflammatory functions of macrophages.

Glycolysis produces pyruvate as an end product can be transported into the mitochondria and be converted to acetyl CoA to feed the Krebs cycle, which generates NADH to the support oxidative phosphorylation. Alternatively, pyruvate can be reduced

to lactate and produce a molecule of NAD+ in the process. The latter fate of pyruvate from glycolysis is less efficient in generating ATP per glucose molecule, but is thought to meet energy requirements by the increased rates of glucose oxidation. In this mechanism, pro-inflammatory macrophages highly consume glucose (Feingold et al., 2012) and are independent of mitochondrial metabolism, as shown by shutdown of mitochondrial respiration in classically activated macrophages and inability to shift to an immunosuppressive phenotype (Van den Bossche et al., 2016). Glucose oxidation yields intermediates that are used for composing amino acids and triglycerides. In LPS-activated macrophages, carbons from glucose have been shown to be incorporated for fatty acid synthesis and engulfed free fatty acids for triglyceride accumulation (Feingold et al., 2012). Mobilization of triglyceride stores and fatty acids are vital for the phagocytosis function of macrophages (Ecker et al., 2010) (Chandak et al., 2010).

GLUT1 overexpression in macrophages increase the expression of pro-inflammatory genes, and the research group showed that this was dependent on the use of glycolysis and superoxide production (Freemerman et al., 2014). Similarly, inhibiting glycolysis by using 2-deoxyglucose in macrophages responding to LPS reduced IL-1β (Tannahill et al., 2013), suggesting that macrophages rely on catabolizing glucose for the ROS and pro-inflammatory cytokine-producing functions.

Glycolysis is also interlinked with the pentose phosphate pathway (PPP), which is important for the synthesis of nucleotides and production of NADPH as electron carriers. The rate-limiting enzyme, glucose-6-phosphate dehydrogenase, has been shown to be capable of influencing the levels of intracellular ROS in macrophages responding to hydrogen peroxide, and that increase in NADPH availability may enhance the ROS levels in naïve macrophages (Ham et al., 2013). In the macrophage population, exacerbate amounts of ROS are produced by M1 in response to pathogens as part of an anti-microbicidal repertoire. The mechanism by which ROS is produced by M1

macrophages are primarily described to be through NOX2, although there has been

evidence that the mitochondria can also be a source of ROS in M1. In brief,

mitochondrial ROS is generated when the electron transport chain (ETC) result in

electron leakage before the last complex of the ETC, and react with oxygen forming

superoxide (Jastroch et al., 2010). The detailed reactions of mitochondrial ROS

production has been reviewed in detail elsewhere (Venditti et al., 2013). NOX2 is a

multimeric enzyme which requires NADPH as an electron donor for the formation of

superoxide from molecular oxygen. The source of NADPH for NOX2 has been described

to be due to the activity of the pentose phosphate pathway (PPP), primarily by its first

and rate-limiting enzyme, glucose-6-phosphate dehydrogenase. The third enzyme in the

PPP, phosphogluconate dehydrogenase, and the two TCA cycle enzymes, malate

dehydrogenase and isocitrate dehydrogenase, are also possible sources of NADPH for

NOX2 activity.

Another reactive molecule produced by macrophages for controlling infectious

microbes is nitric oxide (NO). With superoxide radicals, NO reacts to form peroxynitrite,

a powerful oxidant also capable of damaging pathogens. NADPH is also required as a

co-substrate for the synthesis of NO, which is enzymatically formed by homodimerization

of nitric oxide synthases (NOS) with L-arginine as the precursor for its guanidino

nitrogen group (Stuehr, 2004). Of the three enzyme isoforms, macrophages express the

inducible nitric oxide synthase (iNOS) isoform which differ it's endothelial and neuronal

counterparts by being insensitive to calcium ion concentrations for the control of electron

flux and more strictly transcriptionally regulated (Zhao et al., 2015). iNOS catalyzes the

reaction of L-arginine with molecular oxygen to yield NO and L-citrulline. Some studies

report that in macrophages, L-citrulline can be the precursor for L-arginine biosynthesis

and therefore can support cyclic and continuous NO generation upon pro-inflammatory

activation (Wu and Brosnan, 1992).

A disruption of the Krebs cycle is also important for pro-inflammatory macrophages. The inhibition of succinate dehydrogenase leading to accumulation of succinate was observed in classically activated macrophages (Jha et al., 2015), and it was determined that high levels of succinate leads to succinylation of many proteins and signal the stabilization of the HIF-1α transcription factor for cytokine transcription (Tannahill et al., 2013). The abundance of the Krebs cycle metabolite, citrate, was also deemed important in pro-inflammatory macrophages as it is used to synthesize the anti-bacterial compound, itaconate (Meiser et al., 2016). In addition, the aspartate-arginosuccinate shunt, which produces arginine and connects the Krebs cycle to the urea cycle, was shown to be involved in nitric oxide production, and gene transcription of iNOS and IL-6 in M1 macrophages (Jha et al., 2015).

Accumulation of lipids are also important for the pro-inflammatory macrophage. Cholesterol is taken up by macrophages as low or very low density lipoproteins, and digest to form lipid droplets, which can be used to make inflammatory mediators, or in excess, form cholesterol crystals which can activate the NLRP3 inflammasome or amplify TLR4 and NFKB signaling by reacting with lipid rafts (reviewed in (Moore et al., 2013)). However, these lipid-ridden macrophages, known as foam cells and a hallmark of atherosclerotic lesions (Yu et al., 2013), are thought to contribute to chronic inflammation when cholesterol transport is defective (Tall and Yvan-Charvet, 2015) although other reports observe greater lipid uptake by M2 residing in athersclerotic plaques (reviewed by (Medbury et al., 2014)).

Collectively, these metabolic signatures give insight into what macrophages require for prompt and effective inflammatory function, and useful to better understand how we can devise strategies to enhance pathogen clearance by macrophages.

B3.3: Oxidative Metabolism in Immunomodulatory Mφ.

Immunoregulatory macrophages are grouped in their ability to oppose pro-inflammatory responses, primarily by Th2-related cytokine production, TGF-β which can antagonize iNOS, matrix deposition for tissue remodeling, and type II inflammation association with helminth parasite killing (reviewed in (Martinez and Gordon, 2014)). The activation of the immunomodulatory phenotype of mφ has been shown to use oxidative phosphorylation sourced from lipolysis and fatty acid uptake (Huang et al., 2014), while fatty acid transporter protein 1 activity was shown to be important for transcription levels of M2 marker genes, and limited induction of glycolysis with LPS stimulation (Johnson et al., 2016). As such, lipid catabolism and oxidative phosphorylation has been shown to be crucial for the maintenance of immunomodulatory M2 macrophages.

Induction of M2 with IL-4 activates STAT6 signaling for the induction of the M2 program shown by the failure of STAT6 knockout mφ macrophages to increase the expression of key fatty acid oxidation genes, and shown by recruitment of STAT6 to the arginase 1 promoter with PGC-1 (Vats et al., 2006). Further, the importance of STAT6 signaling has been demonstrated in infectious disease models (Page et al., 2012). PGC-1 is a transcriptional coregulator shown to upregulate fatty acid oxidation, arginase 1 activity, and suppress LPS-induced IL-6 and IL-12 production in mφ (Vats et al., 2006) (Rowe et al., 2010). In addition, PGC-1 knockdown result in poor inhibition of IL-6 and IL-12 in response to LPS in the presence of IL-4 (Vats et al., 2006).

Chemical suppression of oxidative phosphorylation during stimulation of macrophages with IL-4 reduce arginase 1 activity and abolish the suppressive effect of IFN-γ/LPS-induced proinflammatory cytokine production (Vats et al., 2006). After the shutdown of oxidative metabolism in mφs with LPS+IFN-γ treatment, these mφ fail to restore respiration and M2-specific receptors and genes in response to IL-4, although the STAT6 signaling remain intact (Van den Bossche et al., 2016). Additionally, inhibiting

ATP synthase before IL-4 stimulation leads to suppression of M2-specific gene markers in mφ, which suggest that energy-linked oxidative metabolism is crucial for immunomodulatory functions (Van den Bossche et al., 2016). Reducing fatty acid oxidation by modulation of AMP kinase, a sensor responsible for metabolic changes to increase cellular ATP levels, also leads to impairment in inflammatory resolution by macrophages (reviewed in (Steinberg and Schertzer, 2014)).

Glutamine is an amino acid that can replenish the Krebs cycle by its conversion to α-ketoglutarate. Metabolomics analysis showed that Krebs cycle metabolites in M2 macrophages possess more carbon derived from glutamine, and absence of glutamine reduces M2 polarization and genes (Jha et al., 2015).

Peroxisome proliferator-activated receptors (PPARs) are ligand-activated transcription factors which regulate lipid metabolism in a vast variety of tissues. These nuclear receptors heterodimerize with liver X or retinoid X receptors and transcribe key lipid metabolism genes under the PPAR response element (Lemay and Hwang, 2006). Of the α, δ, and γ isotypes, PPAR-γ has been most intensively studied as a regulator of adipogenesis and diabetes, and to play an immuno-regulatory or reparatory function in macrophages (Bouhlel et al., 2007) (Odegaard et al., 2007) (Varga et al., 2016). PPAR-δ agonists have also been shown to suppress the some pro-inflammatory phenotype of macrophages revealed by transcriptome analysis, however these macrophages can enhance IFN-γ production of CD8 T cells (Adhikary et al., 2015). The PPAR-α activation has been shown to improve the cholesterol efflux and reduce lipid accumulation in macrophages (Chinetti et al., 2001) (Haraguchi et al., 2003), which are key mechanisms in reducing lipid-laden inflammatory macrophages in atherosclerotic plaques. These studies suggest that PPAR isotypes control key elements for the resolving macrophage phenotypes. Thus, modulation of PPARs are explored for their therapeutic potential in metabolic and inflammatory diseases.

For the wound healing properties of macrophages, L-arginine is important for the synthesis of collagen from proline for matrix remodeling. Arginases catalyze the formation of ornithine, which is a precursor for proline. As L-arginine is an important amino acid with polarized fates depending on the activation status of macrophages, the activity of iNOS and arginase 1 can serve as a phenotypic indicator of activated macrophages (Rath et al., 2014).

Key metabolic observations that differentiate these macrophage phenotypes are summarized in Table 1.

Table 1. Summary of metabolic changes in pro-inflammatory versus immunoregulatory macrophages.

	Pro-inflammatory Activation	Immunoregulatory Activation
Metabolite markers	Succinate, Lactate, Citrate, arginosuccinate, malate, aspartate,	Glutamine
Pathways used	Warburg glycolysis, pentose phosphate pathway, fatty acid synthesis, aspartate-arginosuccinate shunt,	Glycolysis, Krebs cycle, FA-ox, electron transport chain and oxidative phosphorylation,
Enzyme markers	FBP1, PFKP, GLUT1, iNOS,	Arginase 1
Cell respiration	Low oxygen consumption, unaffected by mitochondrial inhibitors, maximum glycolytic capacity used	High oxygen consumption and spare respiratory capacity, partial glycolytic capacity used

Key differentiating metabolic pathways reported in macrophages activated to pro-inflammatory or immunoregulatory phenotypes *in vitro* are summarized.

B4 Evidence of Mφ Metabolic and Functional Perturbations by Pathogenic

Microbial Infection

The general consensus for appropriate mφ activation in response to intracellular

pathogens is the glycolytic M1 type for pathogen clearance. Indeed, many microbes and

lipopolysaccharide activate mφ to M1 shown by transcriptome and metabolome studies.

However, there are a vast number of microbes that survive the M1 activation or activate

the M2 phenotype in naïve mφ for survival. Various metabolic perturbations have been

reported in macrophages challenged with infectious agents, which is discussed.

B4.1 Viruses

Cholesterol metabolism has been linked to viral entry, replication, and budding in

infected cells. In the case of HIV, the increase in cholesterol biosynthesis induced by

viral infection can result in lipid-laden foam macrophages (reviewed in (Bukrinsky and

Sviridov, 2006)} which secrete inflammatory mediators, activate endothelial cells, and

contribute to cardiovascular disease (Bernard et al., 2014) (Cui et al., 2014), reviewed in

(Crowe et al., 2010)}.

Macrophages infected with HIV or respiratory syncytial virus (RSV) demonstrate

virus survival through lack of glycolysis, as shown by reduced glucose uptake and

glycolysis and pentose pathway intermediates (Hollenbaugh et al., 2011) and enhanced

removal of infected cells by induction of glycolysis in macrophages (Jiang et al., 2016).

Conversely, glycolysis has been suggested to be important in the replication of Dengue

virus in fibroblasts as the inhibition of glucose uptake reduces viral load (Fontaine et al.,

2015). Severe acute respiratory syndrome coronavirus (SARS-CoV) exacerbates the

lung pathology in STAT1 knockout mice, and has been shown that macrophages

polarize to M2 with infection (Page et al., 2012). STAT1/STAT6 double knockout mice

demonstrated low lung pathology, corresponding with STAT6 being essential for M2 activation (Page et al., 2012).

These demonstrate that metabolic processes of the host cell during infection with viruses differ even within pathogenic groups, and that M1-like glycolytic activation may not be beneficial for RSV and Dengue clearance.

B4.2 Bacteria

Salmonella infection of macrophages have been shown to associate with M2 macrophages and a lipid metabolism transcription factor, PPAR-δ, activity has been shown to be important for glucose availability for bacterial replication within cells (Eisele et al., 2013). The importance of glucose availability for *Salmonella* replication within macrophages have also been shown previously (Bowden et al., 2009). This implies that there may be a competition of nutrients between the pathogen and the host cell, and *Salmonella* enhances its survival by switching the host's metabolism to reduce the competition and takeover. *Mycobacterium tuberculosis* pathogenic strain increases the glucose uptake, expression of glucose transporters and glucose-3-phosphate in macrophages, and this ability is suggested to be a determinant of pathogenicity (Mehrotra et al., 2014). The *Francisella tularensis* capsule has been shown to suppress the lactate and HIF-1α stabilization in the secondary response to TLR 7/8 agonism and inhibit aerobic glycolysis in mφ (Wyatt et al., 2016). Inhibition of aerobic glycolysis with 2-deoxyglucose in mφ restores the replication of a capsule mutant of *F. tularensis* (Wyatt et al., 2016). In contrast, NO derivation by mφ can be regulated in L-arginine concentration-dependent manner in response to *Helicobacter pylori* (Chaturvedi et al., 2007). As such, macrophages may be competing for substrates for their pro-inflammatory functions.

B4.3 Intracellular Parasites

Protozoan parasites such as Trypanosomes have shown that type 1 immune responses are important for parasite killing. Arginine metabolism for the synthesis of polyamines, which are used by M2 cells, is important for the persistence of the replicative form of *Leishmania* in the phagocytic vacuole (reviewed in (McConville, 2016)), and where metabolome analysis revealed that the level of M2- associated intracellular metabolites were enhanced while glucose consumption decreased, which also resulted with increase in parasite survival (Lamour et al., 2012). Leishmania infection of mφ have been shown to elicit a metabolic switch from aerobic glycolysis early in the infection to mitochondrial metabolism by enhancing the AMPK-SIRT1 pathway (Moreira et al., 2015).

Toxoplasma gondii* infection of macrophages have suggested that there is reduction of NO production by macrophages for parasite control, possibly due to the use of L-arginine for polyamine synthesis which is used by *T. gondii* for replication (Seabra et al., 2004).

These studies demonstrate that the general glycolytic pro-inflammatory activation of mφ doesn't necessarily correspond to the efficient infectious pathogen clearance mode of mφ. Although infection with communicable diseases do not share a common metabolic impairment in mφ, it is clear that the metabolic processes in mφ play a crucial role in its function to aid in the clearance of infectious pathogens and mitigate disease progression, thereby requires microbe-specific studies on mφ metabolic activation to identify the metabolic pathway that support the mode of clearance by mφ.

Part C: Statement of Purpose and Hypothesis

The purpose of this investigation is to determine how mφ are deficient in *Trypanosoma cruzi* clearance and how the metabolism supports the mφ pro-inflammatory functions. The hypotheses are that mφ infected with *T. cruzi* fail to metabolically and phenotypically shift to the pro-inflammatory phenotype, and that modulating PPAR-α is a strategy to improve mφ function against *T. cruzi*. The anticipated result is that the resulting data will provide a metabolic basis for activating a *T. cruzi*-killing phenotype in mφ.

Chapter 2: Materials and Methods

Majority of this section has been published in Infection and Immunity journal as:

Ethics statement

Human peripheral blood mononuclear cells (PBMCs) were obtained from healthy donors as per an approved IRB protocol (#11-076). All bone marrow harvesting from mice were performed according to the National Institutes of Health Guide for Care and Use of Experimental Animals, and approved by the Institutional Animal Care and Use Committee at the University of Texas Medical Branch (protocol number: 0805029). The work with the pathogen, *Trypanosoma cruzi*, was conducted in a biosafety level 2 laboratory following the regulations of The University of Texas Medical Branch (UTMB) and Centers for Disease Control and Prevention.

Trypanosoma cruzi, cell culture, and treatment

  T. cruzi SYL and TCC trypomastigotes were propagated in C2C12 cells. SYL and C2C12 cells were purchased from American Type Culture Collection (ATCC, Manassas VA), and TCC isolate was kindly provided by Dr. MP Zago (Instituto de Patologia

Experimental, Salta, Argentina). RAW 264.7 mφs (ATCC TIB-71) were cultured in high

glucose DMEM with glutamine (Corning, Corning, NY) containing 10% fetal bovine

serum (FBS) (Invitrogen, Carlsbad, CA), 100 U/ml penicillin, and 100 μg/ml streptomycin

(Corning). RAW264.7 macrophages were used up to passage 14, and maintained in

DMEM with 2% FBS for all experiments. Mycoplasma was tested negative by

visualization of cells with DAPI stain and no amplification of mycoplasma genes shown

by PCR and agarose gel electrophoresis.

THP-1 monocytes (ATCC TIB-202, and a kind gift from Dr. Alfredo Torres at UTMB)

were propagated in RPMI media containing 10% FBS and 100 U/ml penicillin and 100

μg/ml streptomycin (complete RPMI). To generate THP-1 mφs, monocyte cultures were

treated with 50 ng/mL of phorbol 12-myristate 13-acetate (Sigma Aldrich, St. Louis, MO)

in complete RPMI media for 24 h, washed and rested for 48 h before their use in

experiments (Dey et al., 2014, Gupta et al., 2014). To generate primary human mφs,

fresh blood samples were collected from healthy volunteers per our approved IRB

protocol, then monocytes were isolated by using Ficoll-Paque (GE Healthcare,

Pittsburgh PA) and the Human Monocyte Enrichment Kit without CD16 with the Easysep

magnet (Stemcell, Vancouver, Canada) by following the manufacturer's

recommendations. The resulting monocytes were differentiated to mφs over seven days

with 25 ng/mL M-CSF (Peprotech, Rocky Hill, NJ) in complete RPMI. All cells were

maintained in 5% CO_2 humidified incubator at 37°C.

The PPAR-$\alpha^{-/-}$ mice (B6:129S4-$Ppara^{tm1Gonz}$/J) and matching WT mice were

purchased from Jackson Laboratories (Bar Harbor ME). The bone marrow cells were

isolated from the femurs of mice following standard protocol (Zhang et al., 2008). Bone

marrow cells were matured into macrophages over 9 days using 20 ng/mL macrophage-

colony stimulating factor (M-CSF; Biolegend, San Diego CA) in DMEM and Ham's F-12

50:50 mix culture medium (Corning). When used for experiments, bone marrow derived

macrophages (BMDMs) were maintained in 10% FBS / 5-ng/mL M-CSF.

For all experiments, mφs were seeded in 12-well (1×10^6/well), 24-well (5×10^5), or

96-well (6.7×10^4/well) plates, and infected with *T. cruzi* trypomastigotes with parasite: to

cell ratio of 3:1 was used that provided infection of more than 50% of macrophages. In

some experiments, macrophages were infected and incubated for 0, 3, 6, 12, and 18 h in

presence or absence of 50 ng/ml of mouse recombinant interferon gamma (IFN-γ, Gibco,

Carlsbad CA), PPAR-α agonist (5-50 μM GW6471, Tocris Bioscience, Minneapolis MN)

or antagonist (50 μM WY14743, Tocris Bioscience), NOX2 inhibitor (1 mM apocynin,

Tocris Bioscience; or 10 μM diphenyliodinium chloride, Sigma Aldrich, St Louis MO),

glucose transport inhibitor (100 μM apigenin, Cayman Chemical, Ann Arbor MI; or 100

μM SF-31, EMD Millipore, Billerica MA), pyruvate transport inhibitor (100 μM UK5099,

Tocris Bioscience), and phosphogluconate dehydrogenase inhibitor (10 μM 6-

aminonicotinamide (6-AN) Sigma Aldrich). To evaluate the source of carbon needed for

macrophages, cells were incubated in media that was free of glucose, glutamine, and

pyruvate (Gibco) and supplemented with 24 mM D-glucose (Fluka, St Louis MO), 1 mM

pyruvate, 24 mM D-fructose (Fisher Scientific, Waltham MA), or 10 mM glutamine

(Atlanta Biologicals, Flowery Branch GA). Macrophages classically activated with 100

ng/ml lipopolysaccharide (LPS, Sigma Aldrich) and 20 ng/ml IFN-γ were used as positive

controls; Mφs incubated with 20 ng/ml IL-4 (Life Technologies, Carlsbad, CA) (Zajac et

al.) were used as immunomodulatory mφ control. All chemicals were of >99% purity, and

of molecular and cell biology grade.

Cell lysis, fractionation, and Western blotting

To prepare total cell lysates, macrophages (1-2 x 10^6) were washed twice with PBS, and lysed in 200 μL of RIPA buffer containing 150 mM NaCl, 1% Triton X-100, 0.5% sodium deoxycholate, 0.1% SDS, and 50 mM Tris at pH 8.0. The samples were sonicated on ice, twice for 10 second each, and centrifuged at 10,000 rpm for 10 min at 4°C to collect the membrane-cleared supernatants.

For nuclear fractions, macrophages (1 x 10^7) were washed as above, and re-suspended in 500 μL of Buffer A (10 mM HEPES, 10 mM NaCl, 0.1 mM EDTA, 0.1 mM EGTA, and protease and phosphatase inhibitors from Sigma Aldrich). After incubation on ice for 15 min, cells were lysed with 0.5% NP-40 (Thermo Scientific, Waltham MA), vortexed, and centrifuged at 6000 rpm for 2 minutes at 4°C. The resulting pellets were re-suspended in 500 μL of Buffer B (1.7 M sucrose in Buffer A) and nuclei were pelleted by centrifugation at 12000 rpm for 30 min at 4°C. Nuclear pellets were lysed in 500 μL Buffer C (20 mM HEPES, 0.4 M NaCl, 1 mM EDTA, 1 mM EGTA, and protease and phosphatase inhibitors), and suspension was agitated at 4°C for 45 min before centrifugation at 12000 rpm for 5 minutes at 4°C to pellet the nuclear membranes and collection of the nuclear soluble fraction. All cell lysates and fractions were stored at -80°C until analysis, and protein concentration in all samples was quantified by using the bicinchoninic acid assay (Thermo Scientific) by following manufacturer's instructions.

For Western blotting, samples (20 μg) were resolved on 10% polyacrylamide gels (Sigma Aldrich) at 100V for 90 minutes, and proteins were wet-transferred to PVDF membranes (EMD Millipore). The membranes were blocked for 1 h with 3% BSA (Fisher Scientific), and then incubated overnight at 4°C with antibodies against PPAR-α (H-2), PPAR-β/δ (F-10), PPAR-γ (E-8) or gp91phox (NL-7). All 4 antibodies were from Santa Cruz Biotechnology (Dallas TX) and used at 1:500 dilutions in 3% BSA. The membranes were washed 3 times with TBST (TBS + 0.1% Tween-20; Fisher Scientific), and

incubated for 1 h at room temperature with HRP-conjugated anti-mouse antibody (Southern Biotech, Birmingham AL, 1: 10,000 dilution in 3% BSA). Proteins with antibody conjugation were detected by using the chemiluminescence based method (GE Healthcare, Chicago IL), and imaged and analyzed by using an Image Quant LAS4000 system (GE Healthcare) (Schindelin et al., 2012). Nuclear proteins were normalized against TATA binding protein (Abcam, Cambridge MA, 1:1000 dilution in 3% BSA) and proteins from total cell lysates were normalized against β-actin (Santa Cruz Biotechnology).

Enzyme Linked Immunosorbant Assay (ELISA)

Cytokines released by macrophages were measured in the culture media by using IL-6, IL-1β, and TNF-α sandwich ELISA by following recommended instructions and dilutions (BD Biosciences, San Jose CA). The change in absorbance as a measure of cytokine concentration was monitored at 450 nm by using a SpectraMax M5 spectrophotometer (Molecular Devices, Sunnyvale, CA). A standard curve was prepared with 0 -1,000 pg/ml of recombinant cytokines.

Bioenergetic function analysis

The XF24 Extracellular Flux Analyzer (Seahorse Biosciences, North Billerica, MA) was used to measure bioenergetic function (Divakaruni et al., 2014). The optimum number of RAW 264.7 mφ per well was determined as 80,000/0.32 cm^2/well for obtaining a confluent monolayer culture. In all experiments, each treatment was performed in five replicates. Oxygen consumption rate (OCR, moles/min) was measured as an index of mitochondrial function. Cells were equilibrated in XF assay medium (serum-free, bicarbonate free, phenol red-free DMEM (pH 7.4) supplemented with 5 mM glucose and

37

0.5 mM L-glutamine) for 1 h prior to the bioenergetic measurements. A line diagram of

the OCR measurements is shown in **Fig.S1.1A**. After recording the initial basal OCR of

macrophages (± *T. cruzi*, LPS/IFN-γ or IL-4), oligomycin (1 µM), FCCP (1 µM) and

antimycin A (1 µM) were injected sequentially through the ports of the Seahorse Flux

Pak cartridge. The ATP production-dependent OCR was calculated by the decrease in

basal OCR post-oligomycin addition. The remaining OCR is due to proton leak. An

increase in OCR post FCCP addition (OCR_{FCCP}, uncouples respiratory chain from ATP

synthesis) was used to determine the maximal mitochondrial respiration capacity. The

reserve (spare) respiratory capacity (SRC) was calculated as the difference between

OCR_{Basal} and OCR_{FCCP}. Treatment with antimycin A inhibited the flux of electrons through

complex III and O_2 consumption at cytochrome c oxidase, and allowed a measure of

background non-mitochondrial respiration.

The indices of glycolytic function were monitored by the extracellular acidification

rate (ECAR, mpH/min) based on lactate efflux (Vander Heiden et al.), simultaneously as

the OCR. A line diagram of ECAR measurements is shown in **Fig.S1.1B**. The ECAR at

the basal level ($ECAR_{Basal}$) and increase in ECAR with oligomycin addition

($ECAR_{Oligomycin}$) represented the use of glycolysis for energy demand and total glycolytic

capacity, respectively. The glycolytic reserve capacity was calculated as the difference

between $ECAR_{Basal}$ and $ECAR_{Oligomycin}$. Adding 2-deoxyglucose (2DG) inhibited all

glycolytic function and allowed a measure of the non-glycolytic acidification rate

(Divakaruni et al., 2014). In some experiments, OCR and ECAR were normalized by per

µg of total protein.

Nitric oxide (*NO) and Reactive Oxygen Species (ROS) detection

The *NO level in culture supernatants was measured by assaying the nitrite (a stable nitric oxide breakdown product) concentrations in the culture supernatants by using the Griess assay (Kleinbongard et al.). Briefly, 50 µL of supernatant samples were incubated for 5 min with 50 µl of 1% sulfanilamide made in 5% phosphoric acid then with 50 µL of 0.1% N-(1-napthyl) ethylenediamine dihydrochloride (all chemicals from Sigma Aldrich). Formation of diazonium salt was monitored at 545 nm (standard curve: 0–50 µM sodium nitrite). To measure ROS release, 50 µL of culture supernatants were incubated for 5 min with final reaction concentrations of 33 µM Amplex Red reagent (Thermo Scientific, Waltham MA) and 0.1U/ml horseradish peroxidase (final volume 150 µL). The oxidation of amplex red to fluorescent resorufin by H_2O_2 (Ex_{563nm}/Em_{587nm}) was recorded on a SpectraMax M5 microplate reader (standard curve: 0-10 µM H_2O_2) (Gupta et al., 2009). To evaluate intracellular ROS levels, mφs were seeded in black-walled, clear bottom 96-well plates and infected with *T. cruzi* isolates for 3 h or 18 h as described in Parasites and macrophage cultures section. The cells were washed, replenished with 100 µL culture media, and incubated for 30 minutes in presence of 50 µM 2',7'-dichlorodihydrofluorescein diacetate (H_2DCFDA, Molecular Probes, Eugene, OR) at 37°C, 5% CO_2. The cells were washed twice with PBS, loaded with 100 µL PBS, then the intracellular ROS-dependent formation of 2',7'-dichlorofluorescein (DCF) was analyzed at Ex_{485nm}/Em_{538nm} by fluorimetry (Wen and Garg, 2008). To monitor the mitochondrial superoxide, RAW264.7 macrophages were seeded in black-walled, clear bottom 96-well plates and infected with *T. cruzi* isolates for 18 h. Cells were washed twice with PBS, incubated for 30 min in presence of 5 µM MitoSox Red (Molecular Probes), then washed and replenished with 100 µL HBSS. MitoSOX Red is rapidly and selectively targeted to the mitochondria, wherein it's oxidation by superoxide results in release of red fluorescence that was measured at Ex_{510nm}/Em_{580nm} by fluorimetry.

Quantitative reverse transcription polymerase chain reaction

1) Oxidative metabolism

The custom-designed mitoxosome arrays consisting of primer sets for probing the expression profile of 45 key genes related to oxidative phosphorylation and mitochondrial biogenesis (+1 reference gene) were designed in collaboration with Dr. Tom Wood at the Biomolecular Resource Facility at the UTMB Galveston (Table 1). The oligomers were then synthesized (IDT, Coralville IA) and validated for the generation of a single product in qPCR in the thermal cycling conditions described below. All primer sequences are available upon request. Total RNA from the cells were extracted by using the Trizol reagent (Sigma Aldrich) following the manufacturer's instructions. The DNA that might be contaminating the RNA preparation was removed using an RNA purification kit (Ambion, Austin, TX). The RNA pellets were re-suspended in Molecular Grade water (Corning), then quantified by using a NanoDrop-1000 Spectrophotometer (Thermo Scientific, Waltham, MA). The total RNA (500 ng) was reverse transcribed in a 20 µl reaction by using the iScript™ cDNA synthesis kit (Bio-Rad, Hercules CA). The cDNA was distributed equally across the gene array to be used as a template on a CFX Real-Time PCR Detection System (Bio-Rad). The real-time PCR reaction mix (20 µl) consisted of cDNA, 10 µl SYBR Green master mix (Bio-Rad), and 500 nM of each gene-specific oligonucleotides. The thermal cycle conditions were $94°C$ for 15 sec denaturation step followed by annealing and extension at $60°C$ for 1 min, for 40 cycles (Dey et al., 2014). The Ct values for target mRNAs were normalized to the Ct values for *16S* RNA sequence then the relative fold change of each target gene expression was calculated as $2^{-\Delta\Delta Ct}$ by normalizing to control groups using the PrimePCR Analysis

software (Bio-Rad). Values below 1.0 were calculated as negative fold change by dividing from -1, and represented as down-regulated gene expression compared to the expression in no-treatment controls (Dey et al., 2014).

2) Cytokines

Macrophages ($1 \times 10^6 \pm$ *T. cruzi* $\pm$ IFN-γ) were washed with PBS, and total RNA was extracted by using the Aurum Total RNA mini kit (Bio-Rad, Hercules CA) and re-suspended in 30 μl of TE buffer. Total RNA (500 ng) was reverse transcribed by using poly (dT)18 oligonucleotide with an iScript™ kit (Bio-Rad, Hercules CA) in a 20 μL reaction. The cDNA (1 μl) was used as template with 3 μM of each primer (Table 2) and qPCR was performed as done for oxidative metabolism genes. The threshold cycle (C_T) values for target mRNAs were normalized to the C_T values for the HPRT housekeeping gene sequence (ΔC_T), and then converted to linear scale as $2^{(\Delta CT)}$. The relative fold changes in gene expression were calculated compared to no-treatment controls.

Table 2. Oligonucleotides used for RT-qPCR

Gene	NCBI Acc. # and oligonucleotide reference	Forward primer	Reverse primer	Amplicon size (bp)
il-1β	NC_000068.7 (Wan et al., 2016)	gagcttcaggcaggcag	gggatccacactctccagc	439
il-6	NM_031168.2	ttctcatttccacgatttcccag	ttccatccagttgccttcttgg	175
tnf-α	NC_000083.6 (Wan et al.)	gttctatggcccagaccctcaca	taccagggtttgagctcagc	314
hprt	NM_013556.2	cattgtggccctctgtgt	ctacagtcataggaatggatctatca	110

All oligonucleotides were designed by using Primer-BLAST (Ye et al., 2012) based on sequences in corresponding National Center for Biotechnology Information (NCBI) accession numbers, and synthesized by IDT (San Jose CA).

Targeted profiling of metabolites

Reagents and internal standards: High-performance liquid chromatography (HPLC) grade acetonitrile, methanol and water were purchased from Burdick & Jackson (Morristown, NJ). Mass spectrometry grade formic acid and the internal standards, Tryptophan-15N2, Glutamic acid-d5, Thymine-d4, Gibberellic acid, Trans-Zeatin, Jasmonic acid, Anthranilic acid, and Testosterone-d3 were purchased from Sigma Aldrich. The calibration solution containing multiple calibrants in acetonitrile/trifluroacetic acid /water was purchased from Agilent Technologies.

Cell treatments: RAW264.7 mφs (5 x 106) were seeded in T25 flasks, and incubated with media alone, Tc, or Tc + IFN-γ for 18 h. Cell samples (quadruplicates per treatment) were harvested by using the Non-enzymatic Cell Dissociation Solution (C5914, Sigma Aldrich). Cells were washed twice with PBS, counted by using a hemocytometer, pelleted, snap frozen in liquid nitrogen, and then stored at -80°C. Targeted measurement of Krebs cycle and glycolysis metabolites was performed at the Baylor College of Medicine Metabolomics Core.

Extraction of metabolites: Cell pellets were taken through three cycles of freeze-thaw in liquid nitrogen and over ice, and then spiked with 750 µL of ice cold methanol: water (4:1) containing 0.05 mM of internal standards. Cells were homogenized, extracted by using a chloroform-methanol method, and examined by Single Reaction Monitoring as previously performed (31). For quality assurance, we co-analyzed the sample metabolites with 4 liver samples and normalized to two methods using the internal standards. Reproducibility of the metabolite profiling was determined by measuring the instrument variation and process variation, and liver samples spiked with internal standards were used to assess the quality of metabolite extraction. Metabolites were

separated by normal phase chromatography by using methods as previously described (32).

Liquid Chromatography- Mass spectrometry HPLC analysis was performed using an Agilent 1290 series HPLC system equipped with a degasser, binary pump, thermostatted autosampler and column oven (all from Agilent Technologies). The Multiple Reaction Monitoring (MRM)-based measurement of relative metabolite levels, used either reverse phase or normal phase chromatographic separation. All samples were kept at 4°C and 5 µl was used for analysis.

Identification of targeted metabolites: The normal phase chromatographic separation was also used for targeted identification of metabolites by using the Krebs cycle protocol previously described (32), except that the flow rate was increased during the separation from 0.2 mL/min (0–20 mins), 0.3 mL/min (20.1–25 min), 0.35 mL/min (25–30 min), 0.4 mL/min (30–37.99 min) and finally set at 0.2 mL/min (5 min). Metabolites were separated on a Luna Amino (NH2) column (4um, 100A 2.1x150mm, Phenominex). Each sample was assessed in both positive and negative ionization modes by using a dual Electrospray Ionization, and the data were acquired by using a Mass Hunter Software (Agilent). The data was analyzed at 0.25 false discovery rate by t-test and Benjamini-Hochberg test for statistical significance between experimental groups.

Cell viability

For the analysis of cell viability, either 3-(4,5-dimethylthiazol-2-yl)-2,5-diphenyltetrazolium bromide (MTT, from Sigma Aldrich) or Alamar Blue (Thermo Fisher) was used. For MTT, the experimentally treated cells were washed twice with PBS and incubated for 30 min in presence of 0.5 mg/mL of 3-(4,5-dimethylthiazol-2-yl)-2,5-diphenyltetrazolium bromide (MTT, from Sigma Aldrich) in culture media. The reduction

of yellow tetrazolium MTT by dehydrogenase enzymes in metabolically active cells results in the formation of purple formazan crystals. Formazan crystals were solubilized in 100 µL of DMSO, and change in absorbance was measured at 590 nm by using the Spectramax M5 spectrophotometer. Alternatively, Alamar blue was added to cells in 96-well plate for 1 h before measuring fluorescence at Excitation/Emission of 560/590 nm.

Visualization and counting of T. cruzi infection in macrophages

RAW 264.7 macrophages (5 x 10^4 cells per well) were seeded in 8-chamber slides (Thermo Scientific), and infected or treated in triplicate. Cells were fixed for 5 min in methanol, and then flooded in Giemsa-Wright stain (Fisher Scientific) for 2 min. The cells were washed 3 times in pH 6.4 PBS buffer (Corning), air dried, mounted with Permount (Fisher Scientific) and coverslip, and visualized at 40X magnification on a light microscope (BX53F Olympus, Center Valley, PA).

For counting of trypanosome release from macrophages, 5 x 10^5 RAW 264.7 macrophages were seeded in 12-well plates, and infected with *T. cruzi* at cell to parasite ratio of 1:3 in the presence or absence of IFN-γ and 6-aminonicotinamide (6-AN) in 5% FBS DMEM. After 24 h, macrophages were washed twice with PBS to remove free parasites, and then incubated in fresh media, IFN-γ and 6-AN for 48 h. Culture media was collected and replaced with fresh media only. The collected media were centrifuged at 1800 x g for 10 min, and the trypanosome pellets were re-suspended in 15 µL of media before counting by light microscopy.

Small interfering RNA transfection of RAW264.7 macrophages

Silencing of genes encoding for glucose-6-phosphate dehydrogenase (G6PD) and 6-phosphogluconate dehydrogenase (PGD) was performed by using specific siRNA

duplexes directed against mouse G6PD (s66341, Thermo Scientific, 20 nM) and mouse

PGD (110208 locus, OriGene, Rockville MD, 70 nM). RAW264.7 macrophages (5×10^5

per well) were seeded to obtain 50% confluency and transfected with siRNA by using

TKO transfection reagent (Mirus Bio, Madison WI) following manufacturer's

recommendations. After 24 hours, macrophages were washed with PBS and used for

various experiments.

Statistical analysis

All data were analyzed by using a Prism5 (Graphpad, San Diego CA) or SPSS (IBM,

Chicago IL) software. Data are presented as the mean value of minimum of triplicate

observations in two independent experiments ± the standard error of the mean (SEM),

unless indicated. Significance was calculated by using one variable comparison

analyses (1-way ANOVA) with Tukey's *post hoc* test, and multiple comparison analyses

(2-way ANOVA) with Bonferroni post hoc test. Student's t-test was used to compare two

datasets. Significant differences compared to no-treatment controls or as otherwise

stated are annotated as follows: *p value < 0.05; **p value < 0.01; and ***p value $<

0.001$.

Chapter 3: Evaluation of the macrophage pro-inflammatory response to pathogenic and attenuated *Trypanosoma cruzi* isolates.

Introduction

In this study, we investigated how mφs activate to an insufficient inflammatory phenotype in response to *T. cruzi* infection. We evaluated the responses of mouse and human mφs to SYL and TCC isolates of *T. cruzi* by monitoring the generation of reactive oxygen and nitrogen species, cytokine profile, and metabolic functions. Parasite-stimulated and infected mφ were compared to mφs induced with LPS/IFN-γ or IL-4 for pro-inflammatory and immuno-modulatory phenotypes, respectively. Our data suggest that the virulent isolate of *T. cruzi* inhibits the activation of the glycolytic pathway and the oxidative/nitrosative response in mφs. The mitochondrial oxidative metabolism-induced O_2 consumption may constitute a novel mechanism for initiating $^{\bullet}NO$ production and pathogen clearance by mφs to limit disease progression.

ROS and NO production, but not TNF-α, are suppressed in macrophages infected

with T. cruzi. To assess the quality of mφ response to pathogenic *T. cruzi* SylvioX10/4

(SYL), we quantified the secretion of the pro-inflammatory activation markers, TNF-α,

ROS, and ˙NO from murine (RAW 264.7) and human (THP-1 and primary) mφs.

Macrophages were incubated with *T. cruzi* for 3 h and 18 h to capture the state of

parasite-induced mφ stimulation and infection, respectively, and mφs incubated with

LPS/IFN-γ or IL-4 were used as controls. The LPS/IFN-γ-treated murine mφs, as

compared to mφs incubated in media alone, exhibited >1000-fold increase in TNF-α

release within 3 h (**Fig.1.1A**, $p < 0.001_{\text{ANOVA-Tukey's}}$) that was not further increased at 18 h

post-treatment (**Fig.1.1B**). RAW 264.7 mφs infected with SYL (vs. no treatment)

exhibited a rapid and potent increase in TNF-α release at 3 h ($p < 0.001_{\text{ANOVA-Tukey's}}$) that

was slightly lower than that noted in LPS/IFN-γ-treated mφs. By 18 h, SYL-infected

murine mφs exhibited similar or higher level of TNF-α as was noted in LPS/IFN-γ-treated

mφs (**Fig.1.1B**). In comparison, murine mφs incubated with IL-4 exhibited no increase in

TNF-α release above the background levels (**Fig.1.1A&B**). Human (THP-1 and PBMC-

derived) mφs treated with LPS/IFN-γ for 18 h also exhibited a potent increase in TNF-α

release above the background level (**Fig.1.1C&D**, $p < 0.001_{\text{ANOVA-Tukey's}}$). However, human

mφs exhibited no significant increase in TNF-α release in response to SYL infection

(**Fig.1.1C&D**), like that noted in IL-4-treated mφs. No increase was noted in the

immunomodulatory cytokines tumor growth factor-β and IL-10 in murine incubated with

SYL for 3 h or 18 h (data not shown). Together, the results presented in **Fig.1.1**

suggested that a potent activation of TNF-α is a key feature of LPS/IFN-γ induced mφs;

and murine (but not human) mφs are capable of responding to SYL infection by

elicitation of inflammatory cytokine response.

Figure.1.8. Nitrite oxide release from *T. cruzi*-infected macrophages requires mitochondrial oxygen consumption. RAW 264.7 mφs were infected with *T. cruzi* SylvioX10 isolate and co-incubated with 1 µM oligomycin (A&B) or 1 µM FCCP (C) for 18 h. (A&C) Nitric oxide release in culture supernatants were measured by the Griess assay and (B) DCF fluorescence (detects Intracellular ROS) was measured by fluorimetry. Data are presented as mean ± SEM (n ≥ 3 replicates per treatment per experiment), and significance is expressed as compared to not-treated controls unless marked by a horizontal line (*p<0.05, **p<0.01) calculated by one-way ANOVA with Tukey's multiple comparisons test.

Macrophage production of $^{\bullet}NO$ and $O_2^{\bullet-}$, known as nitrosative and oxidative stress, respectively, are important indicators of phagocytes' cytotoxicity. Our data showed that $^{\bullet}NO$ and H_2O_2 release as well as intracellular ROS (DCF fluorescence) levels were not significantly increased above the background levels in murine mφs incubated with LPS/IFN-γ, IL-4 or SYL for 3 h (**Fig.1.2A-C**). By 18 h post-incubation, LPS/IFN-γ induced 10-fold and 5-fold increase in $^{\bullet}NO$ release and intracellular ROS, respectively (**Fig.1.2D&E**, p<0.001$_{ANOVA-Tukey's}$), while no significant differences were observed for H_2O_2 release (**Fig.1.2F**) in murine mφs as compared to that noted in mφs incubated with IL-4 or media alone. RAW 264.7 mφs infected with SYL for 18 h exhibited low levels of $^{\bullet}NO$ (**Fig.1.2D**), and no significant increase in ROS (**Fig.1.2E&F**) when compared to that noted in normal controls. A significant induction of intracellular ROS was also detected in human THP-1 mφs that were incubated with LPS/IFN-γ (p<0.001$_{ANOVA-Tukey's}$) compared to that noted in THP-1 mφs incubated with IL-4, SYL or media alone for 18 h (**Fig.1.2G**). To identify the source of ROS, we stimulated RAW 264.7 mφs with LPS/IFN-γ in presence of an NADPH oxidase (NOX2) inhibitor, diphenyleneiodonium (DPI), then measured the intracellular ROS and mitochondrial ROS using H_2DCFDA and MitoSOX Red fluorescent probes, respectively. We found that the inhibition of NOX2 by DPI abolished the LPS/IFN-γ-induced intracellular ROS (**Fig.1.2H**). Basal mitochondrial ROS that were detected in the no-treatment control mφs were further decreased by LPS/IFN-γ, and co-treatment with DPI prevented the LPS/IFN-γ suppression of mitochondrial ROS in murine mφs (**Fig.1.2I**). Together, the results presented in **Fig.1.2** suggested that murine and human mφs respond by the production of $^{\bullet}NO$ and ROS in the order of LPS/IFN-γ >> SYL > IL-4 = media alone, where ROS release is increased by NADPH oxidase activation.

Figure.1.2. Macrophages elicit sub-optimal •NO and ROS production in response to *T. cruzi* infection. (A-F) RAW 264.7 murine mφs were infected with SYL isolate of *T. cruzi* as in figure 1. Macrophages treated with 100 ng/ml LPS / 20 ng IFN-γ or 20 ng/mL IL-4 were used as controls. Mφs were incubated for 3 h (A-C) or 18 h (D-I). Bar graphs show (A&D) nitrite release, a measure of •NO production, by Griess test; (B&E) DCF fluorescence, a measure of intracellular ROS production and (C&F) H_2O_2 release measured by an Amplex Red assay by fluorimetry. (G) THP-1 mφs were infected with SYL or treated with LPS/IFN-γ or IL-4 for 18 h as above, and DCF fluorescence (intracellular ROS) determined by fluorimetry. (H&I) RAW264.7 mφ were treated with 0.1 µg/mL LPS + 20 ng/mL IFN-γ for 18 h in the presence or absence of NOX inhibitor, diphenyleneiodonium (DPI). Total intracellular ROS (H) and mitochondrial ROS (I) were measured by DCF and MitoSOX Red fluorescence, respectively. Fold change is presented in comparison to no-treatment controls. Data are shown as mean ± SEM (n ≥ 3 replicates per treatment per experiment). Significance was calculated by one-way ANOVA with Tukey's multiple comparisons test, and presented in treatment group vs. no-treatment control unless marked by a horizontal line (*p<0.05, **p<0.01, ***p<0.001).

3 h post-treatment
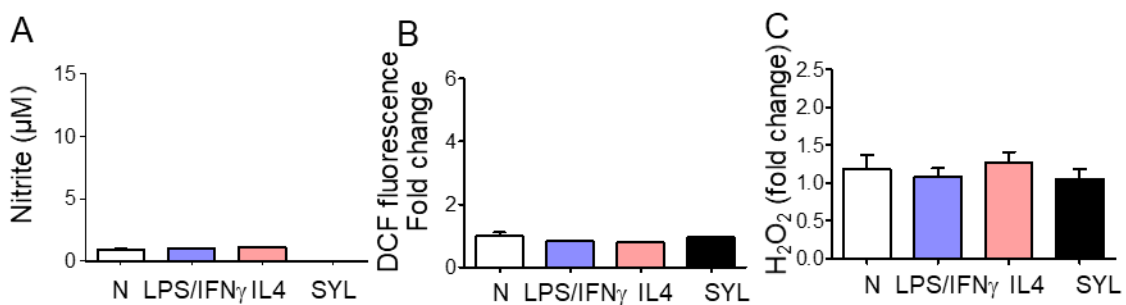
18 h post-treatment
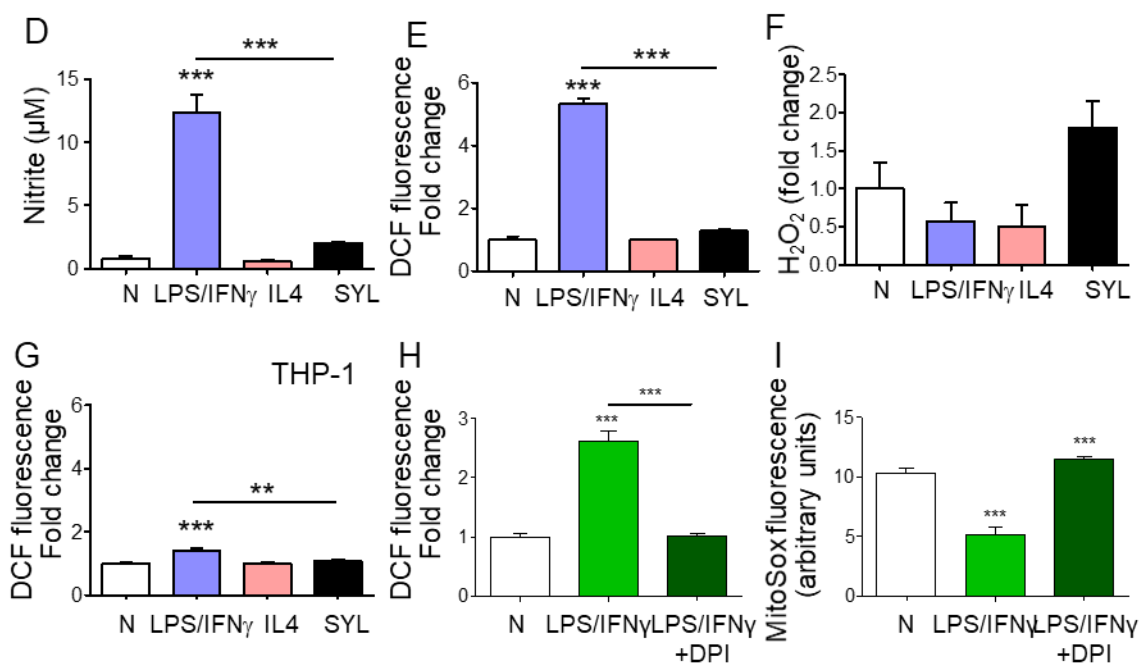
Mitochondrial gene transcription is induced in T. cruzi-infected macrophages.

Cellular metabolic status can serve as a signaling event in the functional activation of

mφs toward diverse phenotypes (Covarrubias et al., 2015). THP-1 mφs were incubated

for 12 h with LPS/IFN-γ or IL-4, or for 18 h with SYL, and we performed RT-qPCR

analysis for the expression of 45 mitoxosome genes by using a custom-designed array

(Table 1). All of the 45 genes were differentially expressed by at least |1.5| fold change

in mφs incubated with LPS/IFN-γ, IL-4 or SYL compared to media alone (**Fig.1.3A**), 22 of

which were statistically significant (p<0.05).

A total of 27 genes were differentially expressed by at least |1.5| fold change (2

upregulated, 25 downregulated) in LPS/IFN-γ-induced mφs (**Fig.1.3B&C**), where the

upregulation of an antioxidant gene (*sod2*) and downregulation of 9 genes (*mt-nd3, mt-

nd6, ndufa5, ndufb5, hspc051, cox5b, mt-co3, mt-atp6, tfam*) involved in the electron

transport chain, mitochondrial fission, and mitochondrial and nuclear gene transcription

were deemed significant compared to the no-treatment mφ group.

In IL-4-treated mφ, only 2 genes (*atp5c1, sod2*) were downregulated (p<0.05)

(**Fig.1.3C**) and 5 genes were upregulated by ≥ |1.5| fold (**Fig.1.3B**) but were not

significantly different compared to the expression in the not treated mφ (Table 1). In

comparison, SYL-infected mφ exhibited upregulation of 27 genes where 19 were

deemed statistically significant (**Fig.1.3B**, Table 1), encoding for genes in the electron

transport chain, mitochondrial fission and fusion, and a nuclear polymerase (**Fig.1.3A**).

Only 4 genes were differentially downregulated but did not show statistical significance

(**Fig.1.3C**, Table 1).

These results suggested that LPS/IFN-γ switched off the mitoxosome at

transcriptional level, and that SYL-infected mφs enhanced the gene expression profile

conducive to oxidative metabolism.
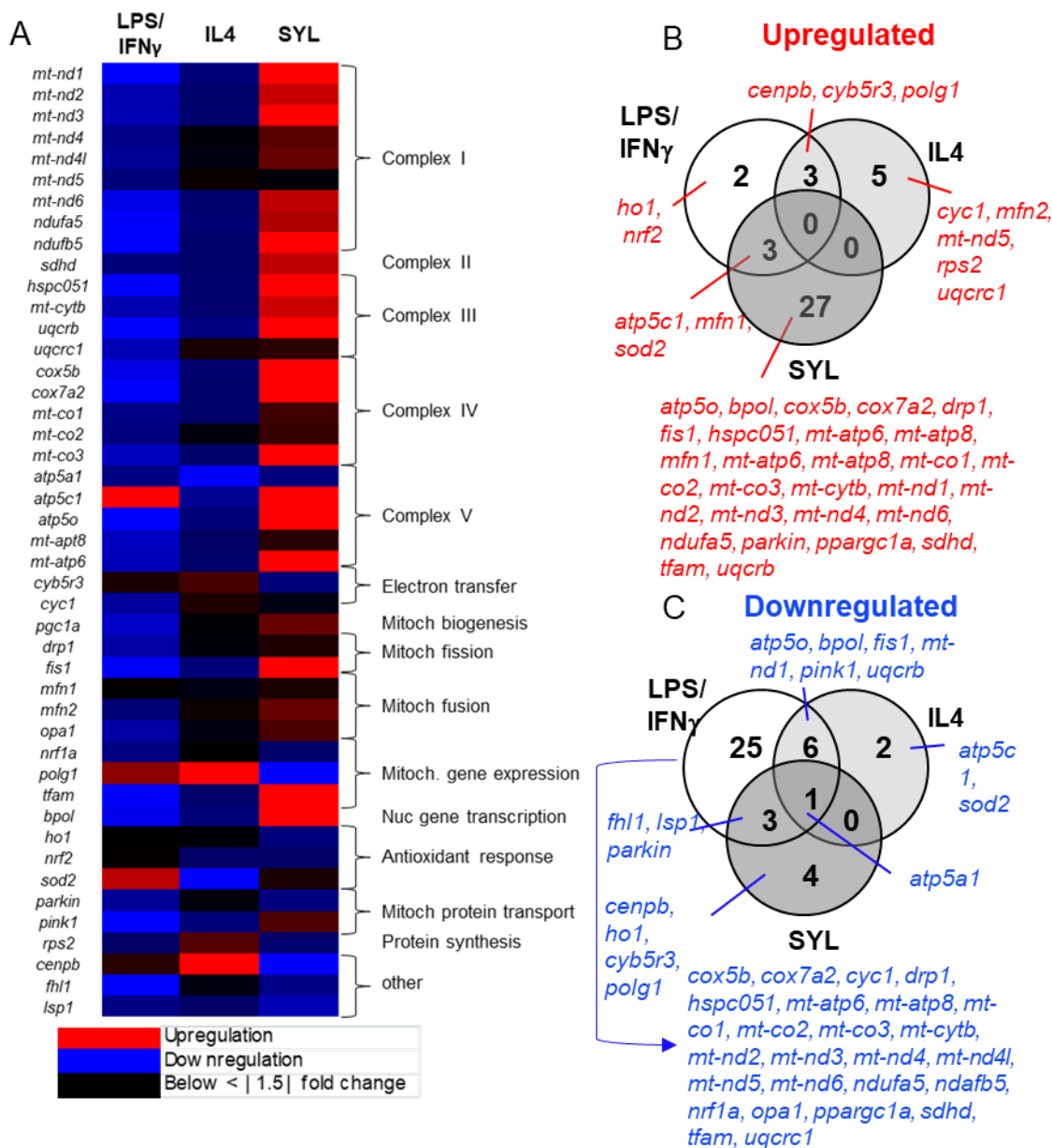
Figure.1.3. Oxidative metabolism related gene expression profile in macrophages infected with *T. cruzi.* THP-1 monocytes were differentiated to resting mφs and incubated in triplicate with LPS/IFN-γ , IL-4, or SYL as described in Materials and Methods. RT-qPCR was performed by using custom-designed arrays to profile the expression of mitochondrial oxidative metabolism-related genes in LPS/IFN-γ, IL-4, and SYL treated mφs. The data were normalized to 16S, and fold change was calculated against the expression levels in mφs incubated in media alone. (A) A heat map of differential gene expression profile. (B&C) Venn diagrams of the genes that were increased (B) or decreased (C) in expression (≥ 1.5-fold change, p<0.05) in mφs incubated with LPS/IFN-γ, IL-4, or SYL with respect to no-treatment controls are shown (n ≥ 2 replicates per treatment).

T. cruzi-infected macrophages fail to switch to glycolytic metabolism. To investigate the metabolic status of mφs at the functional level in response to SYL, we employed the XF24 Analyzer to examine two major pathways of energy production: oxidative metabolism based on mitochondrial oxygen consumption rate (OCR, **Fig.S1.1A**) and glycolysis by extracellular acidification rate (ECAR, **Fig.S1.1B**). The metabolic status of murine mφs incubated with LPS/IFN-γ, IL-4 or SYL for 3 h showed no differences in the levels of basal (OCR_{Basal}-$OCR_{Antimycin}$) and ATP-linked (OCR_{Basal}-$OCR_{Oligomycin}$) OCR, as well as in proton leak ($OCR_{Oligomycin}$-$OCR_{Antimycin}$) in treated (vs. untreated) mφs at 3 h (**Fig.4A.a&b**). However, FCCP induction of mitochondrial maximal respiration capacity (OCR_{FCCP}-$OCR_{Antimycin}$) was found to be 60% ($p<0.001_{ANOVA-BF}$) and 35% ($p<0.05_{ANOVA-BF}$) higher in IL-4-treated and SYL-infected murine mφs, respectively, as compared to that noted in LPS/IFN-γ-treated mφs. Likewise, IL-4-treated and SYL-infected mφs exhibited 7-fold higher level of mitochondrial respiratory reserve capacity (OCR_{FCCP}-OCR_{Basal}, **Fig.1.4A.a&b**, $p<0.01$-$0.001_{ANOVA-BF}$). Basal use of the glycolytic pathway for energy demand was enhanced by 1.6-fold and 2-fold by LPS/IFN-γ and SYL, respectively, as compared to that noted in IL-4-treated mφs (**Fig.1.4B.a&b**, all, $p<0.001_{ANOVA-BF}$). After the addition of oligomycin (inhibits complex V ATP synthase activity), maximal ECAR was increased in all mφ samples; the least increase in ECAR in mφ with IL-4 treatment. Total glycolytic capacity ($ECAR_{Oligomycin}$-$ECAR_{Basal}$) was not statistically different in any of the macrophage samples at 3 h (**Fig.1.4B**). Altogether, at 3 h post-incubation, a) LPS/IFN-γ resulted in reduction of the mitochondrial maximal and reserve respiration capacity and activation of glycolytic metabolism, b) IL-4-induced preferential utilization of oxidative metabolism, and c) SYL infection resulted in an intermediate metabolic state presented with no decline in oxidative metabolism

Figure.1.4. Macrophage utilization of oxidative metabolism is not perturbed in the presence of *T. cruzi* SYL. RAW 264.7 mφs were seeded in XF24 plates (8 x 10^4/well) and incubated with *T. cruzi* (SylvioX10/4), LPS/IFN-γ or IL-4 for 3 h (A&B) or 18 h (C&D). Oxygen consumption rate (OCR = mitochondrial oxidative metabolism rate) and extracellular acidification rate (ECAR = anaerobic glycolytic metabolism) were evaluated by using an XF24 Analyzer. Shown are OCR (A.a&C.a) and ECAR (B.a&D.a) profiles of macrophages in response to sequential administration of pharmacological modulators of mitochondrial electron transport chain, including oligomycin (O), FCCP (F), and antimycin (A). Bar graphs show mean value (± SEM) of OCR (A.b&C.b) and ECAR (B.b&D.b) based parameters, derived from the mean of five replicates (triplicate readings per sample). Significance was calculated by two-way ANOVA with Bonferroni post-hoc test, and is expressed as compared to the LPS/IFN-γ (A.b&C.b) or IL-4 (B.b&D.b) treated (*$p < 0.05$, **$p < 0.01$, ***$p < 0.001$).

3 h post-incubation
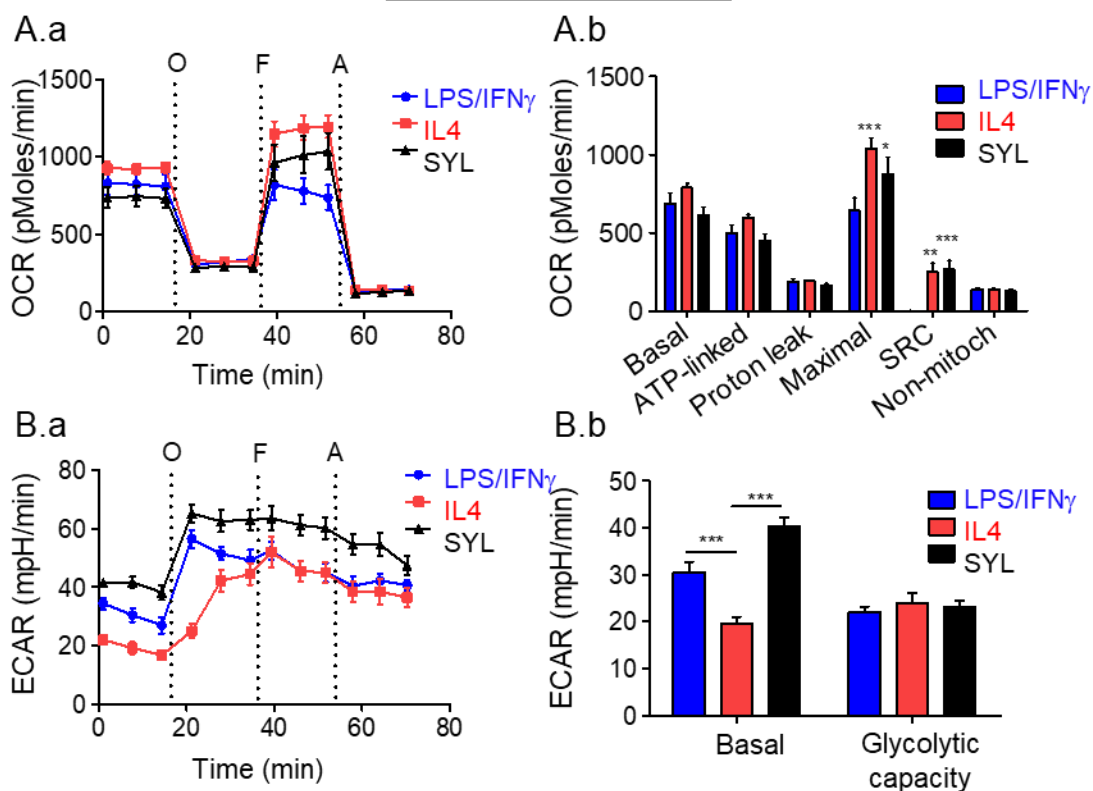
18 h post-incubation
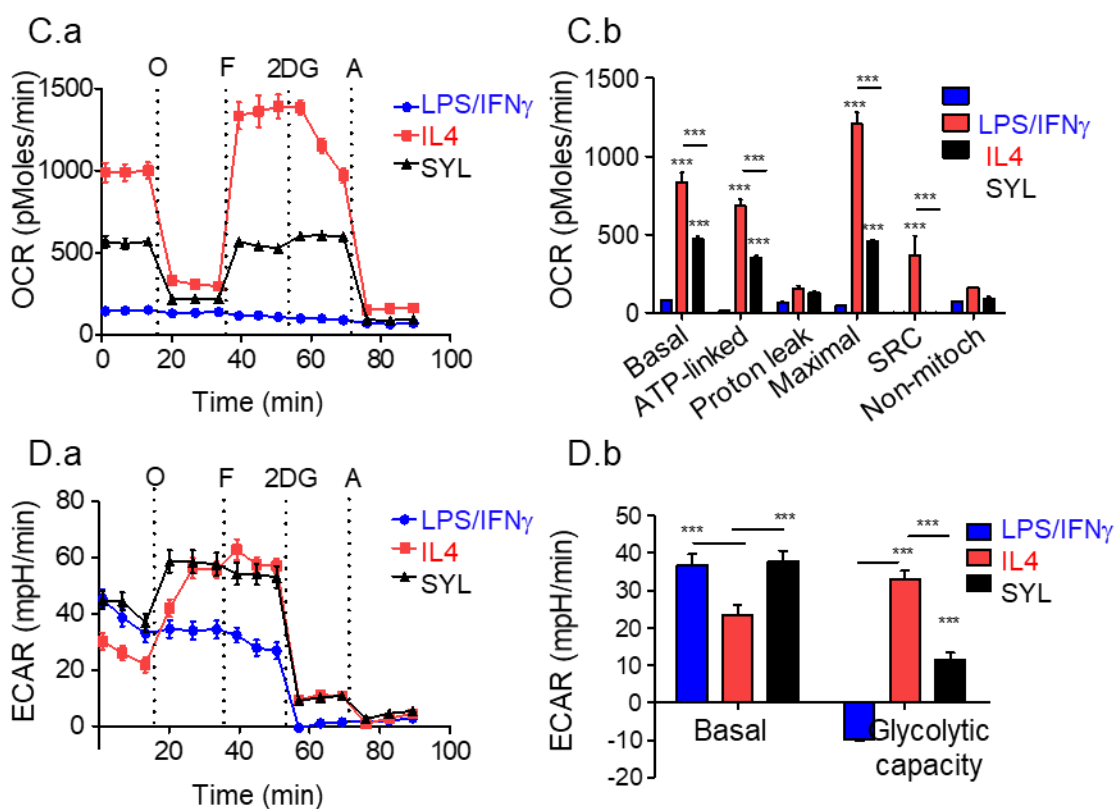
combined with the capability of using glycolysis to meet the energy demand in macrophages.

By 18 h, murine mφs incubated with IL-4 and LPS/IFN-γ were completely polarized in their use of mitochondrial oxidative metabolism and glycolysis, respectively, for energy demand (**Fig.1.4C&D**). LPS/IFN-γ-treated mφs showed no use of mitochondrial respiration (**Fig.1.4C.a&b**). In comparison, IL-4-treated mφs exhibited >10-fold higher levels of basal, ATP-coupled, maximal, and reserve mitochondrial respiration (**Fig.1.4C.a&b**, all $p<0.001_{ANOVA-BF}$) that was abolished by antimycin (inhibits ATP-coupled respiration), thus suggesting that the mitochondrial oxidative metabolism was the major pathway used to fulfill energy demand. Further, SYL-infected murine mφs (vs. LPS/IFN-γ mφs) continued to utilize mitochondrial oxidative metabolism, though basal, ATP coupled, and maximal respiration in SYL-infected mφs at 18 h were at 45-60% of the levels noted in IL-4-treated mφs ($p<0.001_{ANOVA-BF}$), and their reserve respiratory capacity was completely depleted (**Fig.1.4C.a&b**). A 2-fold decline in OCR by 2-deoxyglucose (2DG, inhibits glycolysis) treatment in IL-4-treated mφs suggested that immuno-modulatory mφs utilize the glycolytic pathway to feed the substrate to tricarboxylic acid (TCA) cycle-linked oxidative metabolism (**Fig.1.4C.a&b**).

ECAR measurements in murine mφs incubated for 18 h showed that LPS/IFN-γ and SYL (vs. IL-4) induced 57-61% more utilization of the glycolytic pathway in mφs (ECAR$_{Basal,}$ $p<0.001_{ANOVA-BF}$, **Fig.1.4D.a&b**). When mitochondrial respiration was inhibited by oligomycin, IL-4-treated and SYL-infected (vs. LPS/IFN-γ-treated) mφs were capable of increasing glycolysis as a source of energy and consisted of high levels of glycolytic reserve capacity (**Fig.1.4D.a&b**, $p<0.001_{ANOVA-BF}$). The shutdown of ECAR by the addition of 2DG confirmed that LPS/IFN-γ treated mφs utilized glucose for energy. Altogether, at 18 h post-incubation, a) IL-4-induced mφs continued to utilize

mitochondrial oxidative metabolism as a major source of energy, and b) complete

shutdown of mitochondrial metabolism and switch to glycolysis as a sole source of

energy with no glycolytic reserve capacity occurred in LPS/IFN-γ-treated mφs, and

importantly, c) SYL infection arrested the mφs in an IL-4-like metabolic state, and

prevented the switch to utilize glycolysis as a major source of energy as was noted in

LPS/IFN-γ-treated mφs.

IFN-γ supplementation during T. cruzi infection promotes metabolic switch in

macrophages. We next investigated if providing IFN-γ as a secondary stimulus would

enhance the metabolic shift of mφs treated with *T. cruzi*. Within 3 h, SYL/IFN-γ-treated

mφs exhibited a 57% decline in basal and ATP-linked respiration (**Fig.1.5A.a&b**,

$p < 0.001_{\text{ANOVA-BF}}$), and a partial use of glycolysis (**Fig.1.5B.a&b**) when compared to that

noted in SYL-only treated or no treatment mφs. By 18 h, SYL/IFN-γ-treated mφs

exhibited a shutdown of basal, ATP-linked, and maximal mitochondrial oxygen

consumption (**Fig.1.5C.a&b**) and utilized glycolysis at the maximal capacity

(**Fig.1.5D.a&b**), which is similar to that noted in LPS/IFN-γ-treated mφs (**Fig.1.5C&D**).

These results suggested that a) *T. cruzi* did not irreversibly affect the macrophage's

ability to utilize oxidative or glycolytic metabolism, and b) IFN-γ serves as a sufficient

signal to deactivate macrophage respiration and enhance glycolysis during *T. cruzi*

infection.

Oxidative metabolism and NO production of macrophages are augmented in

response to TCC. The SYL isolate establishes a chronic infection (Postan et al., 1986)

while the TCC isolate fails to persist in mice (Basombrio et al., 1982, Postan et al., 1983).

To determine if a metabolic switch to glycolytic pathway and LPS/IFN-γ-like activation

Figure.1.5. IFN-γ supplementation during *T. cruzi* infection suppress oxygen consumption. RAW264.7 mφ were seeded in XF24 plates (8 x 10⁴/well) and incubated for 3 h (A&B) or 18 h (C&D) with *T. cruzi* SYL in presence or absence of 50 ng/mL IFN-γ. The OCR (A.a&C.a) and ECAR (B.a&D.a) real-time profiles of mφs in response to sequential modulation of mitochondrial electron transport chain were recorded as in Fig.4. Bar graphs show mean value (± SEM) of OCR (A.b&C.b) and ECAR (B.b&D.b) based parameters at 18 h, derived from the mean of 3-4 replicates (triplicate readings per sample). Significance was calculated by two-way ANOVA with Bonferroni post-hoc test is expressed as compared to the LPS/IFN-γ -treated mφs unless marked by a horizontal line (*p<0.05, **p<0.01, ***p<0.001). Note that supplementation of IFN-γ with *T. cruzi* reduced the mφ respiration in comparison to *T. cruzi* treatment only.

3 h post-incubation

A.a

A.b

B.a

B.b

18 h post-incubation

C.a

C.b

D.a

D.b
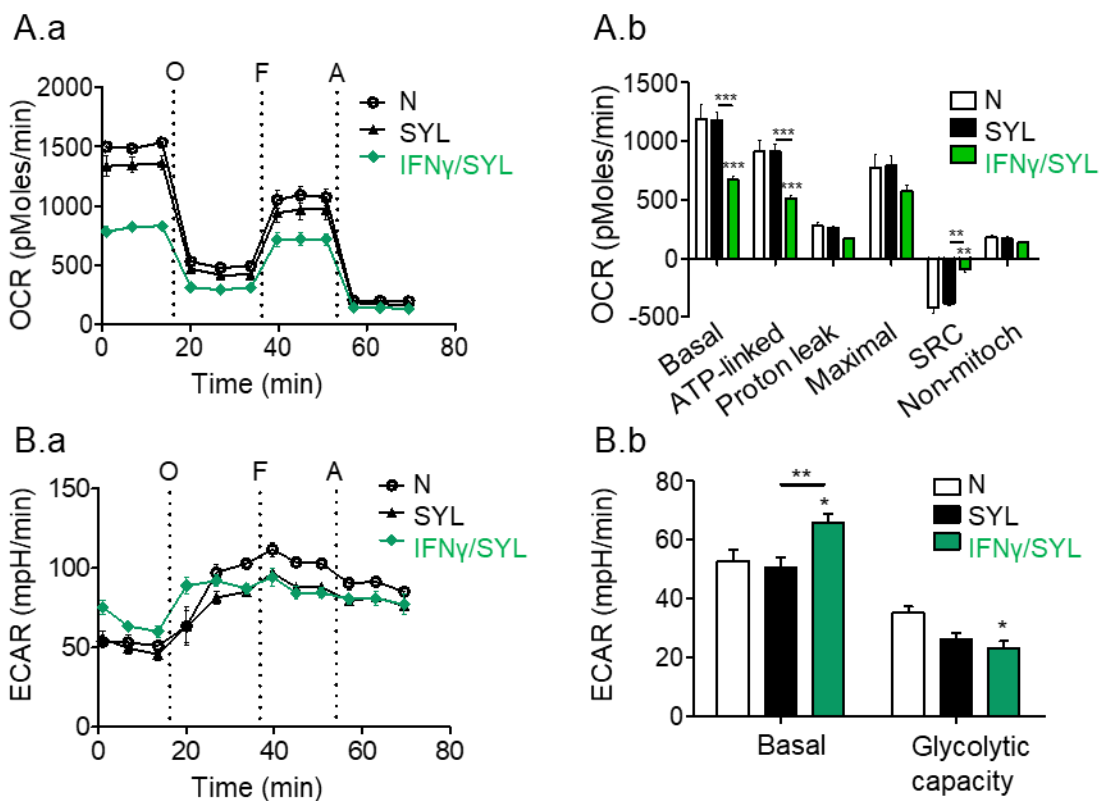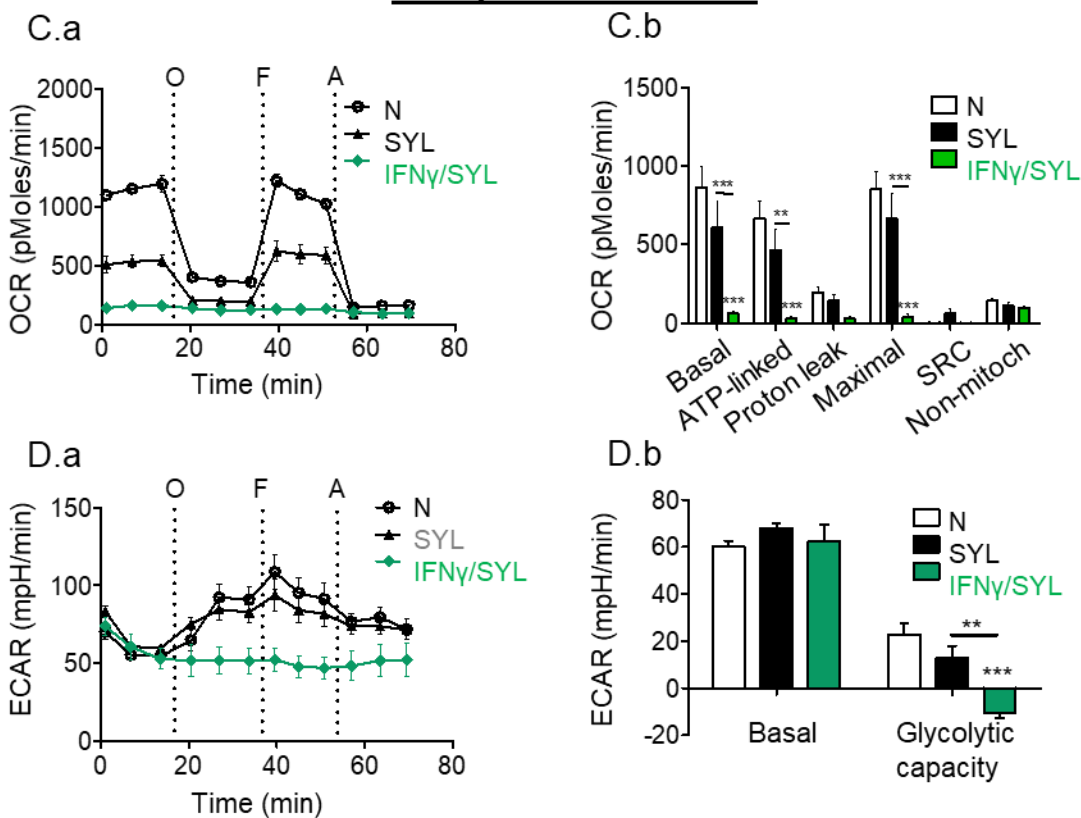
was a prerequisite for mφ control of *T. cruzi*, we challenged the murine mφs with the TCC isolate. Giemsa staining showed no major differences in association of TCC and SYL isolates with RAW264.7 mφs at 3 h (data not shown), and by 18 h, SYL trypomastigotes showed entrance into the host cell cytoplasm whereas some of the TCC trypomastigotes remained attached to the surface of mφs at this time point (**Fig.1.6A.a&b**). In terms of oxidative metabolism at 3 h post-incubation, TCC-infected mφs exhibited 54%, 59%, and 56% higher levels of basal, ATP-linked, and maximal O_2 consumption, respectively, in comparison to SYL-infected mφs (**Fig.1.6B.a&b**, $p<0.01$-$0.001_{ANOVA-BF}$). TCC-infected mφs also exhibited a 60% higher level of mitochondrial spare respiratory capacity (OCR_{FCCP}-OCR_{Basal}) as compared to that noted in SYL-infected mφs (**Fig.1.6B.a&b**, $p<0.001_{ANOVA-BF}$). At 18 h (vs. 3 h) post-infection, the maximal OCR of TCC-infected murine mφs declined by 3-fold (compare **Fig.1.6B.b** with **Fig.1.6C.b**), but remained higher than that of the OCR in SYL-infected mφs (**Fig.1.6C.a&b**, $p<0.01_{ANOVA-BF}$). However, no difference in mitochondrial OCR reserve at 18 h (**Fig.1.6C.b**) and ECARs (basal utilization of glycolytic pathway and glycolytic reserve) at 3 h and 18 h post-incubation were observed in TCC- and SYL-infected mφs (**Fig.S1.2A&B**). These data suggested that TCC-infected mφs utilize higher level of mitochondrial oxidative metabolism than was noted in SYL-infected mφs.

At a functional level, incubation for 3 h elicited no increase in the release of •NO and H_2O_2, and intracellular ROS levels in TCC- and SYL-infected (vs. uninfected) murine mφs (**Fig.1.7A.a-c**), and mφ viability was also not affected by TCC or SYL after 3 h incubation (**Fig.1.7A.d**). After 18 h, TCC- and SYL-infected (vs. no treatment) murine mφs exhibited 4-fold and 2-fold increases in •NO release (**Fig.1.7B.a**, $p<0.001_{ANOVA-Tukey's}$), and 69% and 47% increases in H_2O_2 release (**Fig.1.7B.b**, $p<0.05$-$0.01_{ANOVA-Tukey's}$), respectively, while no significant change in intracellular ROS level (**Fig.1.7B.c**) was

Figure.1.6. SYL-versus-TCC induced changes in oxygen consumption rate in macrophages. (A) RAW 264.7 mφs were seeded in Nunc Lab-Tek 8-well chamber slides (2 x 10^4/well) and incubated with SYL or TCC isolates of *T. cruzi* for 18 h. Slides were stained with Giemsa then visualized at 40X magnification. Intracellular and attached *T. cruzi* trypomastigotes are marked by black and blue arrows, respectively. (B&C) RAW 264.7 mφs were seeded in XF24 plates (8 x 10^4/well) and incubated with SYL or TCC isolates of *T. cruzi* for 3 h (B) and 18 h (C). The OCR was recorded as in Fig.4. Note the basal, ATP-linked, and maximal respiration are augmented in mφ challenged with TCC compared to those challenged with SYL isolate at 3 h (B.a). By 18 h pi, mφs challenged with TCC respired at similar levels as SYL-infected cells, but remain to have enhanced maximum O2 consumption capacity (C.a). Bar graphs show mean value (± SEM) of OCR based parameters at 3 h (B.b) and 18 h (C.b), derived from the mean of four replicates (triplicate readings per sample). Significance was calculated by two-way ANOVA with Bonferroni post-hoc test, and expressed as compared to the SYL-infected mφs (**$p<0.01$, ***$p<0.001$).

A
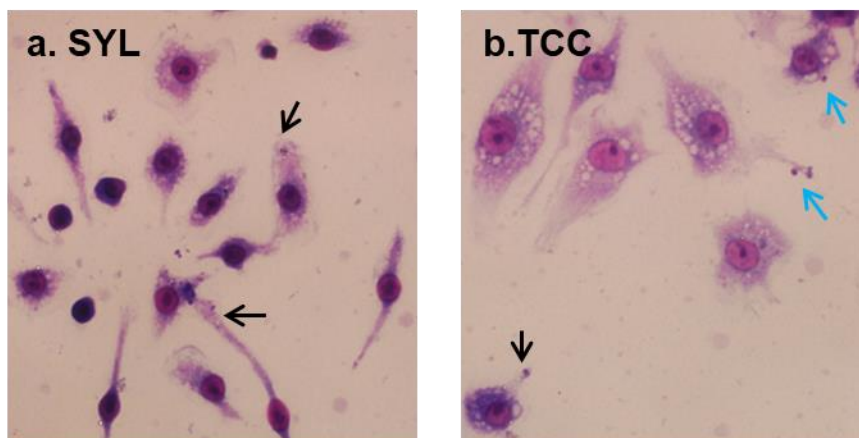
B.a
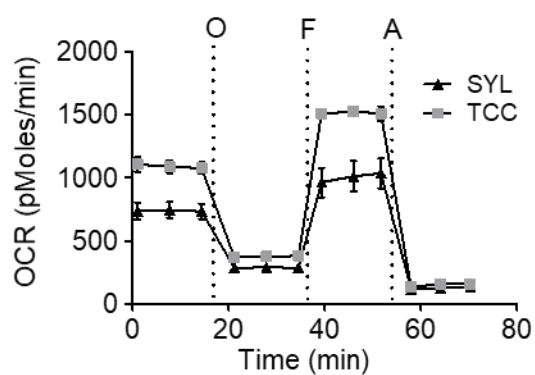
B.b
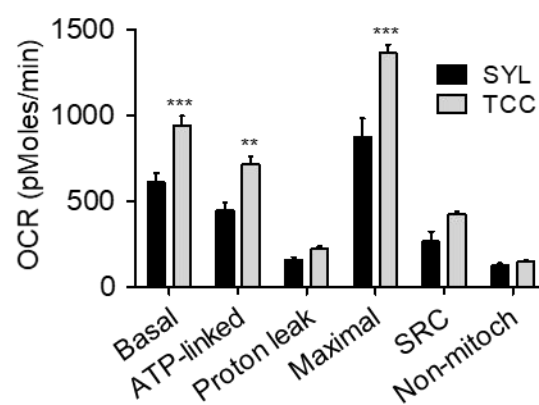
C.a
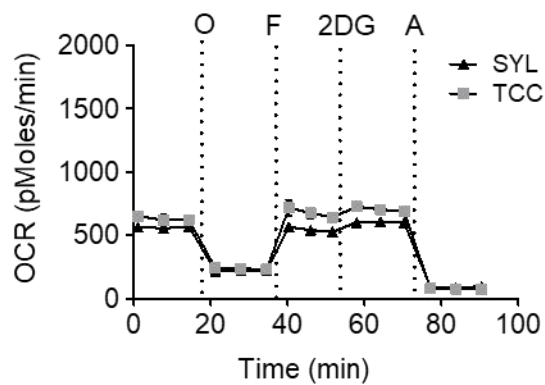
C.b
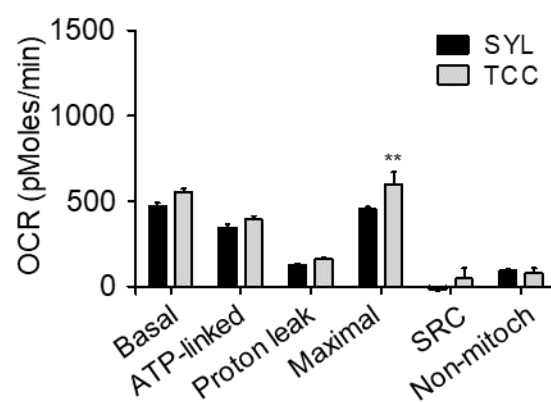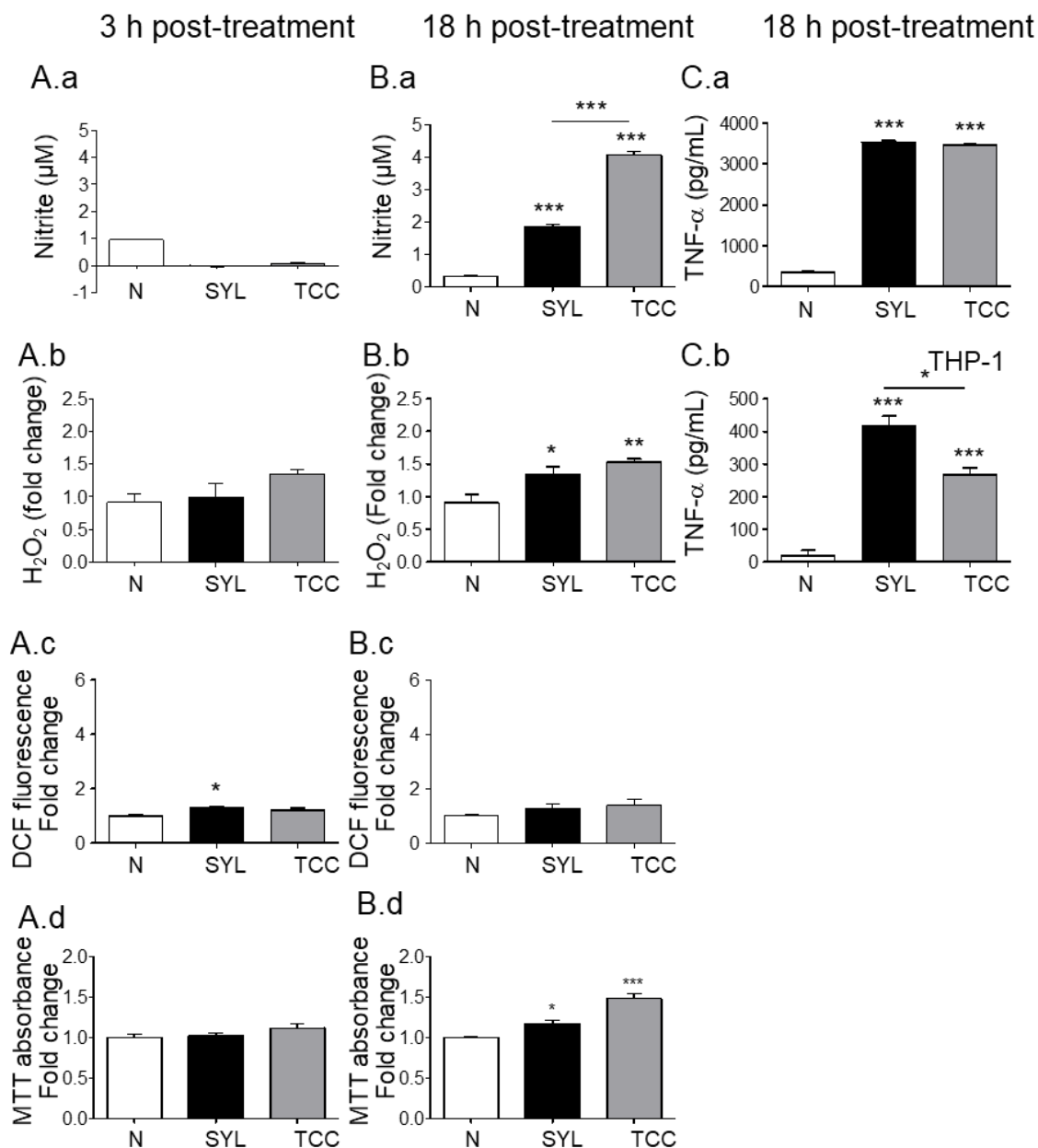
Figure.1.7. SYL-versus-TCC induced functional activation of macrophages. RAW 264.7 mφs were seeded in 24-well plates (5 x 10⁵ per well) and incubated with TCC or SYL isolates of *T. cruzi* at 1:3 cell-to-parasite ratio for 3 h (A) or 18 h (B). Bar graphs show nitrite release by a Griess test (A.a&B.b); H₂O₂ release by an amplex red assay (A.b&B.b); DCF fluorescence, a measure of intracellular ROS production (A.c&B.c); and cell viability and proliferation by MTT absorbance method (A.d&B.d). (C) RAW 264.7 and THP-1 mφs were infected with SYL for 18 h as above. TNF-α production by RAW 264.7 (C.a) and THP-1 (C.b) mφs was measured by an ELISA. Data are presented as the mean ± SEM (n = 3-4 replicates per treatment per experiment). Significance was calculated by one-way ANOVA with Tukey's multiple comparisons test, and is presented as compared to no-treatment control (N) unless marked by a horizontal line (*p<0.05, **p<0.01, ***p<0.001).

observed. The SYL-infected and TCC-infected mφs exhibited 16.5% (p<0.05) and 47.5% (p<0.01), increase in proliferation, respectively (vs. untreated controls) at 18 h post-incubation (**Fig.1.7B.d**). Further, TCC- and SYL-infected (vs. uninfected) murine mφs exhibited a 10-fold increase in TNF-α release (**Fig.1.7C**.a$_{ANOVA-Tukey's}$) at 18 h post-incubation. THP-1 human mφs infected with TCC and SYL isolates for 18 h, when compared to no-infection controls, also exhibited 14-fold and 21-fold increases in TNF-α release, respectively (**Fig.1.7C.b**, p<0.001$_{ANOVA-Tukey's}$), although TNF-α release from infected THP-1 mφs was lower than that observed in LPS/IFN-γ-treated M1 mφs (**Fig.1.1C**). Together, the results presented in **Fig.1.6**, **Fig.1.7**, and **Fig.S1.2A&B** suggested that TCC- and SYL-infected mφs do not differ in their capacity to produce ROS and TNF-α, but TCC-infected mφs exhibit enhanced O$_2$ consumption, mitochondrial oxidative metabolism, and nitrite production as compared to that noted in SYL-infected mφs.

Inhibition of oxygen consumption suppresses the release of •NO in macrophages.
To determine if mφ O$_2$ consumption regulates ˙NO production and constitutes a mechanism in parasite control, we incubated murine mφs with SYL in combination with oligomycin (inhibits ATP synthase and suppresses mitochondrial O$_2$ consumption) or FCCP (uncouples electron transport chain from ATP synthesis and induces maximal O$_2$ consumption), and measured the ˙NO level at 18 h post-treatment. Oligomycin treatment abolished the SYL-induced 2-fold increase in ˙NO levels in infected mφs (p<0.01$_{ANOVA-Tukey's}$, **Fig.1.8A**), while no significant effect of oligomycin was observed on the SYL-induced ROS levels (**Fig.1.8B**). Likewise, FCCP treatment had no inhibitory effects on SYL-induced ˙NO release in infected murine mφs (**Fig.1.8C**). These results

Figure.1.8. Nitrite oxide release from *T. cruzi*-infected macrophages requires mitochondrial oxygen consumption. RAW 264.7 mφs were infected with *T. cruzi* SylvioX10 isolate and co-incubated with 1 µM oligomycin (A&B) or 1 µM FCCP (C) for 18 h. (A&C) Nitric oxide release in culture supernatants were measured by the Griess assay and (B) DCF fluorescence (detects Intracellular ROS) was measured by fluorimetry. Data are presented as mean ± SEM (n ≥ 3 replicates per treatment per experiment), and significance is expressed as compared to not-treated controls unless marked by a horizontal line (*p<0.05, **p<0.01) calculated by one-way ANOVA with Tukey's multiple comparisons test.

suggested that ATP-coupled O_2 consumption may be a mechanism for $^\bullet$NO generation by mφs during *T. cruzi* infection.

Discussion

In this study, we investigated how mφ activation differed in response to *T. cruzi* isolates that had been shown to exhibit different levels of virulence in mice (Zago et al., 2016b). We showed that infection with the virulent SYL isolate arrested the mφs in an intermediate pro-inflammatory state with enhanced TNF-α production, low levels of ROS and $^\bullet$NO release, and partial utilization of glycolysis and oxidative metabolism at the gene expression and functional levels. Importantly, TCC-infected mφs did not differ in their capacity to produce TNF-α and ROS from that noted in SYL-infected mφs; however, exhibited up to 2-fold higher levels of O_2 consumption, oxidative metabolism, and $^\bullet$NO production as compared to the SYL-infected mφs. These results, to the best of our knowledge, provide the first evidence that mitochondrial O_2 consumption constitutes a mechanism for stimulating $^\bullet$NO production in mφs during *T. cruzi* infection. We postulate that enhancing the respiratory capacity will provide an attractive strategy for increasing $^\bullet$NO production and pathogen clearance by mφs to limit disease progression.

The pro-inflammatory markers, TNF-α, ROS, and $^\bullet$NO, are indicators of mφs that have been activated for innate immune defense (Gupta et al., 2013). Indeed, murine and human mφs incubated with LPS/IFN-γ exhibited a >1000-fold increase in TNF-α production at 3 h (**Fig.1.1**) that was succeeded by a robust (>10-fold) increase in $^\bullet$NO, extracellular H_2O_2, and intracellular $O_2^{\bullet-}$ generation at 18 h (**Fig.1.2**). A differential activation between human and mouse cells has also been observed by others (Kuprash et al., 1999). Importantly, both human and mouse mφs elicited low level of oxidative

($O_2\bullet^-$, H_2O_2) and nitrosative ($\bullet$NO) stress upon SYL infection (**Fig.1.2**). Because ROS, NO, and their by-products are strong cytotoxic agents that may directly kill the pathogen (Alvarez et al., 2004) or influence the cellular function by formation of adducts on DNA, proteins, and lipids (Cardoni et al., 1997, Piacenza et al., 2009), our data suggest that *T. cruzi* diminishes the oxidative/nitrosative response to ensure its survival in mφs. Our finding that ROS was inhibited by DPI (NOX2 inhibitor), lack of mitochondrial ROS stimulated by LPS/IFN-γ (**Fig.1.2H&I**) and our prior *T. cruzi* infection studies in splenocytes and human THP-1 mφ (Dey et al., 2014) (Dhiman and Garg, 2011) suggest that NOX2 is the major source of ROS in mφs. How SYL diminishes the NOX2 activation to control ROS/NO levels remains to be further investigated. Others have suggested that an elaborate antioxidant network comprising of peroxiredoxins that scavenges ROS and NO provide a survival advantage to *T. cruzi* in immune cells (Pineyro et al., 2011). These observations, along with our finding of increased NO production in TCC-infected (vs. SYL-infected) mφs (**Fig.1.7**) allow us to propose that intra-phagosomal survival from ROS and $\bullet$NO constitutes at least one key mechanism to the parasite's persistence in the host.

The electron transport chain (ETC)-coupled oxidative phosphorylation (OXPHOS) is the main source of ATP energy in eukaryotic cells. The immuno-modulatory mφs are long-lived and regulate immune functions such as by clearing immune complexes, suppressing inflammatory responses, and promoting wound healing (Huang et al., 2014). Our data showed that IL-4-induced immunomodulatory mφs maintained the transcription levels of ETC and OXPHOS complexes, antioxidant response, and mitochondrial regulatory enzymes, and primarily utilized oxidative metabolism to meet the energy demand. The glycolysis product, pyruvate, may be reduced to lactate resulting in ATP release or provide acetyl CoA to support the TCA

cycle. Our finding of a decline in oxygen consumption rate (OCR) in IL-4-treated mφs

after addition of 2-DG (**Fig.1.4C.a**) suggested that these mφs utilize the glycolytic

pathway to drive pyruvate to feed the TCA cycle and generate reduced (NADH/NADPH)

energy for oxidative metabolism (Dashty, 2013, Carpenter et al., 2015). Our data also

suggest that the use of oxidative metabolism in IL-4-induced mφs was not because of an

incapability to use glycolysis for producing energy, as shown by a metabolic switch to

glycolysis after ATP synthase inhibition (**Fig.1.4D.a**). The LPS/IFN-γ-induced pro-

inflammatory mφs solely utilized the glycolytic pathway for meeting the energy demand

and shut down the oxidative metabolism at transcriptional and functional levels

(**Figs.1.3&1.4**). How the metabolism is shifted and how it may drive the inflammatory vs.

immuno-modulatory phenotype in mφs remains incompletely understood. Some studies

have suggested that poly (ADP-ribose) polymerase 1 (PARP1), a DNA repair enzyme

activated by ROS-induced DNA adducts, depletes the NAD^+ substrate required for

normal activity of sirtuin 1, a metabolic sensor (Canto and Auwerx, 2011, Ba and Garg,

2010) and may activate cells to utilize a glycolytic pathway for energy (Freemerman et

al., 2014). In our present study, we indeed observed the downregulation of mitoxosome

gene expression in mφ stimulated with LPS/IFNγ; but we noted early metabolic

polarization in mφ responding to LPS/IFNγ and IL4 at 3 h (**Fig.1.4A&B**) before

significant increases in ROS and •NO levels at 18 h (**Fig.1.2**). This suggests that ROS-

induced PARP1 activation would occur after the transcriptional inhibition of mitochondrial

oxidative metabolism, and may have a role in the maintenance of glycolysis in cells. In

the mφs responding to SYL, the metabolism and cytotoxic phenotype was arrested at an

intermediate state with an LPS/IFN-γ-like activation of glycolysis with TNF-α production

and an IL-4-like oxidative metabolism at gene expression and functional levels and low

levels of ROS and NO production. The addition of IFN-γ lifted the *T. cruzi*-induced

metabolic block, which suggest that IFN-γ secreted by nearby cells in an *in vivo* disease system could aid in the pro-inflammatory metabolic activation of macrophages for *T. cruzi* killing. How IFN-γ regulates the metabolic state of the mφs remain to be investigated in future studies.

Secreted factors originating from *T. cruzi* influence the host cell signaling pathways for successful infection (reviewed in (Watanabe Costa et al., 2016)). One of these soluble proteins, Cruzipain, has been described to enhance arginase activity (Aoki et al., 2004) which is a key characteristic in immunomodulatory/IL-4-polarized murine mφ (Sheldon et al., 2013). *Trypanosoma* phospholipase A1 is a virulence factor that has been shown to generate secondary lipid messengers and activate protein kinase C in host cells (Belaunzaran et al., 2007), an enzyme that has been shown to promote glycolysis in B-cells (Blair et al., 2012). These *T. cruzi* molecules may prove to be significant in reducing *T. cruzi* pathogenesis or improving the mφ response by swaying the metabolic processes.

TCC is a low pathogenic *T. cruzi* strain that has been previously studied for its immunogenicity (Basombrio et al., 2002), and was recently found to be controlled by mφs (Zago et al., 2016a). Surprisingly, TCC-treated mφs, instead of switching to glycolytic pathway for energy demand, consumed more oxygen and exhibited heightened oxidative metabolism at 3 h pi, and then produced higher levels of •NO when compared to SYL-infected mφs. These results suggest that •NO may contribute to *T. cruzi* killing potentially as multiple reactive nitrogen species (RNS) (Jones et al., 2010). High oxygen consumption has been described to correlate with increased ROS levels in neutrophils and PBMCs activated with diverse stimuli (Dahlgren and Karlsson, 1999, Hartman et al., 2014), and with L-arginine supplement for endothelial NOS activity (Gao et al., 2007). Yet, with *T. cruzi* infection of mφs, we did not observe potent ROS

generation, but rather augmented $^{\bullet}$NO production in response to the TCC isolate.

Arginase 1 (Arg1) competes with iNOS for arginine for the synthesis of ornithine and

polyamines, which result in a net effect of reduced production of RNS (Norris et al.,

1995). Thus, one possibility is that increased O_2 consumption divert the arginine

metabolism from Arg1 towards $^{\bullet}$NO production in TCC-infected mφs; however, a mere

increase in O_2 consumption by FCCP treatment of the SYL-infected mφs did not further

increase $^{\bullet}$NO production (**Fig.1.8**). Instead, inhibiting ATP synthase and OXPHOS with

oligomycin caused a significant decline in $^{\bullet}$NO release in infected mφs (**Fig.1.8**). These

data suggest that O_2 consumption-linked ATP synthesis is important for the generation of

$^{\bullet}$NO by mφs in response to *T. cruzi*. Our observation of a direct relationship between

OXPHOS and $^{\bullet}$NO in *T. cruzi*-infected mφs differs from the literature wherein others

have documented the $^{\bullet}$NO as being an antagonist for O_2 consumption (Giulivi et al.,

2006, Cleeter et al., 1994). The kinetics of O_2 consumption and $^{\bullet}$NO production in *T.*

cruzi-infected mφs will provide further insight into how phagocytes may achieve parasite

clearance while preventing over-activation of mitochondrial function and $^{\bullet}$NO to ensure

host survival.

Antigenic lysates of intracellular pathogens have potential to activate the

inflammatory profile of immune cells. In the context of *T. cruzi*, prepared lysates are

insufficient to activate an inflammatory response in mφ and splenocytes. Human THP-1

mφs were shown to lack the induction of IL-1β with either live *T. cruzi* and *T. cruzi* lysate

stimulation compared to LPS-treatment (Dey et al., 2014). Splenocytes, isolated from

normal mice, respond to *T. cruzi* lysates with production of low levels of H_2O_2 that was

enhanced only when splenic cells were primed with live *T. cruzi* before secondary

stimulation with *T. cruzi* lysate (Dhiman and Garg, 2011). Further, the pro-inflammatory

cytokines IL-1β, IL-6, TNF-1α, and IFN-γ and the immunomodulatory cytokine, IL-4,

were not elicited by *T. cruzi* lysate treatment compared to no-treatment controls (Dhiman

and Garg, 2011). Others have shown that inoculation with heat-killed *T. cruzi* induce

cardiac damage but lack inflammatory qualities in the heart and splenocytes when

compared to *T. cruzi*-infected mice (Bonney et al., 2011). These observations suggest

that immune cells do not respond to heat-killed *T. cruzi* or *T. cruzi* lysates with an

enhanced pro-inflammatory profile compared to live *T. cruzi.*

In summary, we have investigated the anti-microbial and metabolic response of

mφs to *T. cruzi*. Our results suggested that •NO and oxidative metabolism, rather than

complete activation of inflammatory phenotype like LPS/IFN-γ-treated mφs, may be the

key components for the resistance and cytotoxic response of macrophages to *T. cruzi*.

To our knowledge, this is the first report that •NO formation can be dependent on

mitochondria-linked oxygen consumption in mφs, and that mitochondrial respiration can

be beneficial in an anti-microbial response by mφs.

Chapter 4: Delineation of Glycolysis Pathway for ROS and NO generation by Macrophages

This study is in preparation for peer review and publication.

NOX2-dependency of ROS production in T. cruzi+IFN-γ stimulated macrophages.

We have previously observed low intracellular ROS levels in *T. cruzi*-infected

macrophages, but a significant increase of ROS in LPS+IFN-γ-stimulated macrophages

(Koo et al., 2016). We, therefore, first monitored if IFN-γ amplifies the macrophage

response to *T. cruzi.* RAW264.7 macrophages responded to *T. cruzi* with an increase in

ROS level at 3 h that continued through 18 h post-infection (**Fig.1A**). IFN-γ alone did not

elicit ROS production; however, addition of IFN-γ enhanced the *T. cruzi*-induced ROS

level by 2.5-fold in macrophages (**Fig.2.1A&B**, p<0.001). The increase in ROS content

was directly associated with an increase in the protein levels of the gp91phox, the

catalytic subunit of NADPH oxidase (NOX2, **Fig.2.1C.a&b**, p<0.001), and ROS response

was abolished by the NOX2 inhibitors, diphenyliodinium (DPI) (**Fig.2.1B**, p<0.001) and

apocynin (**Fig.2.1D**, p<0.001) in *T. cruzi*+IFN-γ-stimulated macrophages. Likewise,

apocynin treatment abolished the LPS+IFN-γ-induced ROS production (**Fig.2.1E**,

p<0.001) and NO release (**Fig.2.1.F**, p<0.001) in macrophages. These results indicate

that the ROS production in macrophages responding to infection in the presence of IFN-

γ is NOX2-dependent, and correlates with the protein abundance of NOX2 catalytic unit.
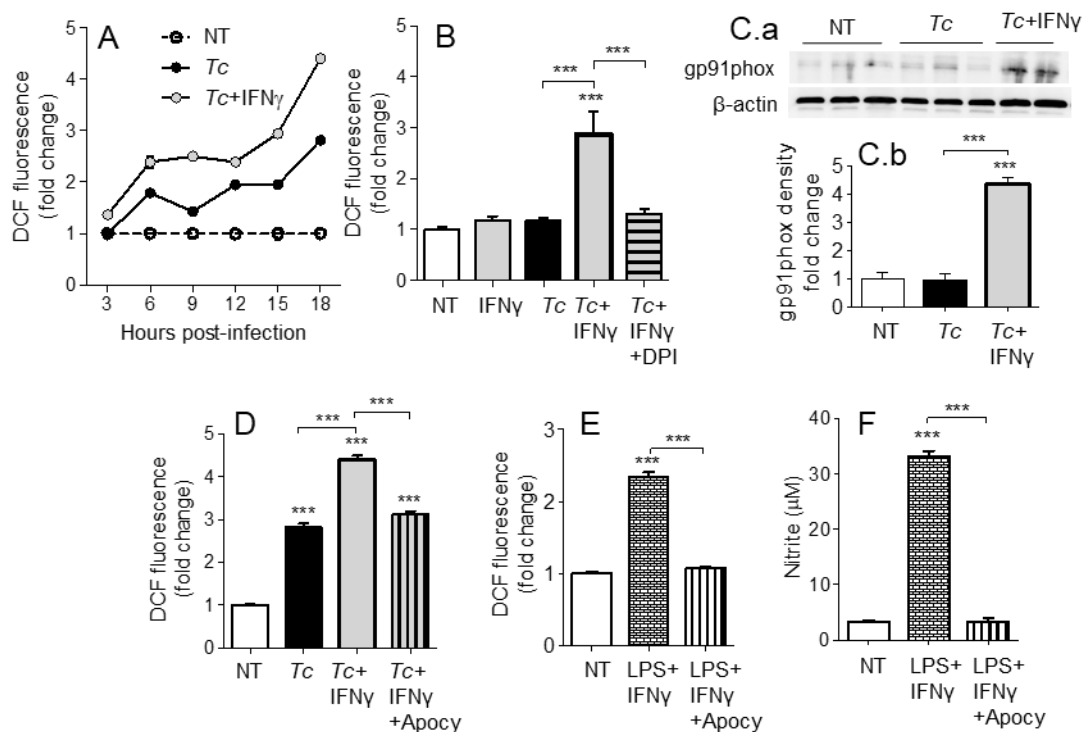
Figure.2.1. NOX2-dependency of ROS/NO generation in macrophages stimulated with *T. cruzi*. RAW264.7 macrophages were stimulated with *T. cruzi* or LPS in presence or absence of IFNγ and inhibitors of NADPH oxidase, diphenyliodinium (DPI) or apocynin (apocy) for 18 h. (A) Intracellular ROS levels measured over 18 h by DCF fluorescence. (B&D) ROS accumulation with NOX2 inhibition by DPI (B) and apocynin (D). (C) Immunoblot analysis of gp91phox in macrophage cell lysates at 18 h pi (panel a), normalized to β-actin loading control (panel b). (E&F) Macrophages activated with LPS+IFNγ in presence or absence of apocynin for 18 h analyzed for ROS level (E) and NO release by Griess assay (F). All data are shown as mean ± SEM of ≥3 biological replicates. Statistical significance is indicated by ANOVA_{Tukey} ***P<0.001 compared to no-treatment controls unless marked by a line over comparing groups.

Expression of PPAR isoforms and effect of PPAR-α modulation on cytokine

response in macrophages infected with T. cruzi. All of the 3 PPAR isoforms are

prime regulators of lipid metabolism in various cell types and may control macrophage

metabolism. In order to determine whether PPARs are involved in macrophage response

to *T. cruzi*, we first evaluated the nuclear expression of PPAR isoforms in RAW264.7

macrophages infected with *T. cruzi* for 0, 3, 6 and 18 h. These data showed that the

nuclear expression of PPAR-α was increased by 5-fold at 18 h post-infection (pi)

(**Fig.2.2A.a&A.b**, p<0.001). The nuclear abundance of δ and γ isoforms of PPARs did

not change significantly over the course of *T. cruzi* infection (**Fig.2.2A.a&A.b**). To test

the role of PPAR-α in modulating proinflammatory response, we incubated the

macrophages with *T. cruzi* in presence or absence of small molecule inhibitor of PPAR-α

(GW6471, 5-50 μM). RAW264.7 macrophages incubated with *T. cruzi* for 3 h or 18 h

exhibited 2- to 22-fold increase in TNF-α release that was not heightened upon co-

incubation with increasing concentrations of GW6471 (**Fig.2.2B** & **Fig.2.2C.a**). Co-

incubation of macrophages with PPAR-α small molecule agonist (WY14743, 50 μM) did

not dampen the TNF-α release at 18 h pi (**Fig.2.2C.a**). Likewise, macrophages infected

with *T. cruzi* for 18 h exhibited >300-fold increase in IL-6, and no effects of PPAR-α

agonist and antagonist were observed on *T. cruzi*-induced IL-6 release in macrophages

(**Fig.2.2C.b**). Normal macrophages incubated with 30-50 μM GW6471 for 18 h also

exhibited TNF-α release (**Fig.2.2B** & **Fig.2.2C.a**). These results suggest that *T. cruzi*

infection induces a significant increase in PPAR-α expression and TNF-α and IL-6

production in macrophages; however, PPAR-α is not the prime regulator of the

proinflammatory cytokine response in infected macrophages.
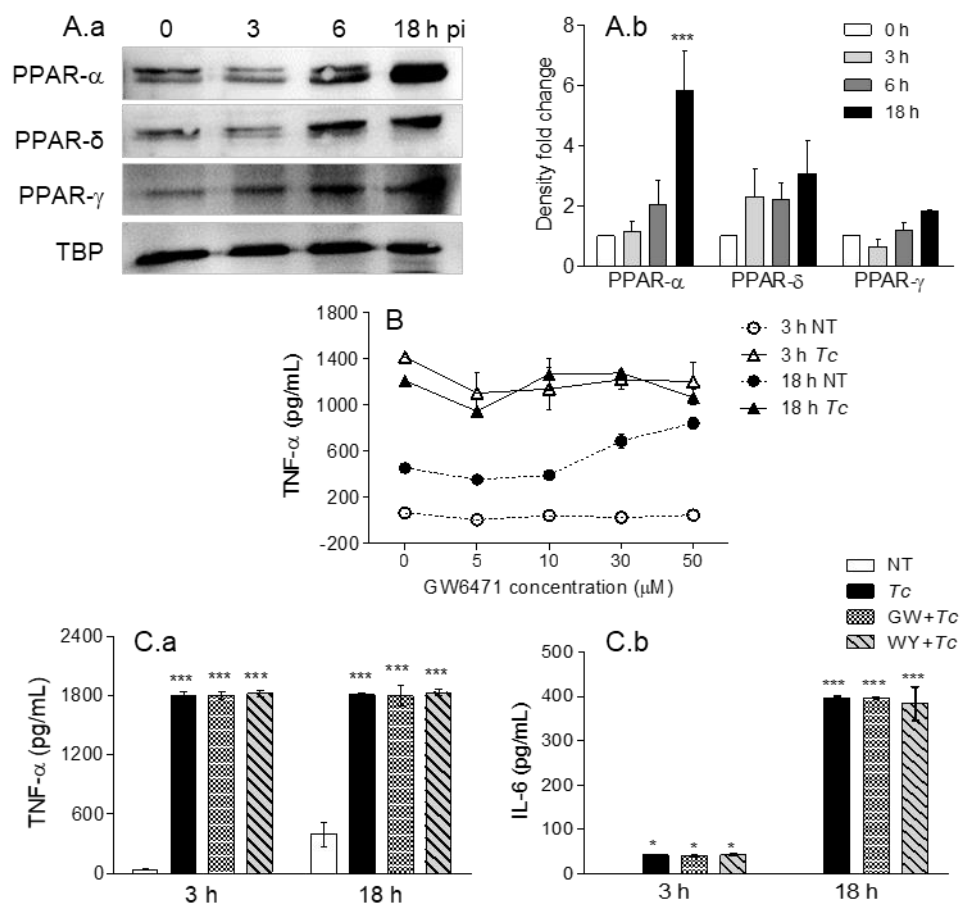
Figure. 2.2. Expression of PPAR isoforms and effect of PPAR-α modulation on cytokine response in macrophages infected by *T. cruzi*. RAW264.7 macrophages were infected with *T. cruzi* for 0, 3, 6, and 18 h. (A) Nuclear abundance of PPAR isoforms and TATA binding protein (TBP, loading control) in infected cells was determined by immunoblotting (A.a). Densitometry calculation of PPAR signal was normalized to TBP (A.b*)*. (B) ELISA analysis of TNF-α production by macrophages infected with *T. cruzi* (± GW6471, PPAR-α inhibitor; 0-50 µM) observed in duplicate. (C) Production of TNF-α (C.a) and IL-6 (C.b) by RAW264.7 infected with *T. cruzi*. Cells were incubated for 3 h or 18 h in presence or absence of 10 µM GW6471 (GW) or 50 µM WY14643 (WY, PPAR-α agonist). All data are shown as mean value ± SEM of ≥3 biological replicates unless stated. ANOVA$_{BF}$ *P<0.05 and ***P<0.001 compared to time point 0 (A.b) or no-treatment controls (C).

PPAR-α modulation of ROS and NO response in macrophages infected with

***T.* cruzi.**

As NO and ROS are important anti-microbials, we examined if PPAR-α is a regulator of these compounds in infected macrophages. We first used bone marrow-derived macrophages (BMDMs) from wild type (WT) and PPAR-α-/- mice. LPS+IFN-γ treatment of WT BMDMs increased the nitrite levels, the breakdown product of NO, from 1 μM to 16 μM within 9 h and to 40 μM in 18 h (Fig.2.3A.a, p<0.001). The PPAR-α-/- BMDMs also exhibited a significant increase in nitrite in response to LPS+IFN-γ; however, this response was 4-fold lower than that noted in WT BMDMs (Fig.2.3A.a, p<0.001). Similarly, WT and PPAR-α-/- BMDMs exhibited 2.5-fold and 50% increase in intracellular ROS levels, respectively, in response to LPS+IFN-γ treatment (Fig.2.3A.b, all, p<0.05). When infected with T. cruzi, both WT and PPARα-/- BMDMs produced low levels of nitrite (<5 μM) by 18 h pi (Fig.2.3A.a). No increase in DCF fluorescence was observed in WT and PPAR-α-/- BMDMs in response to T. cruzi infection for 18 h. Addition of IFN-□ resulted in >5-fold increase in NO release (Fig.2.3B.a, p<0.001) and >1.6-fold increase in intracellular ROS level (Fig.2.3B.b, p<0.05) in T. cruzi-infected WT and PPAR-α-/- BMDMs, the higher levels being observed in WT BMDMs. Likewise, RAW264.7 macrophages responded to *T. cruzi* infection with an increase in nitrite release that was further enhanced by 3-fold with IFN-γ addition (**Fig.2.3C.a**, p<0.001). PPAR-α antagonist (GW6471; 10 μM) resulted in a partial suppression (**Fig.2.3C.a&b**, p<0.05), while PPAR-α agonist (WY14643; 50 μM) had no effect on *T. cruzi*+IFN-γ induced ROS and NO levels in RAW264.7 macrophages at 18 h. Together the results presented in **Fig.2.3** suggest that a) *T. cruzi* stimulates low levels of ROS/NO in primary and cultured macrophages, b) addition of IFN-γ enhances the *T. cruzi*-induced ROS/NO response similar to the levels noted in LPS+IFN-γ stimulated macrophages, and c) genetic and chemical inhibition of PPAR-α decreased the ROS/NO response in
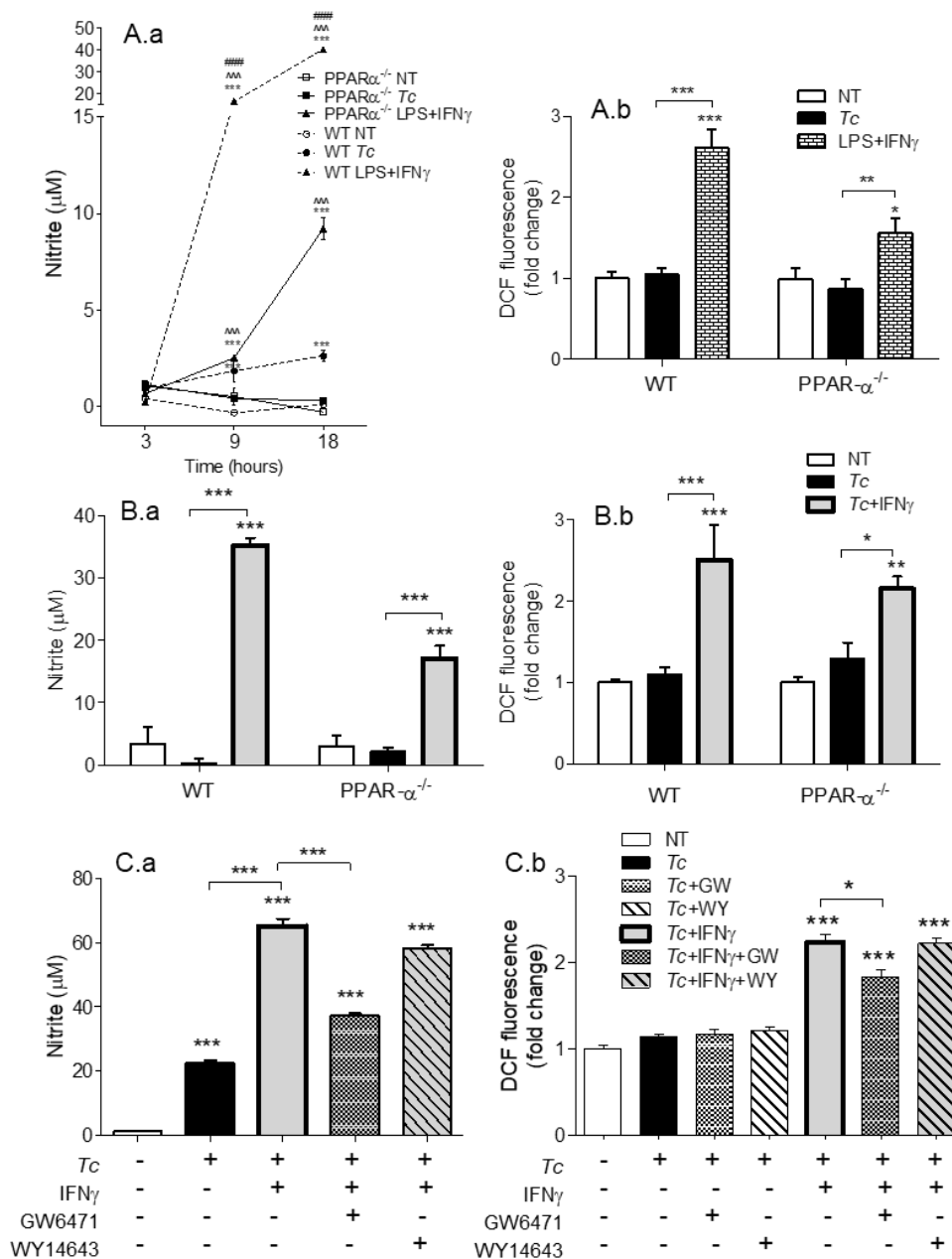
Figure 2.3. PPAR-α modulation of ROS and NO response macrophages (± *T. cruzi*). (A&B) Bone marrow derived monocytes of wild type (WT) and PPAR-α$^{-/-}$ mice were matured into macrophages, and incubated with *T. cruzi, T. cruzi*+IFNγ, or LPS+IFNγ for 0-18 h. The time course of NO release (A.a) and NO release at 18 h (B.a) was determined by Griess assay. The intracellular ROS levels were measured by DCF fluorescence (A.b and B.b). (C) RAW264.7 macrophages were incubated with *T. cruzi* in presence or absence of IFNγ, GW6471 (PPAR-α antagonist), or WY14671 (PPAR-α agonist) for 18 hours. The NO release (C.a) and intracellular ROS (C.b) were measured as above. Data are shown as mean ± SEM of ≥3 biological replicates. ANOVA$_{Tukey}$ or ANOVA$_{BF}$ **$P<0.01$, ***$P<0.001$ compared to no-treatment controls unless marked by line over comparing groups; ^^^$P<0.001$ compared to infection-only group; ###$P<0.001$ compared to PPAR-α$^{-/-}$ LPS+IFNγ treatment.

macrophages. Thus, PPAR-α, rather than suppression of ROS/NO, is involved in production of these compounds in macrophages infected by *T. cruzi*.

PPAR-α regulation of metabolism in macrophages (± T. cruzi). For synthesizing ROS and NO, respectively, the NOX2 and iNOS enzymes require the NADPH substrate that can be produced through pentose phosphate pathway (PPP) and several enzymes of the mitochondrial Krebs cycle. Glycolysis provides substrates for both PPP and Krebs cycle, but only Krebs cycle feeds the oxidative phosphorylation pathway. We therefore, first determined if glycolysis replaces the oxidative phosphorylation in infected macrophages and if PPAR-α plays a role in this metabolic shift in infected macrophages. RAW264.7 macrophages infected with *T. cruzi* alone maintained all aspects of mitochondrial respiration similar to no-treatment control at 3 h and exhibited 45% decline in oxidative metabolism at 18 h pi (**Fig.2.4A-D**). Treatment with PPAR-α inhibitor (GW6471) for 3 h resulted in a 14-28% decline in basal and ATP-linked oxygen consumption rate (OCR) in not-infected and infected macrophages (**Fig.2.4A&C**, $p<0.05$). By 18 h, GW6471 alone (vs. no treatment) resulted in 50% and 20% decline in the basal and ATP-linked OCR, respectively, in macrophages, and further enhanced the *T. cruzi*-induced decline in basal and ATP-linked OCR to 70% and 65%, respectively (**Fig.2.4B&D**). In comparison, co-treatment with IFN-γ abolished the basal and ATP-linked mitochondrial respiration in infected macrophages at 18 h ($p<0.01$).

Concurrent to the decline in OCR, measurement of extracellular acidification rate (ECAR) provides a good indication of Warburg glycolysis. Macrophages exhibited no changes in ECAR values when incubated alone for 3 h (**Fig.2.4E&G**) or 18 h (**Fig.2.4F&H**), or in presence of *T. cruzi* (±GW6471) for 3 h. Treatment with GW6471 alone for 3 h and 18 h resulted in 25-54% decline in glycolytic capacity ($p<0.01$), and GW6471 treatment of infected macrophages resulted in 87% decline in the glycolytic
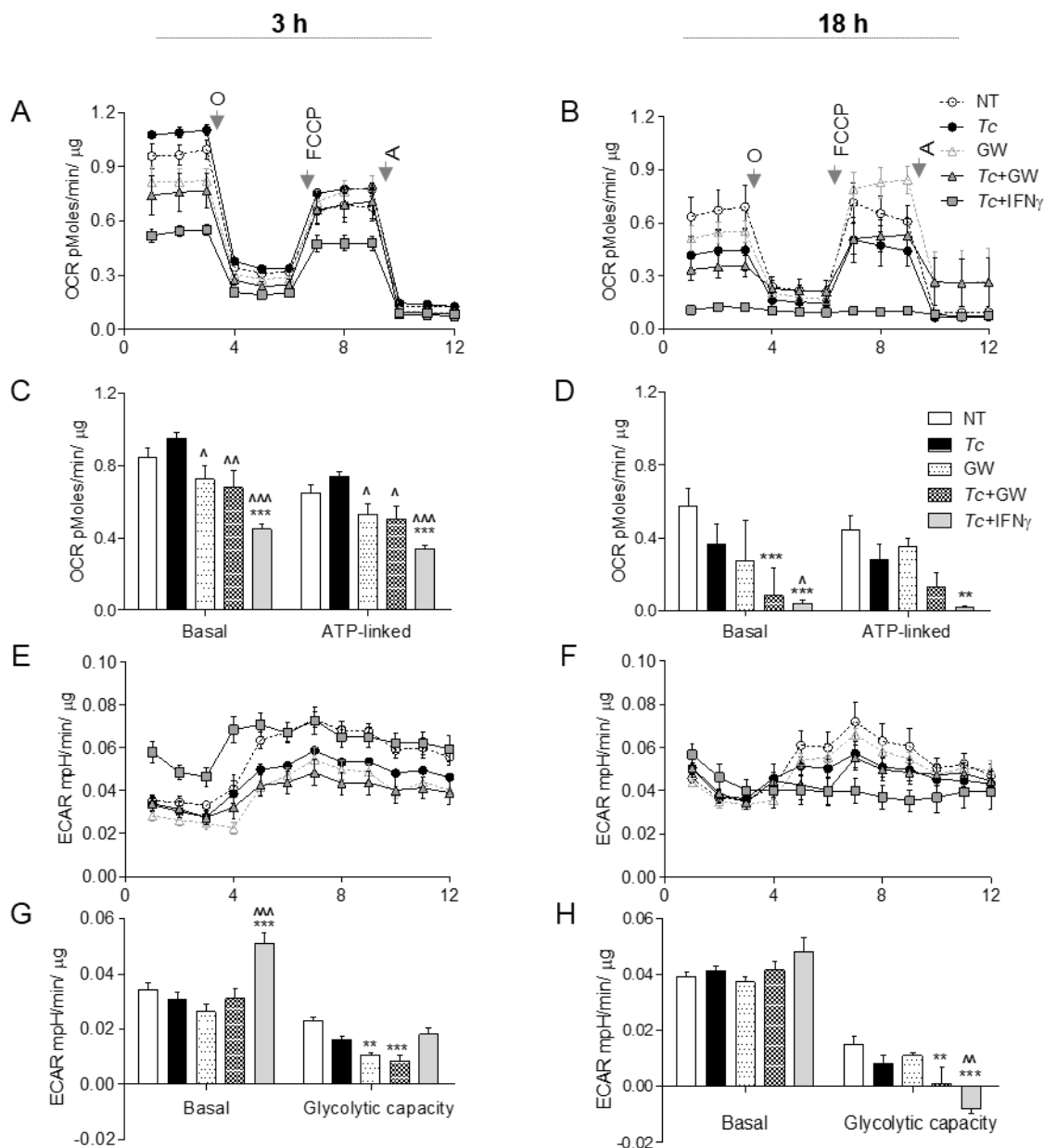
Figure 2.4. Metabolic function of macrophages infected with *T. cruzi* (± PPAR-α antagonist). RAW264.7 macrophages were incubated with *T. cruzi* in presence or absence of IFNγ and GW6471 (PPAR-α antagonist) for 3 h or 18 h. The oxygen consumption rate (OCR) and extracellular acidification rate (ECAR) were monitored by Seahorse Extracellular Flux Analyzer. Shown are the original recordings of OCR (A&B), ECAR (E&F) with sequential addition of oligomycin (O), FCCP, and antimycin (A). Bar graphs show the quantification of mitochondrial stress parameters (C&D) and glycolytic capacity (G&H). All data are shown as the mean ± SEM of four replicates. Statistical significance are marked as ANOVA$_{BF}$ **P<0.01 and ***P<0.001 (infected and/or treated vs. no treatment controls) or ^P<0.05, ^^P<0.01, ^^^P<0.001 (*T. cruzi* infected/treated vs. *T. cruzi* infected).

capacity at 18 h. In comparison, IFN-γ treatment resulted in a 65% and 16% increase in basal ECAR, and 10% decline and complete depletion in glycolytic capacity in infected macrophages at 3 h and 18 h post-incubation, respectively (**Fig.2.4E-H**, p<0.01). Together, these results suggest that chemical inhibition of PPAR-α partially suppresses the oxidative metabolism, and likely contributes to substrate availability for NOX2 and iNOS through the use of Warburg glycolysis. However, PPAR-α inhibition did not result in oxidative to glycolytic metabolic shift as was noted with addition of IFN-γ in infected macrophages.

Role of mitochondrial pyruvate in macrophage activation (± T. cruzi). A broken Krebs cycle can deliver substrate for ROS/NO production as well as metabolic signal for HIF1-α-dependent proinflammatory activation of macrophages (Tannahill et al., 2013). We, therefore, further delineated the role of Krebs cycle in macrophage activation by limiting the mitochondrial availability of pyruvate (provides Acetyl CoA to feed the Krebs cycle). The LPS+IFN-γ induced macrophages produced potent quantities of TNF-α that was not modified upon UK5099 inhibition of pyruvate transport to mitochondria for 3 h (**Fig.2.5A**) or 18 h (**Fig.2.5D**). The IL-6 release was also increased in LPS+IFN-γ treated macrophages at 3 h and 18 h (p<0.001) which was initially delayed at 3 h with UK5099 treatment, but met the final levels of non-UK5099 treated pro-inflammatory macrophages by 18 h (**Fig.2.5B&E**, p<0.001). Interestingly, co-incubation with UK5099 for 18 h suppressed the ROS and NO levels by 2-fold and 6-fold, respectively, in LPS+IFN-γ treated macrophages (**Fig.2.5C&F**, p<0.05). Treatment with UK5099 after differentiation of macrophages to proinflammatory phenotype had no suppressive effect on LPS+IFN-γ induced ROS and NO levels (**Fig.2.5G&H**). In macrophages stimulated with *T. cruzi*+IFN-γ for 18 h, UK5099 treatment suppressed the ROS and NO levels by 2-fold

Figure 2.5. Role of mitochondrial pyruvate in the pro-inflammatory activation of macrophages. (A-F) RAW 264.7 macrophages were incubated with LPS+IFNγ for 3 h (A&B) or 18 h (C-F) in the presence or absence of pyruvate transport inhibitor UK5099 (UK). (G&H) RAW 264.7 macrophages were sequentially incubated with LPS+ IFNγ for 18 h, and UK5099 for 4 h. (I&J) RAW 264.7 macrophages were infected with *T. cruzi*, in presence or absence of IFNγ and UK5099 for 18 h. An ELISA was used to quantify TNF-α (A&D) and IL-6 (B&E) release. Intracellular ROS (C, G, I) and nitrite release (F, H, J) were determined by using H_2DCFDA fluorescence probe and Griess assay, respectively. All data are shown as the mean ± SEM of ≥3 biological replicates. $ANOVA_{Tukey}$ *P<0.05, **P<0.01 and ***P<0.001 compared to no-treatment controls otherwise marked by a line over comparing groups.
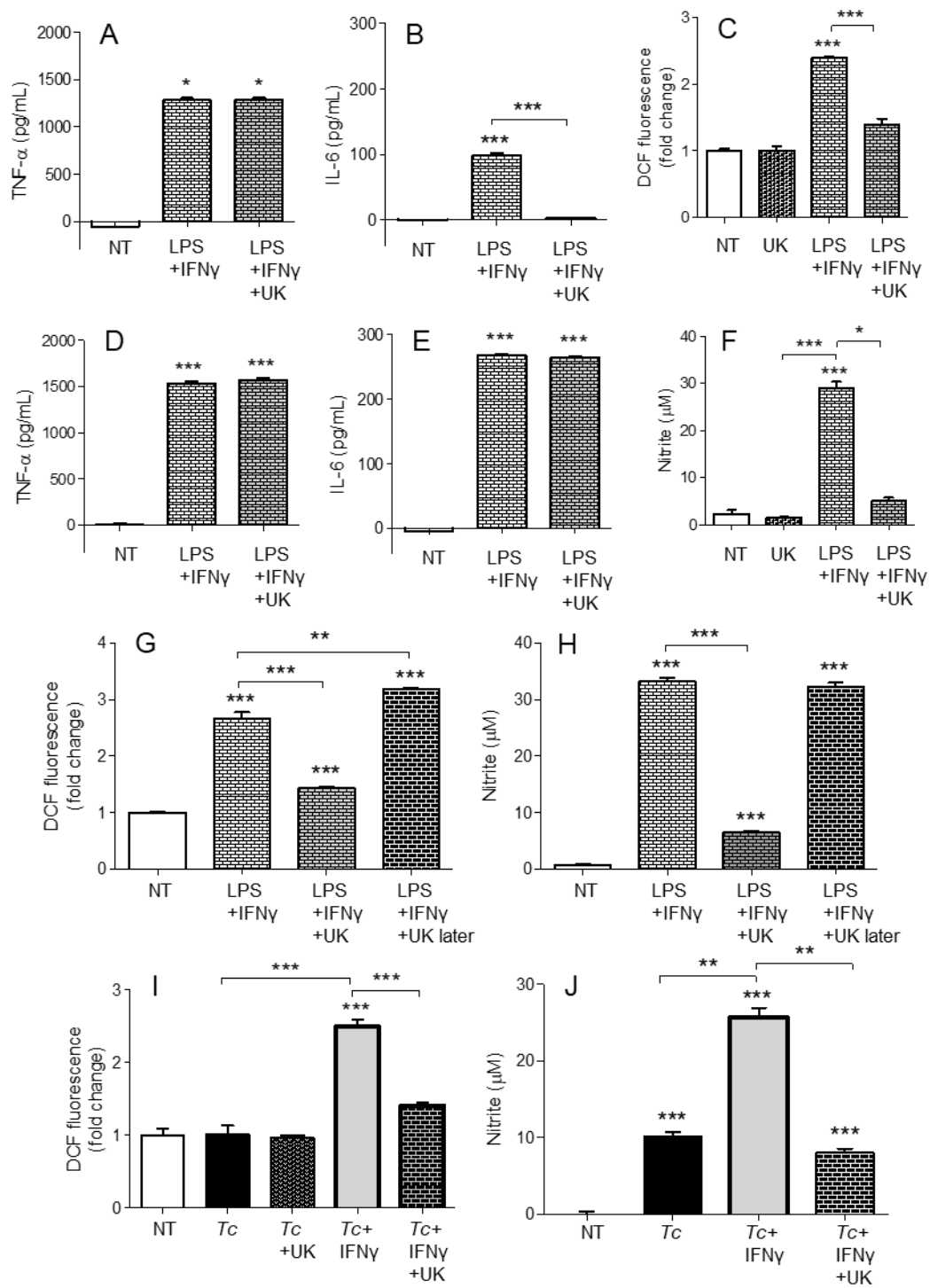
and 3-fold, respectively (**Fig.2.5I&J**, p<0.01). These results suggest that mitochondrial

Krebs cycle does not regulate the proinflammatory cytokine response, but it supports

NOX2 and iNOS activities in macrophages treated with IFN-γ (+ *T. cruzi* or LPS). The

pyruvate uptake-dependent Krebs cycle was dispensable in fully activated macrophages.

Role of glucose uptake on functional activation of macrophages (± T. cruzi).

To confirm our findings that macrophage production of ROS and NO, but not of

cytokines, is dependent on glycolytic shift, we used the inhibitor for glucose transporter 1

(GLUT1), apigenin. As noted above, *T. cruzi* induced a significant release of

proinflammatory cytokines (TNF-α>IL-1β>IL-6) at 3 h (**Fig.2.6A-C**, p<0.001) that was

further enhanced at 18 h (**Fig.2.6D-F**, p<0.001); and addition of IFN-γ elicited greater

quantities of IL-6 in infected macrophages (**Fig.2.6C&F**, p<0.05). These cytokines did

not decline greatly with the inhibition of glucose uptake during stimulation of

macrophages with *T. cruzi*+IFN-γ (**Fig.2.6A-F**). Similar observations were made at gene

expression level; the infection of macrophages led to a significant increase in TNF-α, IL-

1β, and IL-6 mRNA levels, and IL-6 mRNA level was further enhanced with IFN-γ

addition (**Fig.2.6G**, p<0.01). Co-incubation with apigenin had no effect on cytokines'

gene expression in *T. cruzi*+IFNγ treated macrophages (**Fig.2.6G**).

   In contrast, apigenin treatment for 18 h resulted in 2-fold and 17-fold inhibition of

the *T. cruzi*+IFNγ induced ROS (**Fig.2.6H**, p<0.001) and NO (**Fig.2.6I**, p<0.001),

respectively; and 2-fold and 13-fold inhibition of the LPS+IFNγ induced ROS (**Fig.2.6J**,

p<0.001) and NO (**Fig.2.6K**, p<0.001), respectively, in RAW264.7 macrophages. The

decline in *T. cruzi*+IFNγ induced ROS by apigenin treatment was confirmed in BMDMs

(**Fig.2.6L**, p<0.001). Treatment with another GLUT1 inhibitor, STF31, also resulted in a

similar decline in *T. cruzi*+IFN-γ induced ROS (**Fig.2.6M**, p<0.001) and NO levels

Figure 2.6. Modification of cytokine, ROS, and NO response of activated macrophages by glucose uptake. RAW 264.7 macrophages were infected with *T. cruzi* in presence or absence of IFNγ and apigenin (glucose transport 1 inhibitor) for 3 h (A-C) or 18 h (D-I). Shown are quantification of TNF-α (A&D), IL-1β (B&E), and IL-6 (C&F) release by ELISA and gene expression analysis of these cytokines by RT-qPCR (G). Intracellular ROS (H) and nitrite release (I) were determined as in Fig.5. (J&K) RAW 264.7 macrophages were activated with LPS and IFNγ ± apigenin for 18 h and analyzed for ROS (J) and nitrite levels (K). (L) Bone marrow-derived murine macrophages were infected with *T. cruzi* (± IFNγ and apigenin) for 18 h, then intracellular ROS was determined. (M&N) RAW264.7 macrophages were infected with *T. cruzi* in the presence or absence of IFNγ and STF31 for 18 h, then ROS (M) and nitrite release (N) were measured. Data are shown as mean ± SEM of ≥3 biological replicates. ANOVA$_{Tukey}$ *P<0.05, **P<0.01, ***P<0.001 when compared to no-treatment controls unless marked by a line over comparing groups.
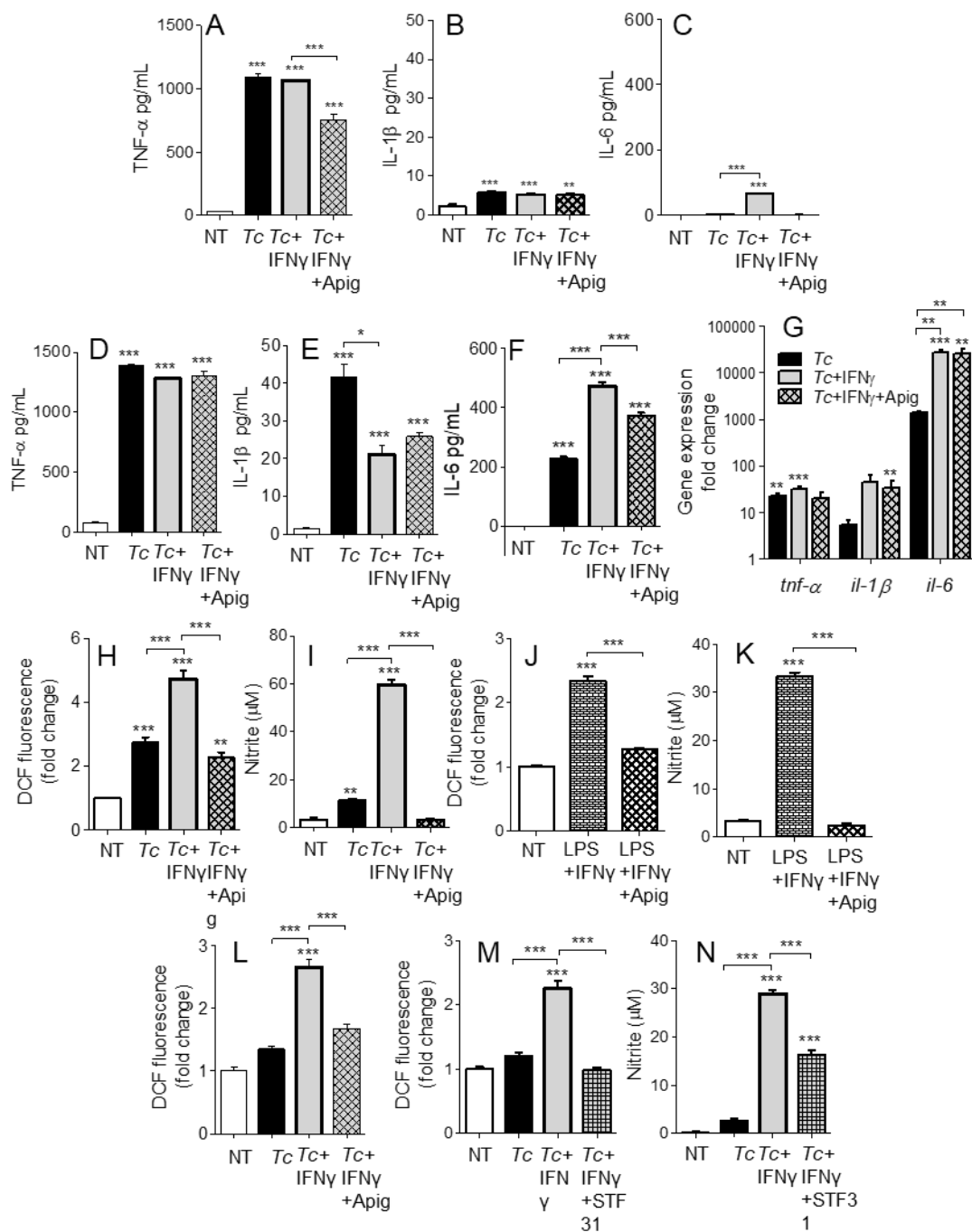
(**Fig.2.6N**, p<0.001) in macrophages. These results confirm our findings, and demonstrate that macrophage stimulation of proinflammatory cytokine response by *T. cruzi* or LPS (+IFNγ) is not dependent on glucose metabolism, while glucose uptake is critical for ROS and NO production in infected macrophages.

Glycolysis supports the pentose phosphate pathway in proinflammatory macrophages.

To delineate the steps in glycolysis and Krebs cycle that signal the differential ROS/NO response, we performed targeted metabolite profiling of the *T. cruzi*-challenged macrophages (± IFN-γ). The detailed data are presented in Table S2.2. We noted increased abundance of glycolysis (FBP/GBP, G6P/F6P, Glyc3P, lactate, and Ru5P) and Krebs cycle (fumarate, malate, oxalate, and succinate) metabolites in infected (vs. normal) macrophages (**Fig.2.7A**). Co-incubation with IFN-γ resulted in a major shift towards glycolysis, evidenced by >2-fold increase in the glycolysis metabolites (3PG/2PG, FBP/GBP, Glyc3P, PEP, and lactate) and ribulose-5-P from the pentose phosphate pathway (PPP) in infected macrophages (**Fig.2.7B**, p<0.05). Glucose and citrate levels declined in both of these groups, glutamine was particularly high (>10-fold, p<0.001) in infected macrophages, and G6P/F6P, Glyc3P, and Ru5P were 2- to 6-fold higher in *T. cruzi*+IFN-γ treated macrophages compared to infection alone (p<0.01).

To elucidate the essentiality of glycolysis linkage to PPP in ROS production, we stimulated macrophages with *T. cruzi* (± IFN-γ) in the presence and absence of glutamine, glucose, or fructose for 18 h (**Fig.2.7C-E**). Glutamine can replenish the Krebs cycle by converting to glutamate and α-ketoglutarate. Glucose is used by both glycolysis and PPP, while fructose does not directly support the PPP as it enters the glycolysis

Figure 2.7. Relevance of glycolysis and pentose phosphate shunt in infected macrophages with IFNγ supplement or classical activation. RAW 264.7 macrophages were infected with *T. cruzi* in presence or absence of IFNγ for 18 h (A-E) or activated with LPS+IFNγ (F&G). (A&B) Targeted profiling of the glycolysis and Krebs cycle metabolites was performed by LC-MS, and data are presented as heat map (A) and fold change compared to no-treatment controls (B). (C-E) Macrophages were incubated with *T. cruzi* ± IFNγ in the absence or presence of glucose, glutamine or fructose for 18 h. The intracellular ROS (C&D) and nitrite release (E) were measured by DCF fluorescence and Griess assay, respectively. (F&G) Macrophages were activated by LPS+IFNγ in the presence or absence of glucose and glutamine. ROS (F) was determined by DCF fluorescence and cell viability (G) was analyzed by Alamar blue fluorescence. Data are shown as the mean of ≥3 biological replicates ± SEM. ANOVA$_{B-H}$ for metabolite analyses and ANOVA$_{BF}$ for ROS and NO levels were used, where *$P<0.05$, **$P<0.01$ and ***$P<0.001$ are compared to no-treatment controls, ^^$P<0.01$ compared to the *T. cruzi*-treated group, otherwise indicated by a line over compared groups. Abbreviations: 3PG/2PG - 3-phosphogluconate/2-phosphogluconate; GBP/FBP – Glucose 1,6-bisphosphate/Fructose 1,6-bisphosphate; Glyc3P – Glycerol 3-phosphate; PEP – Phosphoenolpyruvate; Ru5P – Ribulose 5-phosphate.
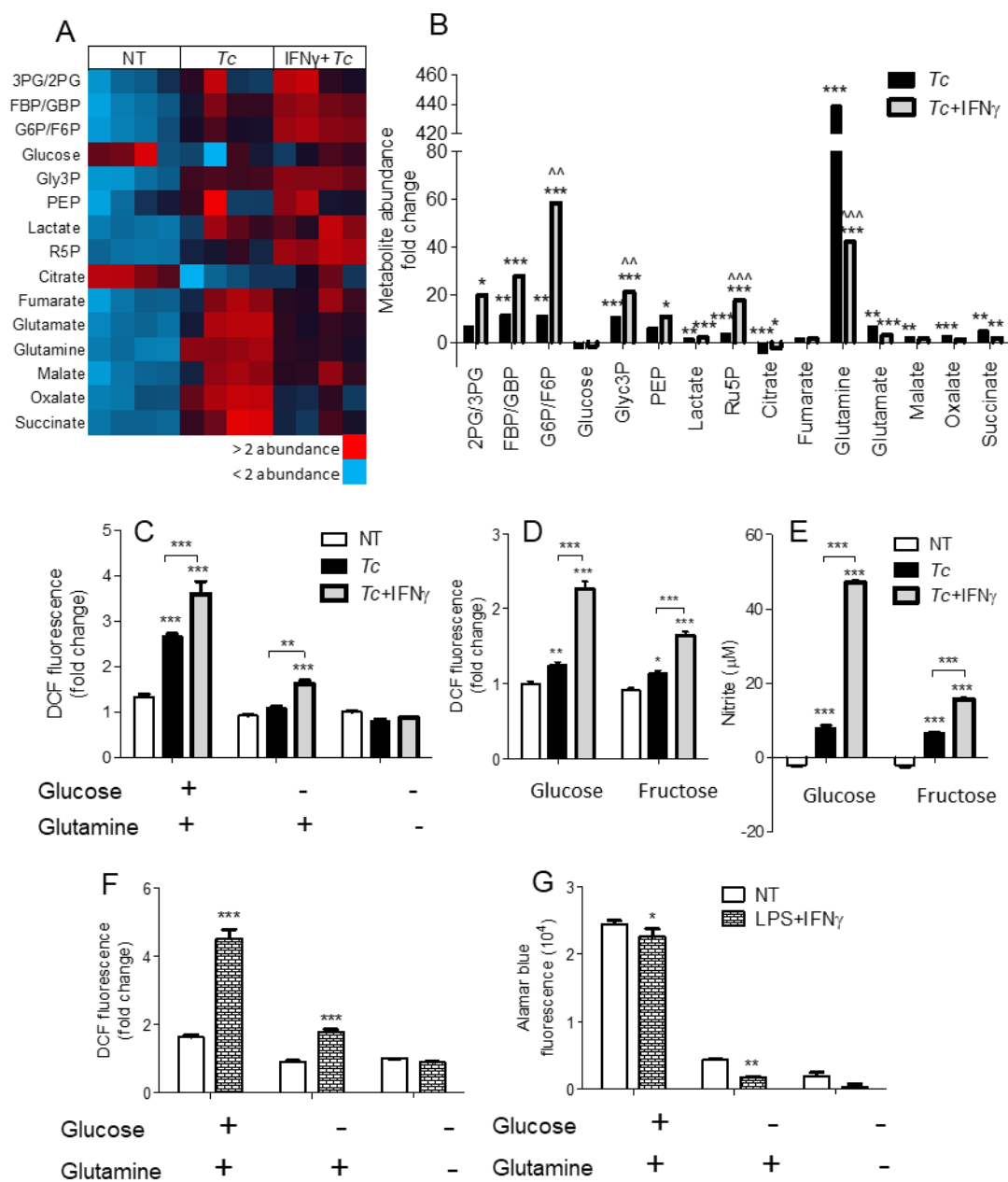
pathway after the divergence to the pentose phosphate shunt. We found that glucose, but not glutamine, supplementation elicited a 2.5-fold increase in ROS response in infected macrophages, which was heightened with IFN-γ addition (**Fig.2.7C&D**, p<0.001). Incubation with fructose allowed <50% increase in the ROS level than was noted in glucose supplemented, *T. cruzi*+IFN-γ stimulated macrophages (**Fig.2.7D**, p<0.001). The NO release by macrophages responding to *T. cruzi*+IFN-γ was also declined by 3-fold when glucose was replaced with fructose in the culture media (**Fig.2.7E**). Similar patterns of ROS production were noted in LPS+IFN-γ activated macrophages where the lack of glucose availability suppressed the ROS level (**Fig.2.7F**) and cell viability (**Fig.2.7G**). Together, the results presented in **Fig.2.7** suggest that glycolysis shunt towards PPP supports the ROS/NO production in macrophages stimulated with *T. cruzi* or LPS (+IFN-γ).

Pentose phosphate shunt is essential for ROS/NO response of macrophages against T. cruzi. To validate the role of PPP in ROS/NO production, we applied an RNAi approach to inhibit the expression of glucose-6-phosphate dehydrogenase (G6PD) and 6-phosphogluconate dehydrogenase (PGD). G6PD is the first step linking glycolysis to PPP, and PGD is the third enzyme in the PPP which catalyzes the production of ribulose-5-phosphate (Ru5P) and NADPH. The G6PD siRNA, but not the scrambled siRNA, resulted in 50% decline in G6PD expression (**Fig.2.8A**). Yet, we observed no major differences in NO (**Fig.2.8B**) and ROS (**Fig.2.8C**) levels in *T. cruzi*+IFN-γ stimulated macrophages. The LPS+IFN-γ stimulated macrophages also did not exhibit a decline in ROS production with G6PD knockdown (**Fig.2.8D**). Silencing of the PGD, even upon use of high concentrations of PGD siRNA duplex, could not be achieved (**Fig.2.8E**). Therefore, we resorted to using the pharmacological inhibitor of PGD, 6-aminonicotinamide (6-AN; 10 μM) during macrophage activation. Co-treatment with

Figure 2.8. Reliance on pentose phosphate shunt by *T. cruzi*+IFNγ-activated macrophages. RAW264.7 macrophages were transfected with G6PD or scrambled (SCR) siRNA for 24 h and then treated with *T. cruzi*+IFNγ for 18 h. Shown are (A) Western blot analysis for G6PD and β-actin (loading control), (B) NO release, and (C) and intracellular ROS levels in infected (± G6PD siRNA) macrophages. (D) Effect of G6PD knockdown by siRNA on LPS+IFNγ induced ROS at 18 h is shown. (E) Western blot for PGD of lysates from RAW264.7 macrophages transfected with siRNA against PGD or scrambled sequence (SCR), or treated with media in absence of transfection vehicle (No vh) for 24 h. (F-H) RAW264.7 macrophages were incubated with *T. cruzi*+IFNγ in the presence or absence of 6-aminonicotinamide (6-AN; 100 µM). The NO (F) and ROS (G) production were determined at 18 h post-incubation. Trypanosome release was quantified at 3, 5, 7, and 9 days post-infection (H). (I) RAW264.7 macrophages (5 x 10^4 per well) were seeded in 8 chamber slides, and incubated with *T. cruzi* (3:1 parasite to cell ratio) in the presence or absence of IFN-γ (50 ng/mL), Apocynin (1 mM), or Apigenin (100 µM). After 18 h post-incubation, macrophages were fixed and stained with Giemsa-Wright solution then ≥ 200 *T. cruzi*-bearing macrophages were counted. The percentages of infected cells are reported. Data shown are represented as the mean ± SEM of ≥3 biological replicates. ANOVA$_{Tukey}$ **$P<0.01$ and ***$P<0.001$ in comparison to no-treatment controls unless indicated by a line over compared groups.

A

B

C

D

E

F

G

H

I

Treatment	Infected	Total cell count	% Infected
Tc	211	421	50.1%
IFNγ+Tc	201	500	40.2%
Apocynin +IFNγ+Tc	202	360	56.1%
Apigenin +IFNγ+Tc	222	342	64.9%
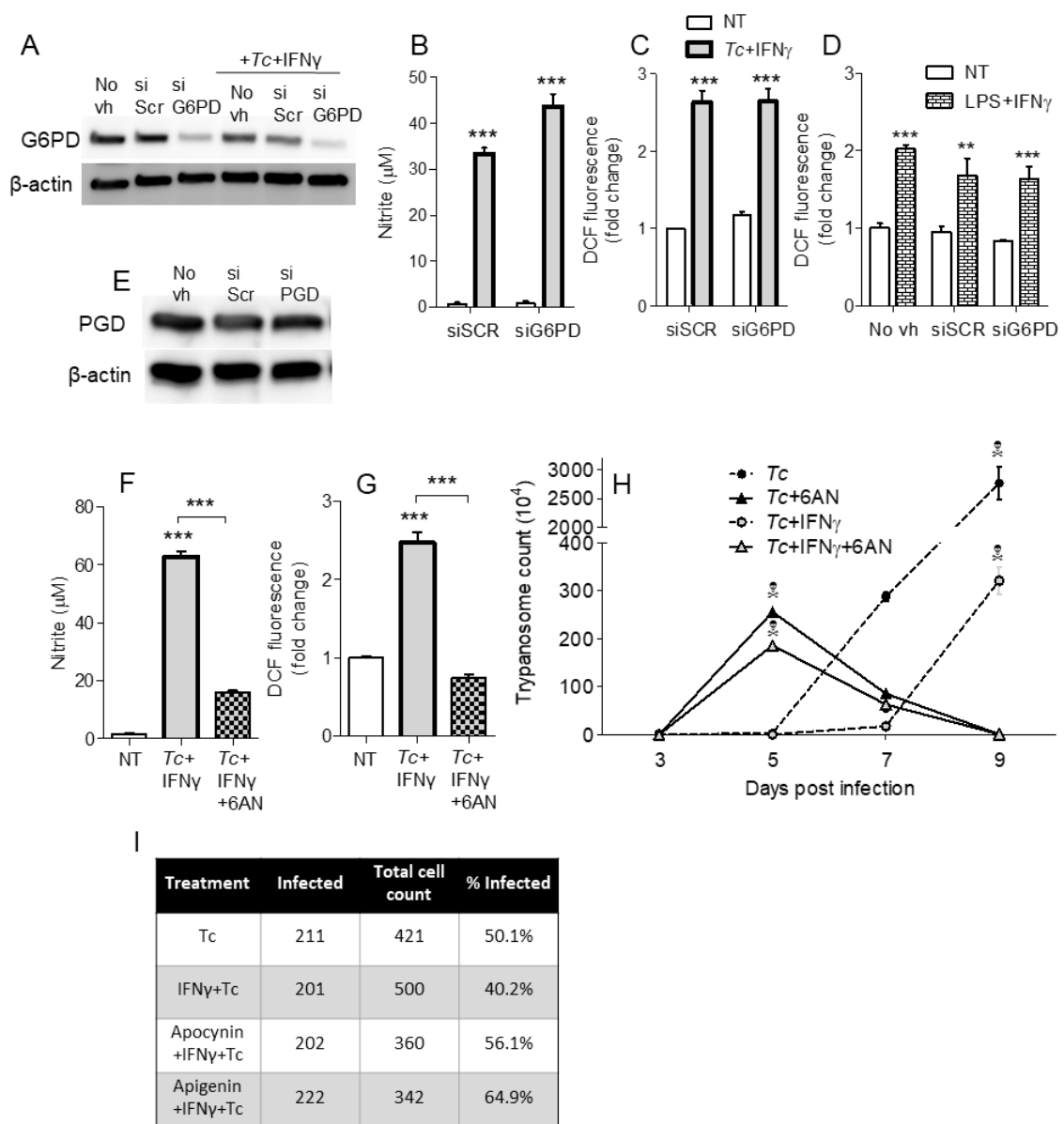
6-AN abolished the NO (**Fig.2.8F**, p<0.001) and ROS (**Fig.2.8G**, p<0.001) formation in *T. cruzi*+IFN-γ stimulated macrophages. These results confirm that glycolytic-PP shunt, and particularly the step producing Ru5P, is essential for ROS and NO response of macrophages.

Finally, we determined the significance of glucose/PPP in controlling parasites in macrophages. Up to 50% of the RAW264.7 macrophages were infected with *T. cruzi* (1:3 cell parasite ratio) at 18 h, and co-incubation with IFN-γ resulted in a 20% decline in infected macrophages (**Fig.2.8H**). Inhibition of glucose transport (apigenin) or NOX2 (apocynin) abolished the IFN-γ effects in limiting parasites in macrophages. Further, treatment of macrophages with 6-AN (inhibits glucose-PPP link) enhanced parasite development in macrophages (**Fig.2.8H**). The peak release of trypomastigotes from *T. cruzi*-infected and *T. cruzi*+IFN-γ treated macrophages was observed during 7 – 9 days pi. In comparison, addition of 6-AN resulted in peak trypomastigotes release at 5 days pi after which cells began to die. These results demonstrate that glucose-PPP supports the NOX2/ROS production for early control of parasite replication in macrophages.

Discussion

In this study, we investigated how the macrophage ability to control *T. cruzi* infection is subdued, and took a metabolic approach to improve the trypanocidal function of macrophages. For this, we have used primary and cell line macrophages coupled with genetic and chemical depletion of PPARs, metabolite profiling followed by supplementation of critical metabolites and chemical and RNAi inhibition of key metabolic enzymes to delineate the macrophage response to *T. cruzi*. Our data showed that macrophages phagocytize *T. cruzi* and elicit a potent, inflammatory cytokine response; however, they lack effective ROS and NO responses against the parasite. We

showed that this is due to macrophages continuing to maintain a PPAR-α-dependent, Krebs cycle-linked oxidative metabolism that has no effect on inflammatory cytokine response, but allow only a partial level of NOX2/iNOS activation upon *T. cruzi* infection. IFN-γ treatment dispensed the macrophages' need to utilize pyruvate-supported Krebs cycle, led to complete metabolic shut down of oxidative metabolism, and enhanced the glycolytic source of energy availability in infected macrophages. Ironically, the glucose uptake and metabolism was diverted towards PPP, and the activity of 6PGD, which produces Ru5P and NADPH, was essential for eliciting potent ROS and NO response in infected macrophages. Inhibition of 6PGD led to decreased ROS/NO, increase parasite replication, and earlier release of trypomastigotes from infected macrophages. To the best of our knowledge, this is the first study providing a detailed view of the metabolic regulation of the macrophage response to an intracellular pathogen. We propose that chemical analogs enhancing the glucose-pentose phosphate shunt will be beneficial in controlling early parasite replication and dissemination in the infected host.

The TLR family of innate immune receptors (TLR1-TLR10) recognize a variety of pathogen ligands and initiate two major pathways: the MyD88-dependent pathway that is used by all TLRs except TLR3 for the activation of NF-kB and AP-1, and the TIR-domain-containing adaptor protein inducing IFN β-dependent pathway that is initiated by TLR3 and TLR4 and activates type I IFN responses. *T. cruzi and T. cruzi* antigens (e.g. GPI-anchored mucins, cruzipain) are shown to engage TLR2 and TLR4, and *T. cruzi* DNA is recognized by TLR9 to induce proinflammatory cytokine response in macrophages (Kayama and Takeda, 2010). Unfortunately, the *T. cruzi* induced cytokine response seems insufficient in controlling parasites. Rather, the predominance of pro-inflammatory cytokines, IFN-γ, TNF-α, IL-17, with TLR2 and TLR4 involvement is pathological to the host, and suggested to be involved in the presentation of cardiac form of disease in infected humans (Mendes da Silva et al., 2017). TLR2 and TLR4 are also

suggested to be involved in the production of ROS and NO; however, in the context of *T. cruzi* infection, TLR2/TLR4 activation appeared to be not sufficient to induce potent ROS/NO response to kill the intracellular parasite. Others have suggested that it is not the inability of macrophages to mount an ROS/NO response, rather the parasite's elaborate antioxidant system of trypanothione-dependent tryparedoxin peroxidases dismutates the ROS/NO (Pineyro et al., 2008, Piacenza et al., 2008). Our study suggests that this might not be the only cause for a sub-par ROS/NO response. Supplementing with IFN-γ during infection was sufficient to activate the macrophage expression and activation of iNOS and NOX2, and production of NO and ROS, respectively. Further studies will be required to identify how IFN-γ complements the *T. cruzi*-generated stimuli in enhancing the ROS/NO response. The two pathways that deserve immediate attention include the interaction of the atypical PKC ζ and TLR2 in the lipid rafts of the plasma membrane and the TLR4-MyD88-IL-1 receptor-associated kinase 4 signaling pathway that activate the p38 MAPK and protein kinase B pathways, which can initiate the phosphorylation of p47^{phox} and subsequent activation of NOX2 and ROS production in macrophages (Shin et al., 2008, Xiang and Fan, 2010).

How energy metabolism is reconfigured to support macrophage activation and effector function has not been fully studied. PPARs (α, γ and δ isoforms) are ligand-activated transcription factors that regulate nearly every facet of fatty acid metabolism. Recent studies have established a role for PPAR-γ and -δ in the regulation of macrophage lipid metabolism and inflammation. Several groups have noted upregulation of PPAR-γ in murine and human macrophages, and initial studies suggested that PPAR-γ attenuates the proinflammatory macrophage response (Bouhlel et al.). Agonism of PPAR-γ coupled the uptake of oxidized low density lipoprotein to cholesterol efflux via induction of liver X receptor-α-mediated transcriptional cascade and the cholesterol

efflux pump Abca1, and was beneficial in providing the atheroprotective effects in

diabetes (Chawla et al., 2001). Others suggested that PPAR-δ-dependent shift towards

oxidative metabolism is accompanied by an influx of fatty acids, and PPAR-δ-dependent

surge in monounsaturated fatty acids synergize with IL-4 to enhance the alternative

gene expression signature (Odegaard et al., 2008). Macrophage-specific knockdown of

PPAR-γ resulted in a loss of alternatively activated macrophages in tissues and

increased susceptibility to diet induced obesity, insulin resistance, and glucose

intolerance in mice (Odegaard et al.). The role of PPAR-α in macrophages is

comparatively less studied. Our study provides the first evidence that PPAR-α

expression increases in murine macrophages by *T. cruzi*-generated stimulus.

Interestingly, genetic and chemical ablation of PPAR-α activity had no effect on the

inflammatory cytokine response of infected macrophages; however, PPAR-α appeared

to stimulate the ROS and NO production at least in response to initial infection. Inhibition

of PPAR-α decreased the oxidative metabolism and the NO and ROS response in

infected macrophages. A similar suppression of NO and ROS was observed with the

inhibition of pyruvate transport to the mitochondria early in pro-inflammatory activation,

which overall suggested that PPAR-α-regulated mitochondrial metabolism may be

involved in the early events that lead to ROS and NO production by infected

macrophages. Inhibiting mitochondrial pyruvate transport had been shown to suppress

iNOS gene transcription in LPS-activated macrophages (Meiser et al., 2016). A broken

Krebs cycle results in accumulation of metabolites, e.g. succinate, that signaled

transcriptional activation of inflammatory response in LPS-stimulated macrophages

(Tannahill et al., 2013). We also observed a moderate increase in Krebs cycle

metabolites including succinate in infected macrophages. Alternatively, a functional

mitochondrial Krebs cycle could support the production of oxidative compounds as it has

two enzymes that produce NADPH, which is utilized by NOX2 and iNOS for synthesizing ROS and NO, respectively. Further studies will be required to delineate the comparative role of PPAR-α in providing transcriptional and metabolic signals for regulating the NOX2/iNOS activation in macrophages. Regardless, PPAR-α inhibition was not sufficient to arrest parasite replication in macrophages.

Recent studies have described an increase in glycolysis-dependent lactate formation and activation of PPP in macrophages after phagocytosis (Kelly and O'Neill, 2015), and that inhibition of sedoheptulose kinase (CARKL), which resulted in accumulation of metabolites in the PPP and a decline in Krebs cycle metabolites, enhanced the proinflammatory cytokine response in LPS-activated macrophages (Haschemi et al., 2012). Others showed that HIF-1α-dependent transcriptional programming is responsible for heightening glycolysis in macrophages (Liu et al., 2016), and GLUT1-mediated glucose uptake drives a proinflammatory phenotype (Freemerman et al., 2014). In this study, we provide evidence that first few steps where glycolysis and PPP are linked, primarily support ROS and NO production in inflammatory macrophages. Our data show that in all instances when glucose availability was limited, achieved by inhibition of GLUT-1, removal of glucose, or replacement of glucose with fructose as a carbon source, the levels of cytokine release were not altered while ROS and NO response was abolished in *T. cruzi*- and LPS-stimulated macrophages. Glutamine, which can replenish the Krebs cycle through its conversion to glutamate and α-ketoglutarate, was also insufficient in the absence of glucose to support cell viability and the ROS/NO response of activated macrophages. The increase in abundance of Glucose-6-P/Fructose-6-P and Glycerol-3-P metabolites of glycolysis pathway and Ru5P of the PPP that reversibly fuel each other provided the first indication that activation of potent ROS/NO response in macrophages requires a coordinated regulation of glycolysis to

PPP, instead of glycolytic formation of pyruvate or lactate. This was also evidenced by the findings that ROS/NO response was abolished by inhibition of 6PGD (produces Ru5P and NADPH) in infected macrophages. Future studies will be required to delineate if glycolytic-pentose phosphate shunt simply provides the NADPH substrate, or it provides metabolic signaling at transcriptional, translational or post-translational levels for NOX2 and iNOS activation in proinflammatory macrophages. Yet, we surmise that activation of glycolytic-pentose phosphate shunt will be beneficial in enhancing the macrophages' ability to achieve early clearance of intracellular parasites.

In summary, the present study shows that early inhibition of mitochondrial metabolism may be detrimental for ROS and NO generation, glycolysis and PPP are important for ROS and NO generation at the metabolite level, and *T. cruzi* infection may program the metabolism of host macrophages differentially at the pentose phosphate shunt compared to pro-inflammatory macrophages. Based on these findings, we extend our understanding of how the synthesis or release of ROS and NO compounds are controlled by metabolism, which may be further studied for potential translational purposes.

Chapter 5: Summary and Final Conclusions

A part of this chapter will be published or has already been published in Infection and Immunity journal as:

5.1 Recapitulation of Purpose and Findings

The aim of this dissertation was to determine how mφ are deficient in *Trypanosoma cruzi* clearance and how the metabolism supports the mφ pro-inflammatory functions. I had hypothesized the *T. cruzi* prevents the macrophage's metabolic shift away from oxidative phosphorylation for pro-inflammatory functions, and that modulating metabolism can enhance parasite killing.

In the first study, I challenged mφs with the *T. cruzi* isolates SylvioX10/4 (SYL, pathogenic) and TCC (attenuated) or treated with LPS/IFN-γ (proinflammatory activation) and IL-4 (immunomodulatory activation). I analyzed the cytokine profile, reactive oxygen species, nitric oxide, and metabolic state by using mitoxosome gene array and Seahorse Flux Analyzer. I showed that LPS/IFN-γ elicit potent increase in TNF-α, ROS and •NO, inhibit oxidative metabolism, and switch to the glycolytic pathway in mφs. SYL infection however, elicited low levels of •NO and ROS, and the mφ presented with an intermediate

metabolic state using both oxidative metabolism and glycolysis for energy demand that could be modulated by IFN-γ. TCC- and SYL-infected mφs exhibited similar capacities to produce TNF-α and ROS, but TCC-infected mφs exhibited 2-fold higher levels of oxidative metabolism and $^{\bullet}$NO production. Lastly, in this study, I showed that inhibiting ATP-coupled oxygen consumption suppressed the $^{\bullet}$NO release in infected mφs. I concluded that mitochondrial O_2 consumption may constitute a mechanism for $^{\bullet}$NO generation, and enhancing the oxidative metabolism provides an opportunity for increasing $^{\bullet}$NO production and pathogen clearance by mφs.

In the second study, I investigated the role of peroxisome proliferator-activated receptors (PPARs) and IFN-γ in metabolic regulation of macrophages during *T. cruzi* SYL infection. For this, primary (wild type and PPAR-$\alpha^{-/-}$) and cultured (RAW264.7) macrophages were infected with *T. cruzi* (±IFN-γ)*,* and evaluated for ROS, NO, and cytokine production in the presence of metabolic modulators of glycolysis, Krebs cycle, and oxidative phosphorylation. I analyzed the metabolic status by Seahorse XF Analyzer and LC-MS, and validated the findings by an RNAi approach.

I found that infection with *T. cruzi* elicited a substantial increase in PPAR-α expression and TNF-α, IL-1β, and IL-6 release, and moderate levels of ROS/NO production in macrophages. Co-delivery of IFN-γ enhanced the *T. cruzi*-induced ROS/NO release to the levels noted in LPS+IFN-γ-stimulated macrophages. Genetic and chemical inhibition of PPAR-α had no effect on cytokine release, partially attenuated the ROS/NO response, and it was not sufficient for complete oxidative to glycolytic metabolic shift as was noted in presence of IFN-γ in *T. cruzi*-infected macrophages. Deprivation of carbon sources (glutamate and glucose) and chemical inhibition of metabolite transport showed that Krebs cycle and glycolysis support NOX2/iNOS activation of ROS/NO but are not essential for inflammatory cytokine response, Krebs

cycle was dispensable in fully activated macrophages, and glucose uptake was critical

for ROS/NO generation in *T. cruzi*+IFN-γ- and LPS+IFN-γ-stimulated macrophages.

Metabolic profiling and RNAi studies showed that glycolysis-pentose phosphate shunt at

6-phosphogluconate dehydrogenase which produces Ru-5-P and NADPH, was essential

for ROS/NO response, and control of parasite replication in macrophages infected by *T.*

cruzi. I concluded that the supplementation with IFN-γ, but not inhibition of PPAR-α,

supports metabolic up regulation of glycolytic-pentose phosphate shunt for eliciting

potent ROS/NO response in *T. cruzi*-infected macrophages. Chemical analogs

enhancing the glucose-PPP will be beneficial in controlling parasite replication and

dissemination by macrophages.

Collectively, the data from these investigations indicated the following:

1) *T. cruzi* infection of macrophages elicit potent pro-inflammatory cytokine response but

poorly activate the ROS, NO, and classical pro-inflammatory metabolic response.

2) Attenuated *T. cruzi* induces a greater NO response, but fails to induce sufficient ROS

linked to higher early mitochondrial metabolism in mφs.

3) PPAR-α inhibition partially declines ROS, NO, and oxidative phosphorylation and

does not synergistically modify these aspects in mφ during *T. cruzi* infection.

4) IFN-γ supplementation during *T. cruzi* infection shuts down mitochondrial metabolism,

enhance the ROS and NO response, and limits infection.

5) ROS and NO production, but less so for inflammatory cytokines, are linked to the use

of glucose for the pentose phosphate pathway.

6) Phosphogluconate dehydrogenase in the pentose phosphate pathway is involved in

regulating ROS, NO, and *T. cruzi* survival and replication in mφ.

These observations provided insight into how *T. cruzi* metabolically drive the mφ to

suppress anti-microbial mechanisms and support parasite survival, which may be used

as the basis of a novel strategy for improving *T. cruzi* clearance. This drives a new

direction of focus on why the pentose phosphate shunt from glycolysis is essential to control *T. cruzi* growth.

5.2 Limitations of this Research and Future Directions

These *in vitro* studies allowed a direct comparison of cell metabolism perturbations caused by *T. cruzi* infection, as opposed to having a mix of cell types of varying default metabolic states and capacities and cell death would convolute these results if for example, macrophages were analyzed after infection *ex vivo*. Yet, high densities of macrophages responding to high numbers of *T. cruzi* and the lack of mediators produced by other responding cells are likely not the course of natural infection. Macrophages infected with *T. cruzi* produced potent amounts of inflammatory cytokines. A future study involving other immune cells, such as to evaluate the antigen presentation of macrophages with enhanced pentose phosphate synthesis, will be useful in determining its role in the interaction with other components of immunity. Isolation of infected macrophages from a mouse model of Chagas disease and evaluating the metabolism of these cells will also be useful, when the capacity allows. Currently with LC-MS, 5×10^6 cells are recommended for evaluation.

It was not the intention to imply that low ROS and NO is a cause of Chagas disease progression nor are the molecules the sole players in *T. cruzi* killing, when many investigators in the field have reported oxidative stress in Chagas disease. The results from this study rather focused on the early macrophage response to *T. cruzi* and uncovering a metabolic relationship to the production of the oxidative molecules. In addition, mφs infected with *T. cruzi* isolates have been shown to produce moderate levels of ROS but at later time points (Zago et al., 2016b), and at 6 hours post-infection in thioglycollate-induced primary mφ (Paiva et al., 2012). I used Sylvio X10/4 as the pathogenic strain in this study. Including other *T. cruzi* strains from other phylogenic

groups that cause Chagas pathology and testing *in vivo* mφ response will be useful in determining whether the pentose phosphate shunt is a common pathway that could be targeted for improving control of all pathogenic *T. cruzi* strains.

Inhibition of the oxidative phosphorylation chain during early stages of infection resulted in suppression of NO production by infected mφ, as was also observed with PPAR-α knockdown and mitochondrial pyruvate transport inhibition. A biphasic metabolic activation in pro-inflammatory mφ has been previously alluded to (Haschemi et al., 2012), and with this data now strongly suggest that future work delineating these metabolic switches is important for fine tuning the modulation of mφ function.

The pentose phosphate pathway has various functions, including generation of NADPH, the precursors for nucleotide and amino acid synthesis, and intermediates that can cycle back into glycolysis. Delineating how the pentose phosphate pathway, especially at the phosphogluconate dehydrogenase step, controls *T. cruzi* survival and replication and the activities of iNOS and NOX2 will be useful in better understanding the modulation of these macrophage functions. *In vivo* Chagas disease studies that target the pentose phosphate pathway in mφ will also implicate whether modulating metabolism during *T. cruzi* infection could be a significant strategy for mitigating chronic Chagas symptoms. Further insight into how *T. cruzi* regulate this pathway could provide a basis for generating an attenuated *T. cruzi* strain to better understand the innate immune response against the parasite in order to mitigate the development of Chagas disease.

5.3 Relevance of Findings to Metabolic Disorders

Metabolic disturbance is a feature of many diseases. Obesity and malnutrition are significant metabolic health concerns which may be predispositions to infectious diseases. Obesity is an overweight state defined by the body mass index (BMI) score,

which moderately correlates with body fat and is calculated by using weight and height measurements. Obesity is a major risk factor for many noncommunicable diseases such as type 2 diabetes, and causes detrimental chronic low-grade inflammation which does not reach the extent of the inflammation achieved during acute phase of infection clearance (Lumeng, 2013). Obese patients have also been shown to have failure of antibiotic treatment for skin infections (Conway et al., 2017), and numerous bacterial infections (Karlsson and Beck, 2010). In the obese state, macrophages have been shown to be recruited to adipose tissue and possess pro-inflammatory phenotypes more than macrophages in lean adipose tissue with regard to a surface receptor marker and cytokine production, yet have been shown to metabolically use lysosomal lipid metabolism and increase fatty acid transporters (Castoldi et al., 2015). In the context of macrophages in the obese microenvironment where free fatty acids are abundant in high glucose and insulin concentrations, macrophages have been shown to activate to produce the pro-inflammatory cytokines, TNF-α and IL-1β in a PPAR-γ-dependent manner, and TLR-4 deficiency suppress adipose tissue inflammation perhaps due to less activation by the circulating LPS originating from the gut microbiota (Castoldi et al., 2015). The ROS production in obesity models have been speculated to be partly from NOX2 in macrophages, although the role this ROS in inflammation of adipose tissue has not been delineated (Han, 2016). Despite this, low-grade inflammation present in obesity may be insufficient for the generic control of infectious pathogens, and the metabolism of host cells and macrophages rather may play a more significant role in pathogen clearance. The increase in macrophage flux to obese adipose tissue may be detrimental to the host if the pathogen is intracellular and uses macrophages as carriers, host cell lipid metabolism for their survival, or if the clearance mechanism by macrophages is dependent on metabolic pathways. Thus, impairment of metabolic shift of macrophages may contribute to disease progression of both obesity and that caused by infection. The

results in this dissertation help solidify the notion that the metabolism used by macrophages is an important link between macrophage function and pathogen survival.

In malnourished populations, the susceptibility to infectious diseases also pose interesting insight into the interactions between nutrition and innate immunity. Malnutrition is defined as the imbalance of deficient dietary uptake or absorption compared to energy expenditure. As such, malnutrition has been correlated with immunodeficiency and increased susceptibility to infectious diseases. Macrophages differentiated from bone marrow cells of malnourished, low protein diet-fed mice exhibit increased arginase activity in response to LPS compared to those from healthy mice, and in the presence of IL-4, these macrophages from mice fed a low protein diet demonstrate increased *Leishmania infantum* parasite burden compared to those isolated from nourished mice (Corware et al., 2014). Suppressed NFκB activity (Fock et al., 2010) and reduction in the production of GM-CSF growth factor (Oliveira et al., 2016) and ROS and NO (Costa et al., 2016) was also observed in peritoneal or alveolar macrophages from malnourished animals, suggesting poor macrophage inflammatory function in nutrition-deficient states. These studies point to the importance of nutritional availability for macrophages to prompt a pro-inflammatory response, and delineating the mechanism of how metabolic deficiency links to function of macrophages in malnourished states will be useful to define novel methods for improving infection outcomes.

APPENDIX
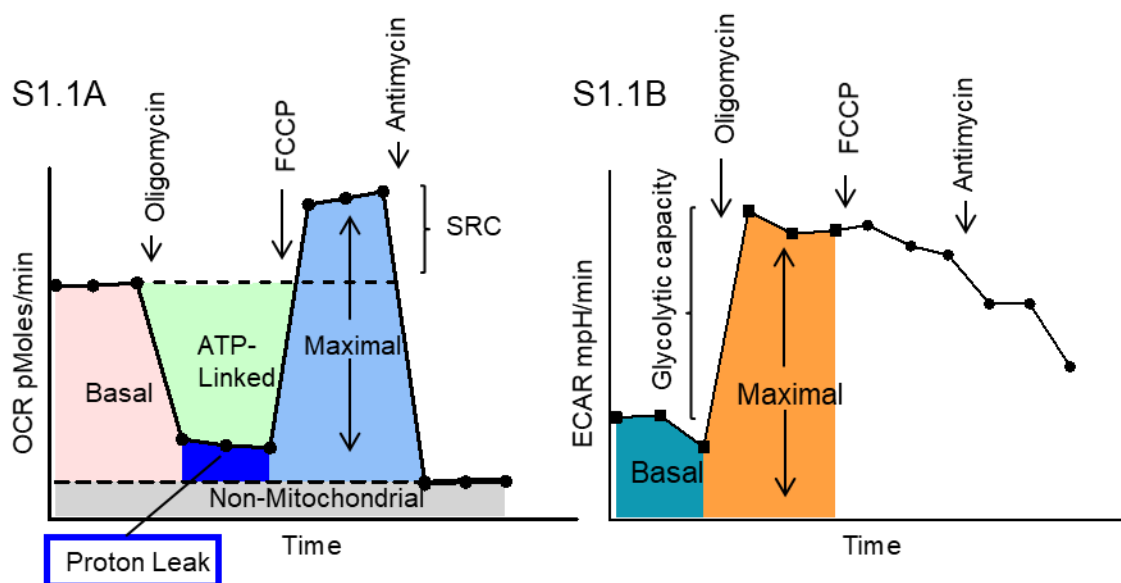
Figure.S1.1. Line diagrams of Seahorse XF cell mito-stress and glycolysis stress tests. (A) The mito-stress test is based on oxygen consumption rate (OCR) and measures the key parameters of mitochondrial function, including basal respiration, ATP production, proton leak, maximal respiration, and spare reserve capacity. (B) The glycolysis stress test is based on extracellular acidification rate (ECAR) and measures three key parameters of glycolytic function including glycolysis, glycolytic capacity and glycolytic reserve. Arrows mark the addition of oligomycin (inhibits ATP-coupled respiration), FCCP (mitochondrial uncoupler), antimycin A (inhibits electron transport from complex III), and 2 deoxy glucose (inhibits glycolysis).
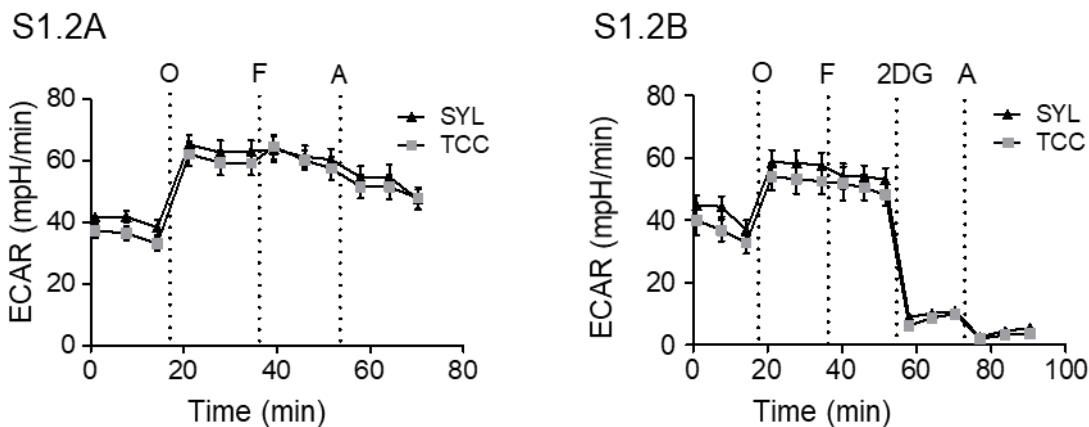
Figure.S1.2. SYL-versus-TCC induced changes in ECAR in macrophages. RAW 264.7 mφs were seeded in XF24 plates (8 x 104/well) and incubated with *T. cruzi* Sylvio (SYL) isolate or TCC isolate for 3 h (A) or 18 h (B), and ECAR (glycolytic metabolism) was evaluated by using an XF24 Analyzer. Shown are ECAR profiles of macrophages in response to the sequential administration of pharmacological modulators of electron transport chain, including oligomycin (O), FCCP (F) and antimycin (A), and inhibition of glycolysis was achieved by 2-deoxyglucose addition. Data are presented as mean ± SEM (n = 5 replicates per treatment per experiment).

LITERATURE CITED

ADEREM, A. & UNDERHILL, D. M. 1999. Mechanisms of phagocytosis in macrophages. *Annu Rev Immunol,* 17**,** 593-623.

ADHIKARY, T., WORTMANN, A., SCHUMANN, T., FINKERNAGEL, F., LIEBER, S., ROTH, K., TOTH, P. M., DIEDERICH, W. E., NIST, A., STIEWE, T., KLEINESUDEIK, L., REINARTZ, S., MULLER-BRUSSELBACH, S. & MULLER, R. 2015. The transcriptional PPARbeta/delta network in human macrophages defines a unique agonist-induced activation state. *Nucleic Acids Res,* 43**,** 5033-51.

AKIRA, S. & TAKEDA, K. 2004. Toll-like receptor signalling. *Nat Rev Immunol,* 4**,** 499-511.

ALVAREZ, M. N., PIACENZA, L., IRIGOIN, F., PELUFFO, G. & RADI, R. 2004. Macrophage-derived peroxynitrite diffusion and toxicity to Trypanosoma cruzi. *Arch Biochem Biophys,* 432**,** 222-32.

AOKI, M. P., GUINAZU, N. L., PELLEGRINI, A. V., GOTOH, T., MASIH, D. T. & GEA, S. 2004. Cruzipain, a major Trypanosoma cruzi antigen, promotes arginase-2 expression and survival of neonatal mouse cardiomyocytes. *Am J Physiol Cell Physiol,* 286**,** C206-12.

ARANDJELOVIC, S. & RAVICHANDRAN, K. S. 2015. Phagocytosis of apoptotic cells in homeostasis. *Nat Immunol,* 16**,** 907-17.

BA, X. & GARG, N. J. 2010. Signaling Mechanism of PARP-1 in Inflammatory Diseases. *Am J Pathol,* 178**,** 946-955.

BARKER, R. N., ERWIG, L., PEARCE, W. P., DEVINE, A. & REES, A. J. 1999. Differential effects of necrotic or apoptotic cell uptake on antigen presentation by macrophages. *Pathobiology,* 67**,** 302-5.

BASOMBRIO, M. A. & BESUSCHIO, S. 1982. Trypanosoma cruzi culture used as vaccine to prevent chronic Chagas' disease in mice. *Infect Immun,* 36**,** 351-6.

BASOMBRIO, M. A., BESUSCHIO, S. & COSSIO, P. M. 1982. Side effects of immunization with liver attenuated Trypanosoma cruzi in mice and rabbits. *Infect Immun,* 36**,** 342-50.

BASOMBRIO, M. A., SEGURA, M. A. & NASSER, J. R. 2002. Relationship between long-term resistance to Trypanosoma cruzi and latent infection, examined by antibody production and polymerase chain reaction in mice. *J Parasitol,* 88**,** 1107-12.

BECKER, L., LIU, N. C., AVERILL, M. M., YUAN, W., PAMIR, N., PENG, Y., IRWIN, A. D., FU, X., BORNFELDT, K. E. & HEINECKE, J. W. 2012. Unique proteomic signatures distinguish macrophages and dendritic cells. *PLoS One,* 7**,** e33297.

BELAUNZARAN, M. L., WAINSZELBAUM, M. J., LAMMEL, E. M., GIMENEZ, G., ALOISE, M. M., FLORIN-CHRISTENSEN, J. & ISOLA, E. L. 2007. Phospholipase A1 from Trypanosoma cruzi infective stages generates lipid messengers that activate host cell protein kinase c. *Parasitology,* 134**,** 491-502.

BERNARD, M. A., HAN, X., INDERBITZIN, S., AGBIM, I., ZHAO, H., KOZIEL, H. & TACHADO, S. D. 2014. HIV-derived ssRNA binds to TLR8 to induce inflammation-driven macrophage foam cell formation. *PLoS One,* 9**,** e104039.

BLAIR, D., DUFORT, F. J. & CHILES, T. C. 2012. Protein kinase Cbeta is critical for the metabolic switch to glycolysis following B-cell antigen receptor engagement. *Biochem J,* 448**,** 165-9.

BONNEY, K. M., TAYLOR, J. M., DANIELS, M. D., EPTING, C. L. & ENGMAN, D. M. 2011. Heat-killed Trypanosoma cruzi induces acute cardiac damage and polyantigenic autoimmunity. *PLoS One,* 6**,** e14571.

BOUHLEL, M. A., DERUDAS, B., RIGAMONTI, E., DIEVART, R., BROZEK, J., HAULON, S., ZAWADZKI, C., JUDE, B., TORPIER, G., MARX, N., STAELS, B. & CHINETTI-GBAGUIDI, G. 2007.

PPARgamma activation primes human monocytes into alternative M2 macrophages with anti-inflammatory properties. *Cell Metab,* 6**,** 137-43.

BOWDEN, S. D., ROWLEY, G., HINTON, J. C. & THOMPSON, A. 2009. Glucose and glycolysis are required for the successful infection of macrophages and mice by Salmonella enterica serovar typhimurium. *Infect Immun,* 77**,** 3117-26.

BUKRINSKY, M. & SVIRIDOV, D. 2006. Human immunodeficiency virus infection and macrophage cholesterol metabolism. *J Leukoc Biol,* 80**,** 1044-51.

CABALEN, M. E., CABRAL, M. F., SANMARCO, L. M., ANDRADA, M. C., ONOFRIO, L. I., PONCE, N. E., AOKI, M. P., GEA, S. & CANO, R. C. 2016. Chronic Trypanosoma cruzi infection potentiates adipose tissue macrophage polarization toward an anti-inflammatory M2 phenotype and contributes to diabetes progression in a diet-induced obesity model. *Oncotarget,* 7**,** 13400-15.

CANTO, C. & AUWERX, J. 2011. Interference between PARPs and SIRT1: a novel approach to healthy ageing? *Aging (Albany NY),* 3**,** 543-7.

CARADONNA, K. L., ENGEL, J. C., JACOBI, D., LEE, C. H. & BURLEIGH, B. A. 2013. Host metabolism regulates intracellular growth of Trypanosoma cruzi. *Cell Host Microbe,* 13**,** 108-17.

CARDONI, R. L., ANTUNEZ, M. I., MORALES, C. & NANTES, I. R. 1997. Release of reactive oxygen species by phagocytic cells in response to live parasites in mice infected with Trypanosoma cruzi. *Am J Trop Med Hyg,* 56**,** 329-34.

CARPENTER, K. L., JALLOH, I. & HUTCHINSON, P. J. 2015. Glycolysis and the significance of lactate in traumatic brain injury. *Front Neurosci,* 9**,** 112.

CASTOLDI, A., NAFFAH DE SOUZA, C., CAMARA, N. O. & MORAES-VIEIRA, P. M. 2015. The Macrophage Switch in Obesity Development. *Front Immunol,* 6**,** 637.

CELENTANO, A. M. & GONZALEZ CAPPA, S. M. 1993. In vivo macrophage function in experimental infection with Trypanosoma cruzi subpopulations. *Acta Trop,* 55**,** 171-80.

CHANDAK, P. G., RADOVIC, B., AFLAKI, E., KOLB, D., BUCHEBNER, M., FROHLICH, E., MAGNES, C., SINNER, F., HAEMMERLE, G., ZECHNER, R., TABAS, I., LEVAK-FRANK, S. & KRATKY, D. 2010. Efficient phagocytosis requires triacylglycerol hydrolysis by adipose triglyceride lipase. *J Biol Chem,* 285**,** 20192-201.

CHATURVEDI, R., ASIM, M., LEWIS, N. D., ALGOOD, H. M., COVER, T. L., KIM, P. Y. & WILSON, K. T. 2007. L-arginine availability regulates inducible nitric oxide synthase-dependent host defense against Helicobacter pylori. *Infect Immun,* 75**,** 4305-15.

CHAWLA, A., BOISVERT, W. A., LEE, C. H., LAFFITTE, B. A., BARAK, Y., JOSEPH, S. B., LIAO, D., NAGY, L., EDWARDS, P. A., CURTISS, L. K., EVANS, R. M. & TONTONOZ, P. 2001. A PPAR gamma-LXR-ABCA1 pathway in macrophages is involved in cholesterol efflux and atherogenesis. *Mol Cell,* 7**,** 161-71.

CHINETTI, G., LESTAVEL, S., BOCHER, V., REMALEY, A. T., NEVE, B., TORRA, I. P., TEISSIER, E., MINNICH, A., JAYE, M., DUVERGER, N., BREWER, H. B., FRUCHART, J. C., CLAVEY, V. & STAELS, B. 2001. PPAR-alpha and PPAR-gamma activators induce cholesterol removal from human macrophage foam cells through stimulation of the ABCA1 pathway. *Nat Med,* 7**,** 53-8.

CLEETER, M. W., COOPER, J. M., DARLEY-USMAR, V. M., MONCADA, S. & SCHAPIRA, A. H. 1994. Reversible inhibition of cytochrome c oxidase, the terminal enzyme of the mitochondrial respiratory chain, by nitric oxide. Implications for neurodegenerative diseases. *FEBS Lett,* 345**,** 50-4.

CONWAY, E. L., SELLICK, J. A., KURTZHALTS, K. & MERGENHAGEN, K. A. 2017. Obesity and Heart Failure as Predictors of Failure in Outpatient Skin and Soft Tissue Infections. *Antimicrob Agents Chemother,* 61.

CORWARE, K., YARDLEY, V., MACK, C., SCHUSTER, S., AL-HASSI, H., HERATH, S., BERGIN, P., MODOLELL, M., MUNDER, M., MULLER, I. & KROPF, P. 2014. Protein energy malnutrition increases arginase activity in monocytes and macrophages. *Nutr Metab (Lond),* 11**,** 51.

COSTA, T. B. D., MORAIS, N. G., PEDROSA, A. L. F., DE ALBUQUERQUE, S., DE CASTRO, M., PEREIRA, V. R. A., CAVALCANTI, M. P. & DE CASTRO, C. 2016. Neonatal malnutrition programs the oxidant function of macrophages in response to Candida albicans. *Microb Pathog,* 95**,** 68-76.

COUPER, K. N., BLOUNT, D. G. & RILEY, E. M. 2008. IL-10: the master regulator of immunity to infection. *J Immunol,* 180**,** 5771-7.

COURA, J. R., DE ABREU, L. L., WILLCOX, H. P. & PETANA, W. 1997. [Comparative controlled study on the use of benznidazole, nifurtimox and placebo, in the chronic form of Chagas' disease, in a field area with interrupted transmission. I. Preliminary evaluation]. *Rev Soc Bras Med Trop,* 30**,** 139-44.

COVARRUBIAS, A. J., AKSOYLAR, H. I. & HORNG, T. 2015. Control of macrophage metabolism and activation by mTOR and Akt signaling. *Semin Immunol,* 27**,** 286-96.

CROWE, S. M., WESTHORPE, C. L., MUKHAMEDOVA, N., JAWOROWSKI, A., SVIRIDOV, D. & BUKRINSKY, M. 2010. The macrophage: the intersection between HIV infection and atherosclerosis. *J Leukoc Biol,* 87**,** 589-98.

CUI, H. L., DITIATKOVSKI, M., KESANI, R., BOBRYSHEV, Y. V., LIU, Y., GEYER, M., MUKHAMEDOVA, N., BUKRINSKY, M. & SVIRIDOV, D. 2014. HIV protein Nef causes dyslipidemia and formation of foam cells in mouse models of atherosclerosis. *FASEB J,* 28**,** 2828-39.

DAHLGREN, C. & KARLSSON, A. 1999. Respiratory burst in human neutrophils. *J Immunol Methods,* 232**,** 3-14.

DASHTY, M. 2013. A quick look at biochemistry: carbohydrate metabolism. *Clin Biochem,* 46**,** 1339-52.

DEY, N., SINHA, M., GUPTA, S., GONZALEZ, M. N., FANG, R., ENDSLEY, J. J., LUXON, B. A. & GARG, N. J. 2014. Caspase-1/ASC inflammasome-mediated activation of IL-1beta-ROS-NF-kappaB pathway for control of Trypanosoma cruzi replication and survival is dispensable in NLRP3-/- macrophages. *PLoS One,* 9**,** e111539.

DHIMAN, M. & GARG, N. J. 2011. NADPH oxidase inhibition ameliorates Trypanosoma cruzi-induced myocarditis during Chagas disease. *J Pathol,* 225**,** 583-96.

DIVAKARUNI, A. S., PARADYSE, A., FERRICK, D. A., MURPHY, A. N. & JASTROCH, M. 2014. Analysis and interpretation of microplate-based oxygen consumption and pH data. *Methods Enzymol,* 547**,** 309-54.

DULGERIAN, L. R., GARRIDO, V. V., STEMPIN, C. C. & CERBAN, F. M. 2011. Programmed death ligand 2 regulates arginase induction and modifies Trypanosoma cruzi survival in macrophages during murine experimental infection. *Immunology,* 133**,** 29-40.

ECKER, J., LIEBISCH, G., ENGLMAIER, M., GRANDL, M., ROBENEK, H. & SCHMITZ, G. 2010. Induction of fatty acid synthesis is a key requirement for phagocytic differentiation of human monocytes. *Proc Natl Acad Sci U S A,* 107**,** 7817-22.

EISELE, N. A., RUBY, T., JACOBSON, A., MANZANILLO, P. S., COX, J. S., LAM, L., MUKUNDAN, L., CHAWLA, A. & MONACK, D. M. 2013. Salmonella require the fatty acid regulator PPARδ for the establishment of a metabolic environment essential for long-term persistence. *Cell Host Microbe,* 14**,** 171-82.

ELAINE CRISTINA NAVARRO, M. M. D. A., FRANCILENE CAPEL TAVARES, JOSÉ EDUARDO CORRENTE, CAMILA MARIA DE ARRUDA, PAULO CÂMARA MARQUES PEREIRA 2013. Indeterminate Form of Chagas' Disease and Metabolic Syndrome: A Dangerous Combination. *American Journal of Medicine and Medical Sciences,* 3**,** 68-73.

FEINGOLD, K. R., SHIGENAGA, J. K., KAZEMI, M. R., MCDONALD, C. M., PATZEK, S. M., CROSS, A. S., MOSER, A. & GRUNFELD, C. 2012. Mechanisms of triglyceride accumulation in activated macrophages. *J Leukoc Biol,* 92**,** 829-39.

FOCK, R. A., ROGERO, M. M., VINOLO, M. A., CURI, R., BORGES, M. C. & BORELLI, P. 2010. Effects of protein-energy malnutrition on NF-kappaB signalling in murine peritoneal macrophages. *Inflammation,* 33**,** 101-9.

FONTAINE, K. A., SANCHEZ, E. L., CAMARDA, R. & LAGUNOFF, M. 2015. Dengue virus induces and requires glycolysis for optimal replication. *J Virol,* 89**,** 2358-66.

FREEMERMAN, A. J., JOHNSON, A. R., SACKS, G. N., MILNER, J. J., KIRK, E. L., TROESTER, M. A., MACINTYRE, A. N., GORAKSHA-HICKS, P., RATHMELL, J. C. & MAKOWSKI, L. 2014. Metabolic reprogramming of macrophages: glucose transporter 1 (GLUT1)-mediated glucose metabolism drives a proinflammatory phenotype. *J Biol Chem,* 289**,** 7884-96.

GALLO, E., KATZMAN, S. & VILLARINO, A. V. 2012. IL-13-producing Th1 and Th17 cells characterize adaptive responses to both self and foreign antigens. *Eur J Immunol,* 42**,** 2322-8.

GAO, Y. T., ROMAN, L. J., MARTASEK, P., PANDA, S. P., ISHIMURA, Y. & MASTERS, B. S. 2007. Oxygen metabolism by endothelial nitric-oxide synthase. *J Biol Chem,* 282**,** 28557-65.

GARCIA, E. S., GENTA, F. A., DE AZAMBUJA, P. & SCHAUB, G. A. 2010. Interactions between intestinal compounds of triatomines and Trypanosoma cruzi. *Trends Parasitol,* 26**,** 499-505.

GARG, N., GERSTNER, A., BHATIA, V., DEFORD, J. & PAPACONSTANTINOU, J. 2004. Gene expression analysis in mitochondria from chagasic mice: alterations in specific metabolic pathways. *Biochem J,* 381**,** 743-52.

GERAIX, J., ARDISSON, L. P., MARCONDES-MACHADO, J. & PEREIRA, P. C. 2007. Clinical and nutritional profile of individuals with Chagas disease. *Braz J Infect Dis,* 11**,** 411-4.

GIULIVI, C., KATO, K. & COOPER, C. E. 2006. Nitric oxide regulation of mitochondrial oxygen consumption I: cellular physiology. *Am J Physiol Cell Physiol,* 291**,** C1225-31.

GREEN, D. S., YOUNG, H. A. & VALENCIA, J. C. 2017. Current prospects of type II interferon gamma signaling and autoimmunity. *J Biol Chem,* 292**,** 13925-13933.

GUPTA, S., BHATIA, V., WEN, J. J., WU, Y., HUANG, M. H. & GARG, N. J. 2009. Trypanosoma cruzi infection disturbs mitochondrial membrane potential and ROS production rate in cardiomyocytes. *Free Radic Biol Med,* 47**,** 1414-21.

GUPTA, S., SILVA, T. S., OSIZUGBO, J. E., TUCKER, L. & GARG, N. J. 2013. Serum mediated activation of macrophages reflects Tcvac2 vaccine efficacy against Chagas disease. *Infection & Immunity,* Submitted.

GUPTA, S., SILVA, T. S., OSIZUGBO, J. E., TUCKER, L., SPRATT, H. M. & GARG, N. J. 2014. Serum-mediated activation of macrophages reflects TcVac2 vaccine efficacy against Chagas disease. *Infect Immun,* 82**,** 1382-9.

HAM, M., LEE, J. W., CHOI, A. H., JANG, H., CHOI, G., PARK, J., KOZUKA, C., SEARS, D. D., MASUZAKI, H. & KIM, J. B. 2013. Macrophage glucose-6-phosphate dehydrogenase stimulates proinflammatory responses with oxidative stress. *Mol Cell Biol,* 33**,** 2425-35.

HAN, C. Y. 2016. Roles of Reactive Oxygen Species on Insulin Resistance in Adipose Tissue. *Diabetes Metab J,* 40**,** 272-9.

HARAGUCHI, G., KOBAYASHI, Y., BROWN, M. L., TANAKA, A., ISOBE, M., GIANTURCO, S. H. & BRADLEY, W. A. 2003. PPAR(alpha) and PPAR(gamma) activators suppress the monocyte-macrophage apoB-48 receptor. *J Lipid Res,* 44**,** 1224-31.

HARTMAN, M. L., SHIRIHAI, O. S., HOLBROOK, M., XU, G., KOCHERLA, M., SHAH, A., FETTERMAN, J. L., KLUGE, M. A., FRAME, A. A., HAMBURG, N. M. & VITA, J. A. 2014. Relation of

mitochondrial oxygen consumption in peripheral blood mononuclear cells to vascular function in type 2 diabetes mellitus. *Vasc Med,* 19**,** 67-74.

HASCHEMI, A., KOSMA, P., GILLE, L., EVANS, C. R., BURANT, C. F., STARKL, P., KNAPP, B., HAAS, R., SCHMID, J. A., JANDL, C., AMIR, S., LUBEC, G., PARK, J., ESTERBAUER, H., BILBAN, M., BRIZUELA, L., POSPISILIK, J. A., OTTERBEIN, L. E. & WAGNER, O. 2012. The sedoheptulose kinase CARKL directs macrophage polarization through control of glucose metabolism. *Cell Metab,* 15**,** 813-26.

HOLLENBAUGH, J. A., MUNGER, J. & KIM, B. 2011. Metabolite profiles of human immunodeficiency virus infected CD4+ T cells and macrophages using LC-MS/MS analysis. *Virology,* 415**,** 153-9.

HOSHINO, T., WINKLER-PICKETT, R. T., MASON, A. T., ORTALDO, J. R. & YOUNG, H. A. 1999. IL-13 production by NK cells: IL-13-producing NK and T cells are present in vivo in the absence of IFN-gamma. *J Immunol,* 162**,** 51-9.

HU, C. J., WANG, L. Y., CHODOSH, L. A., KEITH, B. & SIMON, M. C. 2003. Differential roles of hypoxia-inducible factor 1alpha (HIF-1alpha) and HIF-2alpha in hypoxic gene regulation. *Mol Cell Biol,* 23**,** 9361-74.

HUANG, S. C., EVERTS, B., IVANOVA, Y., O'SULLIVAN, D., NASCIMENTO, M., SMITH, A. M., BEATTY, W., LOVE-GREGORY, L., LAM, W. Y., O'NEILL, C. M., YAN, C., DU, H., ABUMRAD, N. A., URBAN, J. F., JR., ARTYOMOV, M. N., PEARCE, E. L. & PEARCE, E. J. 2014. Cell-intrinsic lysosomal lipolysis is essential for alternative activation of macrophages. *Nat Immunol,* 15**,** 846-55.

JACKSON, Y., ALIROL, E., GETAZ, L., WOLFF, H., COMBESCURE, C. & CHAPPUIS, F. 2010. Tolerance and safety of nifurtimox in patients with chronic chagas disease. *Clin Infect Dis,* 51**,** e69-75.

JASTROCH, M., DIVAKARUNI, A. S., MOOKERJEE, S., TREBERG, J. R. & BRAND, M. D. 2010. Mitochondrial proton and electron leaks. *Essays Biochem,* 47**,** 53-67.

JHA, A. K., HUANG, S. C., SERGUSHICHEV, A., LAMPROPOULOU, V., IVANOVA, Y., LOGINICHEVA, E., CHMIELEWSKI, K., STEWART, K. M., ASHALL, J., EVERTS, B., PEARCE, E. J., DRIGGERS, E. M. & ARTYOMOV, M. N. 2015. Network integration of parallel metabolic and transcriptional data reveals metabolic modules that regulate macrophage polarization. *Immunity,* 42**,** 419-30.

JIANG, H., SHI, H., SUN, M., WANG, Y., MENG, Q., GUO, P., CAO, Y., CHEN, J., GAO, X., LI, E. & LIU, J. 2016. PFKFB3-Driven Macrophage Glycolytic Metabolism Is a Crucial Component of Innate Antiviral Defense. *J Immunol,* 197**,** 2880-90.

JOHNDROW, C., NELSON, R., TANOWITZ, H., WEISS, L. M. & NAGAJYOTHI, F. 2014. Trypanosoma cruzi infection results in an increase in intracellular cholesterol. *Microbes Infect,* 16**,** 337-44.

JOHNSON, A. R., QIN, Y., COZZO, A. J., FREEMERMAN, A. J., HUANG, M. J., ZHAO, L., SAMPEY, B. P., MILNER, J. J., BECK, M. A., DAMANIA, B., RASHID, N., GALANKO, J. A., LEE, D. P., EDIN, M. L., ZELDIN, D. C., FUEGER, P. T., DIETZ, B., STAHL, A., WU, Y., MOHLKE, K. L. & MAKOWSKI, L. 2016. Metabolic reprogramming through fatty acid transport protein 1 (FATP1) regulates macrophage inflammatory potential and adipose inflammation. *Mol Metab,* 5**,** 506-26.

JONES, G. E. 2000. Cellular signaling in macrophage migration and chemotaxis. *J Leukoc Biol,* 68**,** 593-602.

JONES, M. L., GANOPOLSKY, J. G., LABBE, A., WAHL, C. & PRAKASH, S. 2010. Antimicrobial properties of nitric oxide and its application in antimicrobial formulations and medical devices. *Appl Microbiol Biotechnol,* 88**,** 401-7.

KARLSSON, E. A. & BECK, M. A. 2010. The burden of obesity on infectious disease. *Exp Biol Med (Maywood),* 235**,** 1412-24.

KAYAMA, H. & TAKEDA, K. 2010. The innate immune response to Trypanosoma cruzi infection. *Microbes Infect,* 12**,** 511-7.

KELLY, B. & O'NEILL, L. A. 2015. Metabolic reprogramming in macrophages and dendritic cells in innate immunity. *Cell Res,* 25**,** 771-84.

KIM, J. W., TCHERNYSHYOV, I., SEMENZA, G. L. & DANG, C. V. 2006. HIF-1-mediated expression of pyruvate dehydrogenase kinase: a metabolic switch required for cellular adaptation to hypoxia. *Cell Metab,* 3**,** 177-85.

KLEINBONGARD, P., RASSAF, T., DEJAM, A., KERBER, S. & KELM, M. 2002. Griess method for nitrite measurement of aqueous and protein-containing samples. *Methods Enzymol,* 359**,** 158-68.

KOO, S. J., CHOWDHURY, I. H., SZCZESNY, B., WAN, X. & GARG, N. J. 2016. Macrophages Promote Oxidative Metabolism To Drive Nitric Oxide Generation in Response to Trypanosoma cruzi. *Infect Immun,* 84**,** 3527-3541.

KRYSKO, D. V., DENECKER, G., FESTJENS, N., GABRIELS, S., PARTHOENS, E., D'HERDE, K. & VANDENABEELE, P. 2006. Macrophages use different internalization mechanisms to clear apoptotic and necrotic cells. *Cell Death Differ,* 13**,** 2011-22.

KUPRASH, D. V., UDALOVA, I. A., TURETSKAYA, R. L., KWIATKOWSKI, D., RICE, N. R. & NEDOSPASOV, S. A. 1999. Similarities and differences between human and murine TNF promoters in their response to lipopolysaccharide. *J Immunol,* 162**,** 4045-52.

LA FLAMME, A. C., KAHN, S. J., RUDENSKY, A. Y. & VAN VOORHIS, W. C. 1997. Trypanosoma cruzi-infected macrophages are defective in major histocompatibility complex class II antigen presentation. *Eur J Immunol,* 27**,** 3085-94.

LAMOUR, S. D., CHOI, B. S., KEUN, H. C., MÜLLER, I. & SARIC, J. 2012. Metabolic characterization of Leishmania major infection in activated and nonactivated macrophages. *J Proteome Res,* 11**,** 4211-22.

LEMAY, D. G. & HWANG, D. H. 2006. Genome-wide identification of peroxisome proliferator response elements using integrated computational genomics. *J Lipid Res,* 47**,** 1583-7.

LIU, L., LU, Y., MARTINEZ, J., BI, Y., LIAN, G., WANG, T., MILASTA, S., WANG, J., YANG, M., LIU, G., GREEN, D. R. & WANG, R. 2016. Proinflammatory signal suppresses proliferation and shifts macrophage metabolism from Myc-dependent to HIF1alpha-dependent. *Proc Natl Acad Sci U S A,* 113**,** 1564-9.

LUMENG, C. N. 2013. Innate immune activation in obesity. *Mol Aspects Med,* 34**,** 12-29.

MARTINEZ, F. O. & GORDON, S. 2014. The M1 and M2 paradigm of macrophage activation: time for reassessment. *F1000Prime Rep,* 6**,** 13.

MARTINEZ, F. O., GORDON, S., LOCATI, M. & MANTOVANI, A. 2006. Transcriptional profiling of the human monocyte-to-macrophage differentiation and polarization: new molecules and patterns of gene expression. *J Immunol,* 177**,** 7303-11.

MCCONVILLE, M. J. 2016. Metabolic Crosstalk between Leishmania and the Macrophage Host. *Trends Parasitol,* 32**,** 666-8.

MEDBURY, H. J., WILLIAMS, H. & FLETCHER, J. P. 2014. Clinical significance of macrophage phenotypes in cardiovascular disease. *Clin Transl Med,* 3**,** 63.

MEHROTRA, P., JAMWAL, S. V., SAQUIB, N., SINHA, N., SIDDIQUI, Z., MANIVEL, V., CHATTERJEE, S. & RAO, K. V. 2014. Pathogenicity of Mycobacterium tuberculosis is expressed by regulating metabolic thresholds of the host macrophage. *PLoS Pathog,* 10**,** e1004265.

MEISER, J., KRAMER, L., SAPCARIU, S. C., BATTELLO, N., GHELFI, J., D'HEROUEL, A. F., SKUPIN, A. & HILLER, K. 2016. Pro-inflammatory Macrophages Sustain Pyruvate Oxidation through

Pyruvate Dehydrogenase for the Synthesis of Itaconate and to Enable Cytokine Expression. *J Biol Chem,* 291**,** 3932-46.

MENDES DA SILVA, L. D., GATTO, M., MIZIARA DE ABREU TEODORO, M., DE ASSIS GOLIM, M., PELISSON NUNES DA COSTA, E. A., CAPEL TAVARES CARVALHO, F., RAMOS RODRIGUES, D., CAMARA MARQUES PEREIRA, P., VICTORIANO DE CAMPOS SOARES, A. M. & CALVI, S. A. 2017. Participation of TLR2 and TLR4 in Cytokines Production by Patients with Symptomatic and Asymptomatic Chronic Chagas Disease. *Scand J Immunol,* 85**,** 58-65.

MOON, J. S., LEE, S., PARK, M. A., SIEMPOS, II, HASLIP, M., LEE, P. J., YUN, M., KIM, C. K., HOWRYLAK, J., RYTER, S. W., NAKAHIRA, K. & CHOI, A. M. 2015. UCP2-induced fatty acid synthase promotes NLRP3 inflammasome activation during sepsis. *J Clin Invest,* 125**,** 665-80.

MOORE, K. J., SHEEDY, F. J. & FISHER, E. A. 2013. Macrophages in atherosclerosis: a dynamic balance. *Nat Rev Immunol,* 13**,** 709-21.

MOREIRA, D., RODRIGUES, V., ABENGOZAR, M., RIVAS, L., RIAL, E., LAFORGE, M., LI, X., FORETZ, M., VIOLLET, B., ESTAQUIER, J., CORDEIRO DA SILVA, A. & SILVESTRE, R. 2015. Leishmania infantum modulates host macrophage mitochondrial metabolism by hijacking the SIRT1-AMPK axis. *PLoS Pathog,* 11**,** e1004684.

NAGAJYOTHI, F., KULIAWAT, R., KUSMINSKI, C. M., MACHADO, F. S., DESRUISSEAUX, M. S., ZHAO, D., SCHWARTZ, G. J., HUANG, H., ALBANESE, C., LISANTI, M. P., SINGH, R., LI, F., WEISS, L. M., FACTOR, S. M., PESSIN, J. E., SCHERER, P. E. & TANOWITZ, H. B. 2013. Alterations in glucose homeostasis in a murine model of Chagas disease. *Am J Pathol,* 182**,** 886-94.

NAGAJYOTHI, F., ZHAO, D., MACHADO, F. S., WEISS, L. M., SCHWARTZ, G. J., DESRUISSEAUX, M. S., ZHAO, Y., FACTOR, S. M., HUANG, H., ALBANESE, C., TEIXEIRA, M. M., SCHERER, P. E., CHUA, S. C., JR. & TANOWITZ, H. B. 2010. Crucial role of the central leptin receptor in murine Trypanosoma cruzi (Brazil strain) infection. *J Infect Dis,* 202**,** 1104-13.

NORRIS, K. A., SCHRIMPF, J. E., FLYNN, J. L. & MORRIS, S. M., JR. 1995. Enhancement of macrophage microbicidal activity: supplemental arginine and citrulline augment nitric oxide production in murine peritoneal macrophages and promote intracellular killing of Trypanosoma cruzi. *Infect Immun,* 63**,** 2793-6.

O'FARRELL, A. M., LIU, Y., MOORE, K. W. & MUI, A. L. 1998. IL-10 inhibits macrophage activation and proliferation by distinct signaling mechanisms: evidence for Stat3-dependent and -independent pathways. *EMBO J,* 17**,** 1006-18.

ODEGAARD, J. I., RICARDO-GONZALEZ, R. R., GOFORTH, M. H., MOREL, C. R., SUBRAMANIAN, V., MUKUNDAN, L., RED EAGLE, A., VATS, D., BROMBACHER, F., FERRANTE, A. W. & CHAWLA, A. 2007. Macrophage-specific PPARgamma controls alternative activation and improves insulin resistance. *Nature,* 447**,** 1116-20.

ODEGAARD, J. I., RICARDO-GONZALEZ, R. R., RED EAGLE, A., VATS, D., MOREL, C. R., GOFORTH, M. H., SUBRAMANIAN, V., MUKUNDAN, L., FERRANTE, A. W. & CHAWLA, A. 2008. Alternative M2 activation of Kupffer cells by PPARdelta ameliorates obesity-induced insulin resistance. *Cell Metab,* 7**,** 496-507.

OLIVEIRA, D. C. D., HASTREITER, A. A., BORELLI, P. & FOCK, R. A. 2016. The influence of protein malnutrition on the production of GM-CSF and M-CSF by macrophages. *Brazilian Journal of Pharmaceutical Sciences,* 52**,** 375-382.

ORTEGA-GOMEZ, A., PERRETTI, M. & SOEHNLEIN, O. 2013. Resolution of inflammation: an integrated view. *EMBO Mol Med,* 5**,** 661-74.

PAGE, C., GOICOCHEA, L., MATTHEWS, K., ZHANG, Y., KLOVER, P., HOLTZMAN, M. J., HENNIGHAUSEN, L. & FRIEMAN, M. 2012. Induction of alternatively activated

macrophages enhances pathogenesis during severe acute respiratory syndrome coronavirus infection. *J Virol,* 86**,** 13334-49.

PAIVA, C. N., FEIJO, D. F., DUTRA, F. F., CARNEIRO, V. C., FREITAS, G. B., ALVES, L. S., MESQUITA, J., FORTES, G. B., FIGUEIREDO, R. T., SOUZA, H. S., FANTAPPIE, M. R., LANNES-VIEIRA, J. & BOZZA, M. T. 2012. Oxidative stress fuels Trypanosoma cruzi infection in mice. *J Clin Invest,* 122**,** 2531-42.

PEREZ BRANDAN, C. & BASOMBRIO, M. A. 2012. Genetically attenuated Trypanosoma cruzi parasites as a potential vaccination tool. *Bioengineered,* 3**,** 242-6.

PIACENZA, L., ALVAREZ, M. N., PELUFFO, G. & RADI, R. 2009. Fighting the oxidative assault: the Trypanosoma cruzi journey to infection. *Curr Opin Microbiol,* 12**,** 415-21.

PIACENZA, L., PELUFFO, G., ALVAREZ, M. N., KELLY, J. M., WILKINSON, S. R. & RADI, R. 2008. Peroxiredoxins play a major role in protecting Trypanosoma cruzi against macrophage- and endogenously-derived peroxynitrite. *Biochem J,* 410**,** 359-68.

PINAZO, M. J., MUNOZ, J., POSADA, E., LOPEZ-CHEJADE, P., GALLEGO, M., AYALA, E., DEL CACHO, E., SOY, D. & GASCON, J. 2010. Tolerance of benznidazole in treatment of Chagas' disease in adults. *Antimicrob Agents Chemother,* 54**,** 4896-9.

PINEYRO, M. D., ARCARI, T., ROBELLO, C., RADI, R. & TRUJILLO, M. 2011. Tryparedoxin peroxidases from Trypanosoma cruzi: high efficiency in the catalytic elimination of hydrogen peroxide and peroxynitrite. *Arch Biochem Biophys,* 507**,** 287-95.

PINEYRO, M. D., PARODI-TALICE, A., ARCARI, T. & ROBELLO, C. 2008. Peroxiredoxins from Trypanosoma cruzi: virulence factors and drug targets for treatment of Chagas disease? *Gene,* 408**,** 45-50.

POSTAN, M., CHEEVER, A. W., DVORAK, J. A. & MCDANIEL, J. P. 1986. A histopathological analysis of the course of myocarditis in C3H/He mice infected with Trypanosoma cruzi clone Sylvio-X10/4. *Trans R Soc Trop Med Hyg,* 80**,** 50-5.

POSTAN, M., DVORAK, J. A. & MCDANIEL, J. P. 1983. Studies of Trypanosoma cruzi clones in inbred mice. I. A comparison of the course of infection of C3H/HEN- mice with two clones isolated from a common source. *Am J Trop Med Hyg,* 32**,** 497-506.

RATH, M., MULLER, I., KROPF, P., CLOSS, E. I. & MUNDER, M. 2014. Metabolism via Arginase or Nitric Oxide Synthase: Two Competing Arginine Pathways in Macrophages. *Front Immunol,* 5**,** 532.

ROWE, G. C., JIANG, A. & ARANY, Z. 2010. PGC-1 coactivators in cardiac development and disease. *Circ Res,* 107**,** 825-38.

SCHINDELIN, J., ARGANDA-CARRERAS, I., FRISE, E., KAYNIG, V., LONGAIR, M., PIETZSCH, T., PREIBISCH, S., RUEDEN, C., SAALFELD, S., SCHMID, B., TINEVEZ, J. Y., WHITE, D. J., HARTENSTEIN, V., ELICEIRI, K., TOMANCAK, P. & CARDONA, A. 2012. Fiji: an open-source platform for biological-image analysis. *Nat Methods,* 9**,** 676-82.

SEABRA, S. H., DAMATTA, R. A., DE MELLO, F. G. & DE SOUZA, W. 2004. Endogenous polyamine levels in macrophages is sufficient to support growth of Toxoplasma gondii. *J Parasitol,* 90**,** 455-60.

SEDGER, L. M. & MCDERMOTT, M. F. 2014. TNF and TNF-receptors: From mediators of cell death and inflammation to therapeutic giants - past, present and future. *Cytokine Growth Factor Rev,* 25**,** 453-72.

SHELDON, K. E., SHANDILYA, H., KEPKA-LENHART, D., POLJAKOVIC, M., GHOSH, A. & MORRIS, S. M., JR. 2013. Shaping the murine macrophage phenotype: IL-4 and cyclic AMP synergistically activate the arginase I promoter. *J Immunol,* 191**,** 2290-8.

SHIN, D. M., YANG, C. S., LEE, J. Y., LEE, S. J., CHOI, H. H., LEE, H. M., YUK, J. M., HARDING, C. V. & JO, E. K. 2008. Mycobacterium tuberculosis lipoprotein-induced association of TLR2 with

protein kinase C zeta in lipid rafts contributes to reactive oxygen species-dependent inflammatory signalling in macrophages. *Cell Microbiol,* 10**,** 1893-905.

SILVA, G. C., NAGIB, P. R., CHIARI, E., VAN ROOIJEN, N., MACHADO, C. R. & CAMARGOS, E. R. 2004. Peripheral macrophage depletion reduces central nervous system parasitism and damage in Trypanosoma cruzi-infected suckling rats. *J Neuroimmunol,* 149**,** 50-8.

STEINBERG, G. R. & SCHERTZER, J. D. 2014. AMPK promotes macrophage fatty acid oxidative metabolism to mitigate inflammation: implications for diabetes and cardiovascular disease. *Immunol Cell Biol,* 92**,** 340-5.

STUEHR, D. J. 2004. Enzymes of the L-arginine to nitric oxide pathway. *J Nutr,* 134**,** 2748S-2751S; discussion 2765S-2767S.

SU, X., YU, Y., ZHONG, Y., GIANNOPOULOU, E. G., HU, X., LIU, H., CROSS, J. R., RATSCH, G., RICE, C. M. & IVASHKIV, L. B. 2015. Interferon-gamma regulates cellular metabolism and mRNA translation to potentiate macrophage activation. *Nat Immunol,* 16**,** 838-849.

TALL, A. R. & YVAN-CHARVET, L. 2015. Cholesterol, inflammation and innate immunity. *Nat Rev Immunol,* 15**,** 104-16.

TANNAHILL, G. M., CURTIS, A. M., ADAMIK, J., PALSSON-MCDERMOTT, E. M., MCGETTRICK, A. F., GOEL, G., FREZZA, C., BERNARD, N. J., KELLY, B., FOLEY, N. H., ZHENG, L., GARDET, A., TONG, Z., JANY, S. S., CORR, S. C., HANEKLAUS, M., CAFFREY, B. E., PIERCE, K., WALMSLEY, S., BEASLEY, F. C., CUMMINS, E., NIZET, V., WHYTE, M., TAYLOR, C. T., LIN, H., MASTERS, S. L., GOTTLIEB, E., KELLY, V. P., CLISH, C., AURON, P. E., XAVIER, R. J. & O'NEILL, L. A. 2013. Succinate is an inflammatory signal that induces IL-1beta through HIF-1alpha. *Nature,* 496**,** 238-42.

VAN DEN BOSSCHE, J., BAARDMAN, J., OTTO, N. A., VAN DER VELDEN, S., NEELE, A. E., VAN DEN BERG, S. M., LUQUE-MARTIN, R., CHEN, H. J., BOSHUIZEN, M. C., AHMED, M., HOEKSEMA, M. A., DE VOS, A. F. & DE WINTHER, M. P. 2016. Mitochondrial Dysfunction Prevents Repolarization of Inflammatory Macrophages. *Cell Rep,* 17**,** 684-696.

VAN DYKEN, S. J. & LOCKSLEY, R. M. 2013. Interleukin-4- and interleukin-13-mediated alternatively activated macrophages: roles in homeostasis and disease. *Annu Rev Immunol,* 31**,** 317-43.

VANDER HEIDEN, M. G., CANTLEY, L. C. & THOMPSON, C. B. 2009. Understanding the Warburg effect: the metabolic requirements of cell proliferation. *Science,* 324**,** 1029-33.

VARGA, T., MOUNIER, R., PATSALOS, A., GOGOLAK, P., PELOQUIN, M., HORVATH, A., PAP, A., DANIEL, B., NAGY, G., PINTYE, E., POLISKA, S., CUVELLIER, S., LARBI, S. B., SANSBURY, B. E., SPITE, M., BROWN, C. W., CHAZAUD, B. & NAGY, L. 2016. Macrophage PPARgamma, a Lipid Activated Transcription Factor Controls the Growth Factor GDF3 and Skeletal Muscle Regeneration. *Immunity,* 45**,** 1038-1051.

VATS, D., MUKUNDAN, L., ODEGAARD, J. I., ZHANG, L., SMITH, K. L., MOREL, C. R., WAGNER, R. A., GREAVES, D. R., MURRAY, P. J. & CHAWLA, A. 2006. Oxidative metabolism and PGC-1beta attenuate macrophage-mediated inflammation. *Cell Metab,* 4**,** 13-24.

VENDITTI, P., DI STEFANO, L. & DI MEO, S. 2013. Mitochondrial metabolism of reactive oxygen species. *Mitochondrion,* 13**,** 71-82.

WAN, X., WEN, J. J., KOO, S. J., LIANG, L. Y. & GARG, N. J. 2016. SIRT1-PGC1alpha-NFkappaB Pathway of Oxidative and Inflammatory Stress during Trypanosoma cruzi Infection: Benefits of SIRT1-Targeted Therapy in Improving Heart Function in Chagas Disease. *PLoS Pathog,* 12**,** e1005954.

WATANABE COSTA, R., DA SILVEIRA, J. F. & BAHIA, D. 2016. Interactions between Trypanosoma cruzi Secreted Proteins and Host Cell Signaling Pathways. *Front Microbiol,* 7**,** 388.

WEN, J. J. & GARG, N. J. 2008. Mitochondrial generation of reactive oxygen species is enhanced at the Q(o) site of the complex III in the myocardium of Trypanosoma cruzi-infected mice: beneficial effects of an antioxidant. *J Bioenerg Biomembr,* 40**,** 587-98.

WU, G. Y. & BROSNAN, J. T. 1992. Macrophages can convert citrulline into arginine. *Biochem J,* 281 (Pt 1)**,** 45-8.

WYATT, E. V., DIAZ, K., GRIFFIN, A. J., RASMUSSEN, J. A., CRANE, D. D., JONES, B. D. & BOSIO, C. M. 2016. Metabolic Reprogramming of Host Cells by Virulent Francisella tularensis for Optimal Replication and Modulation of Inflammation. *J Immunol,* 196**,** 4227-36.

XIANG, M. & FAN, J. 2010. Association of Toll-like receptor signaling and reactive oxygen species: a potential therapeutic target for posttrauma acute lung injury. *Mediators Inflamm,* 2010.

YE, J., COULOURIS, G., ZARETSKAYA, I., CUTCUTACHE, I., ROZEN, S. & MADDEN, T. L. 2012. Primer-BLAST: a tool to design target-specific primers for polymerase chain reaction. *BMC Bioinformatics,* 13**,** 134.

YU, X. H., FU, Y. C., ZHANG, D. W., YIN, K. & TANG, C. K. 2013. Foam cells in atherosclerosis. *Clin Chim Acta,* 424**,** 245-52.

ZAGO, M. P., HOSAKOTE, Y. M., KOO, S. J., DHIMAN, M., PINEYRO, M. D., PARODI-TALICE, A., BASOMBRIO, M. A., ROBELLO, C. & GARG, N. J. 2016a. TcI isolates of Trypanosoma cruzi exploit antioxidant network for enhanced intracellular survival in macrophages and virulence in mice. *Infect Immun*.

ZAGO, M. P., HOSAKOTE, Y. M., KOO, S. J., DHIMAN, M., PINEYRO, M. D., PARODI-TALICE, A., BASOMBRIO, M. A., ROBELLO, C. & GARG, N. J. 2016b. TcI Isolates of Trypanosoma cruzi Exploit the Antioxidant Network for Enhanced Intracellular Survival in Macrophages and Virulence in Mice. *Infect Immun,* 84**,** 1842-56.

ZAJAC, E., SCHWEIGHOFER, B., KUPRIYANOVA, T. A., JUNCKER-JENSEN, A., MINDER, P., QUIGLEY, J. P. & DERYUGINA, E. I. 2013. Angiogenic capacity of M1- and M2-polarized macrophages is determined by the levels of TIMP-1 complexed with their secreted proMMP-9. *Blood,* 122**,** 4054-67.

ZHANG, X., GONCALVES, R. & MOSSER, D. M. 2008. The isolation and characterization of murine macrophages. *Curr Protoc Immunol,* Chapter 14**,** Unit 14 1.

ZHANG, X. & MOSSER, D. M. 2008. Macrophage activation by endogenous danger signals. *J Pathol,* 214**,** 161-78.

ZHAO, Y., VANHOUTTE, P. M. & LEUNG, S. W. 2015. Vascular nitric oxide: Beyond eNOS. *J Pharmacol Sci,* 129**,** 83-94.

VITA

Sue-jie Koo was born in Corvallis, Oregon, on March 3rd, 1988, the daughter of Gill-soon Kwon and Chang-duck Koo. After completing high school at Villa Maria College in Christchurch, New Zealand, she attended Oregon State University in Corvallis where she studied Microbiology and graduated with a Bachelor of Science in June, 2010. She moved to Houston, Texas and worked on muscle nutrition research at Baylor College of Medicine before starting her graduate studies at the University of Texas Medical Branch in August 2012.

She lives with her husband in Seattle, Washington.

This dissertation was typed by the author with advising from her supervisory chair Nisha Garg, supervisory committee members, and collaborators listed.